BaBar Note # 233

Date: 11/28/95

Author: T. O'Connor, R.J.S. Greenhalgh, P. Fabbricatore, D.E. Baynham
S. Farinon, R. Parodi, F.S. Carr, J. Butterworth, P.L. Sampson
D.A. Cragg, W. Burgess, W.M. Craddock

Title: Design Study for the BaBar Superconducting Solenoid

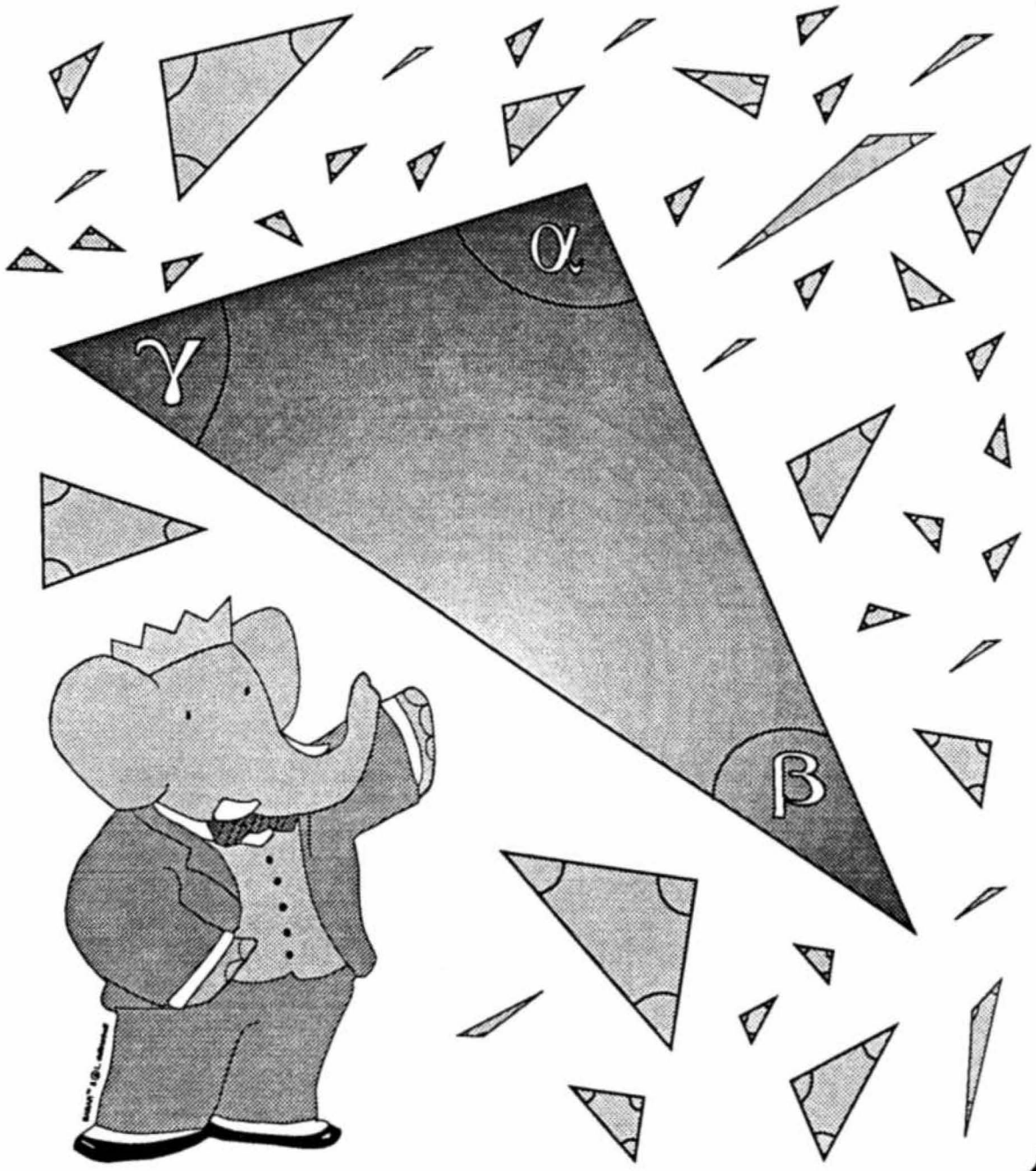

SLAC AHO 2003-032B2f17

BaBar Note No.: 233

Date: 11/28/95

Author(s): Edited by: R.J.S. Greenhalgh, P. Fabbricatore, T.G. O'Connor
Contriubtors: D.E. Baynham, P. Fabbricatore, S. Farinon, R.J.S Greenhalgh, R. Parodi, F.S Carr, J. Butterworth, P.L. Sampson, D.A. Cragg, W. Burgess, W.M. Craddock

Title: Design Study for the BaBar Superconducting Solenoid

Abstract:

Detector System: (Check all that apply)

- [ ] Machine-Detector Interface
- [ ] EM Calorimeter
- [ ] DAQ
- [ ] Vertex Detector
- [ ] IFR
- [ ] Computer On-line
- [ ] Drift Chamber
- [X] Magnet
- [ ] Computer Off-line
- [ ] Particle ID
- [ ] Trigger

Functions: (Specify keywords)

- [ ] Engineering - Electrical
- [ ] Engineering - Software
- [ ] Technical Board
- [X] Engineering - Mechanical
- [ ] ES&H

Keywords: (Check all that apply)

- [X] Specification
- [ ] Operations
- [ ] Monte Carlo
- [ ] Prototype
- [ ] Calibration
- [ ] Algorithms
- [ ] Construction
- [ ] Performance
- [ ] GUI
- [ ] Installation
- [ ] On-line Analysis
- [ ] Tutorial
- [ ] Commissioning
- [ ] Off-line Analysis

Physics Topics: (Check all that apply)

- [ ] *B* Meson
- [ ] Charmed Baryon
- [ ] Two Photon
- [ ] *B* Baryon
- [ ] Tau Lepton
- [ ] QCD
- [ ] Upsilon
- [ ] *CP* Violation
- [X] Other
- [ ] Charmed Meson
- [ ] Mixing

Comments:

Format:

- [ ] TEX PHYZZX
- [ ] Word
- [x] Postscript
- [ ] Paper Only
- [ ] TEX LATEX
- [ ] FrameMaker
- [ ] ASCII
- [ ] TEX DVI

File Location:
~occonor/Babar_Notes/B_Notes.233.ps

Tanya Boyson

BABAR Note 233

Design Study For The BABAR Superconducting Solenoid

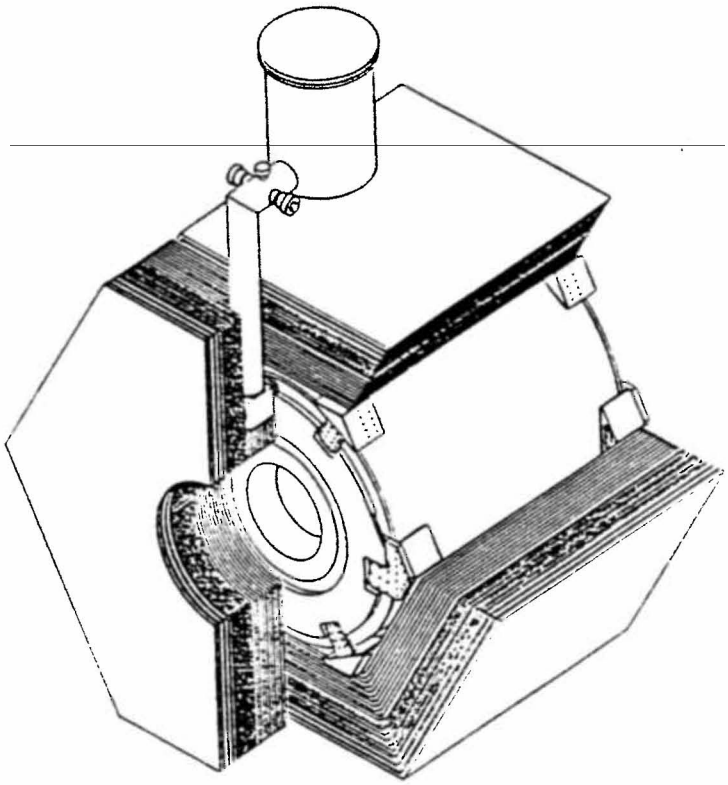

May 1995

Edited by:
R.J.S. Greenhalgh[1], P. Fabbricatore[2] and T.G. O'Connor[3]

Contributors:
D.E. Baynham[1], P. Fabbricatore[2], S. Farinon[2], R.J.S. Greenhalgh[1], R. Parodi[2], F.S. Carr[1], J. Butterworth[1], P.L. Sampson[1], D.A. Cragg[1] W. Burgess[4], W.M. Craddock[4]

[1] Rutherford Appleton Laboratory, Chilton, Didcot, Oxfordshire. OX11 0QX UK
[2] Istituto, Nazionale di Fisica Nucleare, Sezione di Genova. Via Dodecaneso 33, 16146 Genova
[3] Lawrence Livermore National Laboratory, Livermore, CA 94550
[4] Stanford Linear Accelerator Center, Menlo Park, CA

SLAC AHO 2003-032B2f17

Table Of Contents

INTRODUCTION **1**

1. OVERVIEW OF THE SOLENOID **3**

1.1 REQUIREMENTS 3
1.2 COLD MASS 3
1.3 CRYOSTAT 3
1.4 COOLING 4

2. MAGNETIC DESIGN **6**

2.1 THE MODEL 6
2.2 CENTRAL FIELD AND UNIFORMITY 7
2.3 PEAK FIELD AT THE SOLENOID 9
2.4 MAGNETIC FORCES AT THE SOLENOID 9
2.5 MISALIGNMENT IN THE IFR 10
2.6 FORCES IN THE IFR 11
2.7 COMPARISON WITH OTHER CODES 15
2.8 3-D MAGNETIC ANALYSIS 15

3. CONDUCTOR **16**

3.1 AL-STABILIZED CONDUCTOR 16
3.2 ELECTRICAL INSULATION 19
3.3 CONDUCTOR STABILITY 19
3.3.1 Stability Modeling *19*
3.3.2 BABAR Conductor Stability *20*

4. COLD MASS **23**

4.1 DESIGN CONCEPT 23
4.2 SUPPORTING CYLINDER 23
4.3 STRESS CALCULATIONS 24
4.3.1 1-D Analysis For Circumferential Stress *25*
4.3.2 Finite Element Analysis For Circumferential Stress *27*
4.3.3 1-D analysis For Axial Stress *28*
4.3.4 Finite Element Analysis Of The Overall Magnetic Stress *30*
4.3.5 Overall Stress State In Cold Mass *32*
4.3.6 Concluding Remarks *33*
4.4 MANUFACTURING METHOD 34

5. CRYOSTAT **36**

5.1 DESIGN CONCEPT 36
5.2 VACUUM VESSEL 36
5.3 RADIATION SHIELDS 38
5.4 SUPERINSULATION 38

6. SUPPORTS **39**

6.1 DESIGN CONCEPT 39
6.2 LOADS 39
6.2.1 Overview *39*
6.2.2 Details *39*
6.3 INTERNAL SUPPORTS (TIE RODS) 40
6.3.1 Design Criteria *40*
6.3.2 Axial Rods *41*

6.3.3 Radial Rods *41*
6.3.4 Sizes, Details Of Stresses, Heat Loads, Etc. *42*
6.4 EXTERNAL SUPPORTS 43

7. CRYOGENICS 44

7.1 BABAR OVERALL CRYOGENIC CONCEPT 44
7.2 SOLENOID CRYOGENICS CONCEPTS 44
7.2.1 Cool down *45*
7.2.2 Operational Mode *45*
7.2.3 Heat Loads *45*
7.3 COOLING CIRCUIT DESIGN 46
7.3.1 Radiation Shields *46*
7.3.2 Coil *46*
7.3.3 Transfer Lines *46*
7.4 LOCAL CRYOGENICS 46
7.4.1 Services Chimney *46*
7.4.2 Turret Valve Box and Helium Reservoir *46*
7.5 CRYOGENIC CONTROL 47
7.6 FAULT CONDITIONS 47
7.6.1 Warm Up after a Fault Condition *47*

8 VACUUM SYSTEM 49

8.1 DESIGN CRITERIA 49
8.2 CHOICE OF HIGH VACUUM PUMPS 49
8.3 DESIGN 50
8.3.1 Design Calculations *50*
8.4 SYSTEM DEFINITION 50
8.5 SYSTEM INSTALLATION 50
8.5.1 Location/Mounting *50*
8.6 SYSTEM OPERATION 51
8.7 TURRET VALVE BOX 51
8.8 TRANSFER LINES 51
8.9 RELIEF VALVE 51
8.10 CONTROL SYSTEM 51
8.10.1 Interlocks *52*
8.11 REFERENCES 52
8.12 TABLES 53

9. DC POWERING AND QUENCH PROTECTION 54

9.1 CONCEPT 54
9.2 QUENCH ANALYSIS 55
9.2.1 Adiabatic Hot Spot Analysis *55*
9.2.2 Quench Analysis *56*
9.3 QUENCH DETECTION 57

10. INSTRUMENTATION AND CONTROL 58

10.1 GENERAL 58
10.2 TRANSDUCER FUNCTIONS 58
10.2.1 Temperature Monitoring *58*
10.2.2 Force/Loads *59*
10.2.3 Voltages/Currents *59*
10.2.4 Cryogen Flow *59*
10.2.5 Magnetic Fields *59*
10.2.6 Position Sensors *59*

SLAC AHO 2003-032B2f17

10.3 TRANSDUCER LISTING 59
10.4 MONITORING AND CONTROL 59

11. INTERFACES 61

11.1 SPACE 61
11.2 STRUCTURAL 61
11.3 ELECTRICAL/CONTROL 61
11.4 CRYOGENICS 61
11.5 ASSEMBLY REQUIREMENTS 62
11.6 INTEGRATED EARTHQUAKE DESIGN 62
11.7 GENERAL 62

12 ASSEMBLY, TRANSPORT AND INSTALLATION 63

A. EARTHQUAKE LOADS ON BABAR SOLENOID 64

A.1 DESIGN APPROACH 64
A.2 MAGNITUDE OF EARTHQUAKE ACCELERATIONS 64
A.3 APPLICATION OF FORCES 64
A.4 SURVIVAL 64
A.5 DAMAGE 64

B. MATERIAL PROPERTIES 65

C. BABAR EARTHQUAKE LOAD CASES: THE COLD MASS 68

C.1 THE MODEL 68
C.1.1 Finite element model 68
C.1.2 Dimensions 68
C.2 LOAD CASES 68
C.3 RESULTS 69
C.3.1 Files 70

D. EARTHQUAKE LOAD CASES; THE VACUUM VESSEL 71

D.1 THE MODEL 71
D.1.1 Load Cases 71
D.1.2 Results 71
D.1.3 Files 72

E. MANUAL CHECK OF STRESSES IN EXTERNAL SUPPORTS 73

F. BABAR COLD MASS - DETAILED ANALYSIS OF THE STRUCTURE 74

F.1 INTRODUCTION 74
F.2 THE MODEL 74
F.3 THE CALCULATIONS 74
F.4 MATERIAL PROPERTIES 74
F.5 RESULTS 75
F.6 MAGNETIC FORCES 76

G. ADDENDUM 2: CHANGES TO SUPPORTS, ETC 77

G.1. THE CHANGES TO THE REQUIREMENTS 77
G.2. CHANGES TO THE OVERALL STRESSES IN THE COLD MASS 77
G.3. CHANGES TO THE STRESSES AND DEFLECTIONS IN THE VACUUM VESSEL 77
G.4. CHANGES TO THE LOADS ON THE SUPPORTS 78
G.5. CHANGES TO THE DESIGN OF THE EXTERNAL SUPPORTS 80

SLAC AHO 2003-032B2f17

SLAC AHO 2003-032B2f17

INTRODUCTION

This report describes the engineering study of the superconducting solenoid for BABAR magnet. The actual design includes the cold mass, the cryostat with the chimney for hydraulic and electrical feedings, the current leads cryostat and the ancillary equipment. Special problems as the supporting system of the coil to the Iron Flux Return are extensively discussed. Information about the magnetic forces at the IFR are also given.

The superconducting solenoid design is based on the criteria developed in the last 15 years for the aluminum stabilized thin solenoids. The first magnet of this class can be considered CELLO, built at Saclay for Petra Collider at DESY. The common feature of these magnets consists in the use of aluminum stabilized conductors indirectly cooled. The cooling pipes are connected to the supporting structure, made by aluminum alloy. The technique developed for CELLO was subsequently improved on building several thin solenoids like CDF, TOPAZ, VENUS, AMY, ALEPH, DELPHI, CLEO-II, H1 and ZEUS, with bore up to 5 m.

Table I Main characteristics of some thin solenoids

	CDF	ZEUS	CLEO II	ALEPH	BABAR
Location	FNL	DESY	CORNEL	CERN	SLAC
Manufacturer and year of completion	Hitachi 1984	Ansaldo 1988	Oxford 1987	SACLAY 1986	? 1997
Central Field (T)	1.5	1.8	1.5	1.5	1.5
Inner Bore (m)	2.86	1.85	2.88	4.96	3.01
Length (m)	5	2.5	3.48	7	3.47
Stored Energy (MJ)	30	12.5	25	137	27
Current (A)	5000	5000	3300	5000	6830
Total weight (t)	11	2.5	7.0	60	7.0
Radiation Length	0.85	0.9	-	1.6	1.4 max
Conductor overall dimensions (mm)	3.89 x 20	4.3 x 15 5.56 x 15	5 x 16	3.6 x 35	3.2 x 32 5.8 x 32
Overall Current density A/mm^2	64	78 60	42	40	67 37

SLAC AHO 2003-032B2f17

Table I shows the main characteristics of some of these solenoids compared with the ones of BABAR solenoid. At the present time the huge superconducting magnets for LHC detectors, ATLAS and CMS are being developed starting from the same technology we are using for the design of the BABAR solenoid.

A special remark must be given to the conductors used for these magnets, made by a flat Rutherford cable of NbTi/Cu immersed in a pure aluminum matrix. The coupling of the Rutherford to the matrix is usually obtained through a co-extrusion process. The large Al matrix allows both an adequate protection in case of quenching and a good stability margin with respect thermal disturbances.

SLAC AHO 2003-032B2f17

CHAPTER 1

1. OVERVIEW OF THE SOLENOID

1.1 REQUIREMENTS

The present design is related to a superconducting solenoid to be used in the BABAR detector. The required central magnetic field is 1.5 T. The field uniformity in the tracking chamber must be maximum ±2 %. The chamber extends axially up to 1483 mm and radially up to 800 mm. The solenoid has to be transparent to radiation; the nuclear interaction length should be limited to 0.4 λ_{int}. The allowable space for the cryostat is limited from a radius of 1380 mm to 1730 mm. The cryostat maximum length is 3850 mm. In designing the solenoid, the segmented flux return and the end doors shields must be considered for their effects on field, field uniformity and offset forces on the solenoid.

1.2 COLD MASS

The cold mass at the operating temperature of 4.5 K is composed of the winding supported by an outer Al alloy cylinder and the supporting system to the vacuum chamber. The winding is made by a flat superconducting cable composed of 20 multifilamentary NbTi/Cu wires. The cable is stabilized by cladding it in a pure aluminum (99.998) matrix. The conductor is insulated by a fiber-glass tape. The winding is directly wound (740 turns) inside the supporting cylinder and impregnated using two components epoxy-resin under vacuum. In order to obtain the required field uniformity, the current density at the solenoid end is designed to be higher than in the central portion. This is made by using two different conductors: thinner at the sides (3.6 mm) and thicker in the center (6.2 mm). The operating current is 6830 A. The peak field at the winding is 2.5 T.

1.3 CRYOSTAT

The function of the cryostat is to maintain the environment for the cold mass. It consist of a tubular vacuum vessel containing the cold mass at 4.5 K and a set of radiation shields kept at 80K by

SLAC AHO 2003-032B2f17

circulating coolant through pipes connected to the shields. The cryostat is supported to the IFR using support brackets, which take vertical, radial and axial loads

1.4 COOLING

The cold mass will be indirectly cooled by circulation of two-phases helium in circuits attached to the cold mass support cylinder. A thermosyphon process is proposed as the coolant driver.

SLAC AHO 2003-032B2f17

1.5 SUMMARY OF MAJOR DESIGN PARAMETERS

Coil mean conductor radius	Warm Cold	1505mm 1498.5mm
Coil length (conductors only)	Warm Cold	3470mm 3455mm
Field	Central Peak	1.5T 2.5T
Number of turns	Central region Side regions (each) Total	310 215 740
Design current		6833 A
Conductor size	Central portion Ends	32 x 5.8 mm^2 (bare) 32.4 x 6.2 mm^2 (insulated) 32 x 3.2 mm^2 (bare) 32.4 x 3.6 mm^2 (insulated)
Cryostat limiting dimensions (including maximum tolerances)	Internal radius External radius length excluding support brackets	1380mm 1730mm 3850mm
Cryostat nominal dimensions	Internal radius External radius length excluding support brackets	1390mm 1720mm 3848mm
Mass	Solenoid Radiation shields Vacuum vessel Total inc. misc items	7300kg 1000kg 5200kg 13500kg
Earthquake design loads	Vertical Horizontal	2g 1.2g
Magnetic forces on solenoid	Geometric offset Alignment errors	10t axial 20t (2cm errors)
Supports - external	Vertical Radial Axial	Four positions on horizontal center plane, shared with inner detectors Ditto Four positions each end, each acts in one direction only. Inner detectors supported from coil end flange
Supports - internal	Radial+vertical Axial	8 tie-rods, four each end 6 tie-rods one end

SLAC AHO 2003-032B2f17

SLAC AHO 2003-032B2f17

CHAPTER 2

2. MAGNETIC DESIGN

2.1 THE MODEL

The magnetic analysis is based on the 2D model shown in Fig. 2.1 The model includes:

1. The solenoid;
2. The laminated barrel and end caps flux return , composed each by 20 steel plates of different thickness;
3. The Q2 shield in the forward end door (see Fig.2.2);
4. An iron shield in the backward end door, (see Fig.2.3);

The model also includes a gap of 150mm between barrel and end caps.
The backward shield is designed to accommodate a DIRC detector, which is supported by two steel rings, which are also included in the model. The main role of the backward shield is to symmetrize the magnetic field , to balance the magnetic force on the solenoid due to the Q2 shield and to improve the field uniformity in the backward region of the tracking chamber. With respect to the real magnet, having hexagonal structure, the main magnetic analysis was carried out for the plane intersecting the hexagon at the center of two opposite sides. A 3 D analysis for a simplified model was also carried out.
The computations were carried out using a 2D magnetic element of ANSYS code (version ANSYS 50 a) , implemented on a Digital ALPHA-VAX and on HP730 stations.
The magnetic steel properties used for computation are in agreement with HOT ROLLED CARBON STEEL having the magnetic properties shown in Fig. 2.4, also called in the present design *US Mild Steel* . In order to study the effect due to the use of not homogeneous steel, some element of the IFR was also considered to be made by *Russian steel* (See fig.2.4 for the BH curve) , as explained later.
The mesh for the magnetic analysis, shown in Fig.2.5, was suited in order not to exceed 15000 plane elements, so that acceptable CPU time was required for calculations. This approach allowed the study of several magnetic configurations leading to an optimization of the field homogeneity.
The coil is meshed into 60 elements of rectangular shape. The radial thickness is 1 cm, in order to reproduce the thickness of the Rutherford cable. The coil axial length is the cold length, i.e. the length at

SLAC AHO 2003-032B2f17

4.5 K. The solenoid radius also is considered at 4.5 K. The axial dimensions of the mesh elements are 6.38 cm for the central region and 5.13 cm for the two end regions.

2.2 CENTRAL FIELD AND UNIFORMITY

The aim of the magnetic design was to obtain a magnetic field of 1.5T with uniformity ±2% in the tracking region. This region approximately covers the axial range from -1483 mm backward to +1287 mm forward, with respect the magnetic center; the radial limit is 800mm. Fig. 2.6 shows the details of this region. The uniformity is obtained by grading the current density of the solenoid in three regions. A central region covering ±961 mm including 310 turns and two end regions of length 774mm including 215 turns each. The current density in the end regions is 1.7 times that one of the central part. The magnetic field of 1.5T is obtained by powering the solenoid with a current of 6833 A, the total ampere-turns are 5.0564 10^6. The three sections of the magnet are connected electrically in series. Table 2.1 summarizes the main characteristic of the solenoid.

Fig. 2.7 shows the graph of the field lines over the full detector region. Fig 2.8. shows the field uniformity in the central region defined by 0.225 m<r <0.80 m and -1483mm < z <1275 mm.. The target uniformity of ±2% is obtained in the whole region of interest except at the backward edge, where the uniformity decreases to a minimum of - 3%. In the forward direction a better field uniformity is obtained due to the symmetry.

Generally speaking a better field uniformity could be obtained by reducing the axial length of the two end regions. Nevertheless this causes an increase of the current to generate the same field with a consequent reduction of the stability against thermal disturbance. For the initial design we assumed, as maximum current density in the conductor, the maximum value used up to now for the magnets of this kind, i.e. ≈ 80 A/mm^2 (ZEUS magnet). Using a conductor of cross section ≈ 90 mm^2 , the maximum current results to be ≈ 7000 A. The present design can be considered a compromise between the opposite requirements coming from field uniformity and stability. The chosen operating current of 6833 A gives a current density in the conductor of 66 A/mm^2, which can be considered an upper limit. An increase of the current would cause the coil to be spliced into two layers .

SLAC AHO 2003-032B2f17

Table 2.1 Overall coil parameters

Central Induction	1.5T
Conductor peak field	2.5T
Uniformity in the tracking region (r< 800mm -1483 mm < z < 1287 mm)	± 2% (3% at the backward edge)
Winding Length	3470 mm *warm* 3455 mm *cold*
Winding mean radius	1505 mm *warm* 1498.5 mm *cold*
Amp turns	5.0564 10^6
Operating current	6833 A
Inductance	1.15 H
Stored Energy	27 MJoule
The coil is made by two conductors forming 3 regions with different current density: 1 Central region: length Number of turns 2 Side regions: length Number of turns	 1922 mm *warm* 1913.63 mm *cold* 310 770.56mm *cold* 774 mm *warm* 215
Total turns	740
Total length of conductor	6998 m

An interesting feature is that, in spite of the iron a-symmetry, the magnetic field is very close to being symmetric so that a residual net force of only 90 kN is applied directed backward. This fact must be

SLAC AHO 2003-032B2f17

considered in trying adjustment of the geometry leading to an improved field uniformity. As an example, Fig. 2.9 shows the field uniformity obtained by moving the end plug of 40 mm inward. The better uniformity is compensated by the a growth of the net forces on the solenoid from 90 to 220 kN.

2.3 PEAK FIELD AT THE SOLENOID

As described in section 2.1 the solenoid was modeled in form of a thin cylinder of radial thickness 1 cm. The real situation is quite different because the current is shared by 740 turns and flows in the Rutherford conductors, which have a radial thickness of 11 mm and axial thickness of 1.42 mm. In order to evaluate the peak field at the solenoid the real current distribution must be taken into account. The peak fields occur at the two opposite axial ends of the solenoid in the higher current density regions. We have replaced a small part of one of this region, for an axial length of 36 mm, with 10 smaller zones having the dimensions of the Rutherford cable. Fig. 2.10 shows the variation from the usual to the improved solenoid model. This allows to take into account, for the conductors at the solenoid end, both the field and the self field. The peak field is just applied at the last conductor (at the solenoid end) and has a value of 2.35 T. In the present design we will consider , for safety reasons, a peak field slightly higher, i.e. 2.50 T.

2.4 MAGNETIC FORCES AT THE SOLENOID

Axial and radial magnetic forces are applied to the solenoid as shown in fig. 2.11, where the forces at each element of mesh are displayed as arrows.. The general characteristics of these forces are:

1- The radial forces are higher at the end regions than at the central region

2- The axial forces are inward directed for the end regions and outward directed for the central region

The radial pressure as function of the axial position is shown in fig. 2.12. The pressure applied to the central region, with lower current density, is quite independent on position and equal to 0.85 MPa. The pressure at the end regions is much higher, ranging from 1.15 MPa to 1.52 MPa. There is a strong gradient of the radial pressure at the interface between higher and lower current density regions. The pressure falls from 1.52 MPa to 0.86 MPa in few millimeters. In the stress analysis these two zones will be studied more carefully.

Fig. 2.13 shows the axial forces at each element of the mesh as function of the position of the elements. The force is substantially compressive for the end regions as also displayed by fig. 2.11. An important parameter is the maximum axial force applied at a single element. From Fig. 2.13 this force is 1.3 MN, applied to the end elements of the end regions. In performing shear stress calculation , this force must

SLAC AHO 2003-032B2f17

be taken into consideration. The integral force as function of the position is shown in fig. 2.14. The total compressive force at each end region is 4.8 MN, while the outward directed force at half central region is 1.6 MN, so that the coil is compressed with a total force of 3.2 MN.

2.5 MISALIGNMENT IN THE IFR

As already mentioned, due to the IFR a-symmetry, the total axial force at the solenoid is not zero but there is a net force of 90 kN backward directed. Due to the non-linearity of the B-H curve, the net force strength and direction depends on the field: at half the field (B=0.75 T) the net force on the solenoid is 35 kN forward directed. We have studied what are the consequences on the offset force at the nominal field due to misalignment of the coil in the IFR or to the variation of position of some elements of the IFR. We performed several exercises as following:

1) The first exercise was made moving the solenoid with respect to the IFR of 20 mm in the backward direction. The net axial force changed from 90 to 300 kN, so that we have the information that the axial misalignment causes a force of 10.5 kN/mm.
2) The second exercise consisted in removing the inner plate of the backward end cap. The calculated axial force at the solenoid changed of 200 kN, (From 90 backward directed to 190 forward directed). The information coming from this result is that changes in the IFR as big as expected (plate mispositioning) do not cause the solenoid to suffer for high loads (being of course adequately supported).
3) The third exercise was to move axially the backward end plug. Apart the effect on the field uniformity, the result on the axial force is 3.3 kN per mm of the end plug displacement. The force at the solenoid is backward directed moving inward or forward directed moving outward. The consequence of this calculation is that a movement of the backward plug outward of 28 mm reduces to zero the net force at the solenoid. Generally speaking the backward plug can be used to trim the magnetic force due to misalignment of the coil or to IFR a-symmetry caused by plate mispositioning.
4) We studied the effect of changing the magnetic properties of the iron. A big change in the net axial force was expected by using two different steels for the end caps. We performed a calculation using *US mild steel* (the usual steel used in the present design) for the forward end cap (Q2 shield included) and *Russian steel* (see Fig. 2.4) for the backward end cap. The observed change in the axial force was few kN. In order to take into account the non-linear effect of the iron, this computation was also made at half the nominal current (i.e. at 3400 A). We found a force of 40 kN

SLAC AHO 2003-032B2f17

forward directed, i.e. a change of 130 KN with respect the force at the nominal current. A result very similar to the one obtained when using only one steel for both the doors . A little worst field uniformity was also observed. Though this result would not encourage the use of whatever steel for the IFR, we have the important information that IFR elements of not homogeneous steel, do not cause *catastrophic* loads at the solenoid.

5) As last exercise we changed the gap distance between the plates of the backward end caps from 30 to 33 mm (Fig. 2.15). This was made in order to give a tolerance on the space reserved for the RPC detectors. The offset force on the solenoid changed from 90 to 30 kN, with no effect on the field uniformity at the tracking chamber.

After analyzing the net axial force, we studied the effect of radial displacement of the solenoid with respect to the IFR. A correct study of this effect would require the use of a 3D code. Nevertheless important information can be drawn from a 2D analysis. We calculated the total radial force applied at a solenoid with the same axial dimension and Ampere-turns, but with a mean radius of 20 mm higher than the real solenoid. Gluing together half solenoid of the real case and the solenoid with higher radius, we obtain a fictitious solenoid radially moved 10 mm with respect the original one. Looking at the total radial force of this fictitious solenoid we obtained 100 kN outward directed so that we have a force per unit displacement of 10 kN/mm.

These exercises were used to determine the maximum mechanical loads, which can be applied at the solenoid, in relation to the tolerances of the coil and IFR positioning.

2.6 FORCES AT THE IFR

The magnetic analysis, required for the solenoid design, was made using the IFR geometry under design, as already pointed out in section 2.1. As consequence of this approach, the complete force configuration at the IFR was available as shown in fig. 2.16 for the whole IFR and fig. 2.17 and 2.18 for the end caps.

SLAC AHO 2003-032B2f17

Table 2.1 Magnetic Forces at the backward end cap

Element	Axial force (kN)	Radial force (kN)
End Plug	- 1568	+512
DIRC support inner ring	- 274	+245
DIRC support outer ring	-284	+412
I plate (the inner)	-519	-118
II	-352	-29
III	-264	-29
IV	-206	-29
V	-157	-39
VI	-108	-39
VII	-69	-49
VIII	-39	-59
IX	-10	-59
X	+10	-59
XI	+20	-59
XII	+39	-108
XIII	+39	-98
XIV	+29	-78
XV	+29	-69
XVI	+20	-49
XVII	+20	-39
XVIII	+20	-69
IX	+20	-59
XX	+10	-49

The forces at each elements of the IFR are also listed in Table 2.1, 2.2 and 2.3 , where the values, are given over 2 p. The sign minus (-) means that the force (axial or radial) is directed from outer the magnet toward the inner.

SLAC AHO 2003-032B2f17

Table 2.2 Magnetic forces at the Forward end cap

Element	Axial force (kN)	Radial force (kN)
Q2 shield I shield II shield III shield	 - 1372 -29 -10	 +? (*) + 88 +$
I	-617	?
II	-392	?
III	-304	?
IV	-235	?
V	-176	?
VI	-127	?
VII	-88	?
VIII	-69	?
IX	-49	?
X	-29	?
XI	-20	?
XII	-20	?
XIII	-20	?
XIV	-10	?
XV	-10	?
XVI	-5	?
XVII	-6	?
XVIII	-5	?
IX	-3	?
XX	-4	?

(*) The radial force between the first Q2 shield and the forward plates can not be known because there is no air gap between them. For the model used, the first Q2 shield and forward plates constitute a single element. However an indication of the force can be obtained looking at the force between backward plates and backward end plug.

SLAC AHO 2003-032B2f17

Table 2.3 Magnetic forces at the barrel

Element	Axial force (kN)	Radial force (kN)
I	-3	-402
II	-2	-314
III	-2	-235
IV	-2	-176
V	-2	-137
VI	-2	-98
VII	-2	-69
VIII	-2	-49
IX	-2	-39
X	-2	-20
XI	-1	-5
XII	-1	-29
XIII	-1	-4
XIV	-2	-4
XV	-2	+5
XVI	-2	+6
XVII	-2	+7
XVIII	-2	+8
IX	-3	+29
XX	-2	+245

SLAC AHO 2003-032B2f17

2.7 COMPARISON WITH OTHER CODES

In order to have a confirmation of the results obtained by using ANSYS code , we carried out a magnetic analysis on a simplified 2D model of the BABAR magnet. The model is shown in fig. 2.19 . The same model was used to perform magnetic field calculation using PE2D at LLNL. The results obtained by ANSYS and PE2D are shown respectively in fig. 2.20.a and 2.20.b for the field in the drift chamber. The absolute field at the center of the solenoid is 1.5274 as given by PE2D and 1.5209 by ANSYS. The field uniformity in the drift chamber region is quite the same. As conclusion we can say that the results obtained by ANSYS code, and discussed in the present technical design, are confirmed by this comparison test.

2.8 3 D MAGNETIC ANALYSIS

The IFR has hexagonal structure. A more realistic magnetic analysis should be carried out using a complete 3D model. Nevertheless a 3D model containing all the elements of the IFR (60 plates and the shields) would be a very hard task. We tried a different approach by using a simplified 3D model, which is shown in fig.2.21. The used symmetry is 1/2. The main difference with respect the 2D model is that the barrel and the end caps are modeled as 3 single pieces with averaged and anisotropic magnetic properties. This simple model allows to evaluate the effect on field uniformity due to the hexagonal shape and the forces on the solenoid due to non-symmetric iron distribution (as the lack in the backward end cap for leaving the space to the chimney).

When calculating the field uniformity in the plane normal to Z axis at Z=-1400 mm, i.e. at the backward border of the drift chamber., where we have more effect of the IFR geometry, we found that the field variation due to the hexagon shape is less than 0.15 %, so that we can conclude that the 2D analysis is substantially correct.

Presently we have not still ready the calculation of the effect of the lack of iron due to the chimney. Nevertheless a preliminary evaluation seems to show that an axial magnetic load of 90 KN, applied to the solenoid in the forward direction, and a vertical load of 30 KN, downward directed, take place.

SLAC AHO 2003-032B2f17

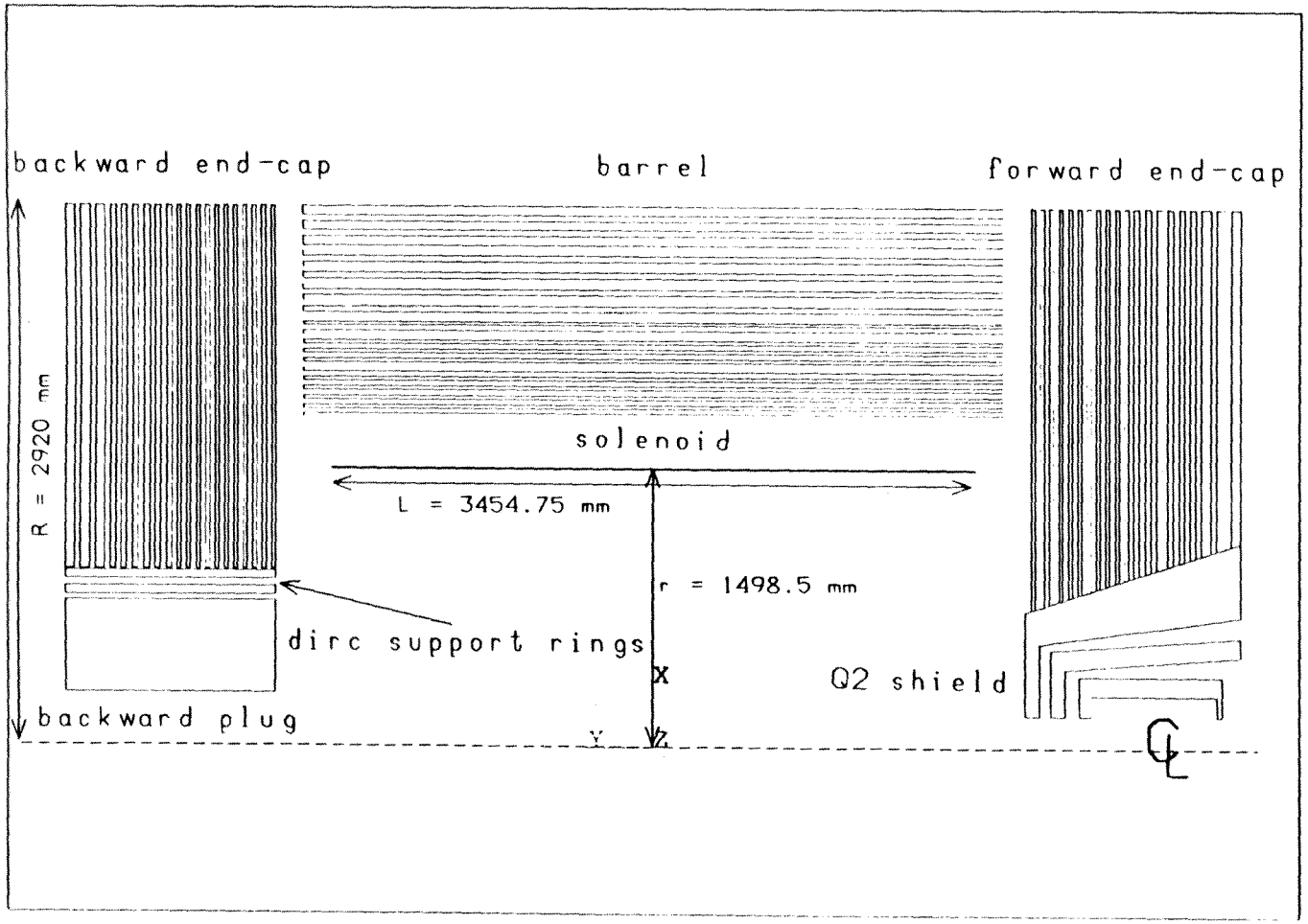

ANSYS 5.0 A
MAY 26 1995
15:44:58
PLOT NO. 1
AREAS
TYPE NUM

ZV =1
DIST=2.441
XF =1.548
A-ZM=90
EDGE

Fig. 2.1: BaBar magnet model

SLAC AHO 2003-032B2f17

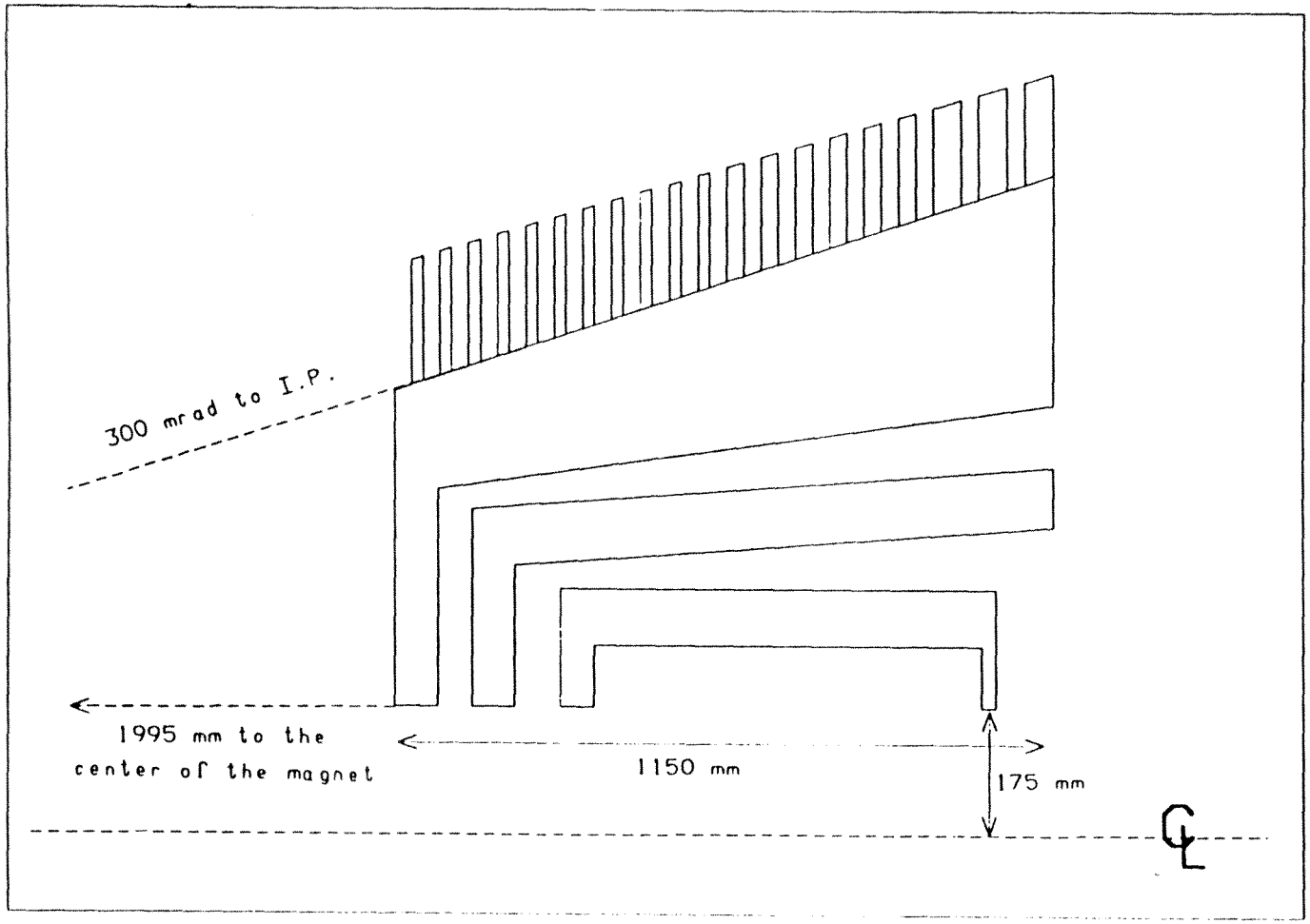

ANSYS 5.0 A
MAY 26 1995
16:48:24
PLOT NO. 1
ELEMENTS
TYPE NUM

ZV =1
*DIST=0.796742
*XF =0.606742
*YF =-2.451
A-ZM=90
EDGE

AREAS
TYPE NUM

ZV =1
*DIST=0.796742
*XF =0.606742
*YF =-2.451
A-ZM=90
EDGE

Fig. 2.2: Forward end-door

SLAC AHO 2003-032B2f17

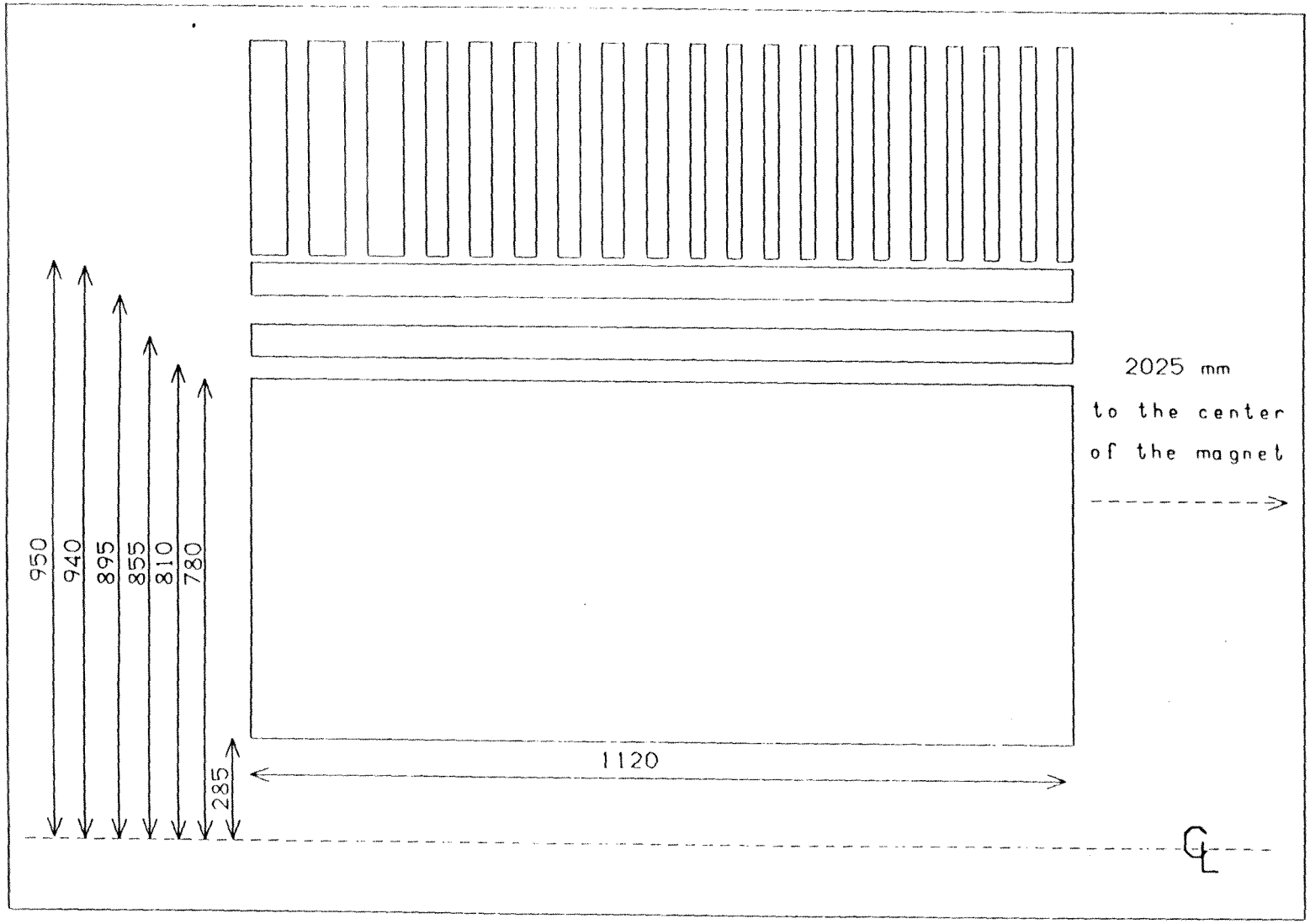

Fig. 2.3: Backward end-door

SLAC AHO 2003-032B2f17

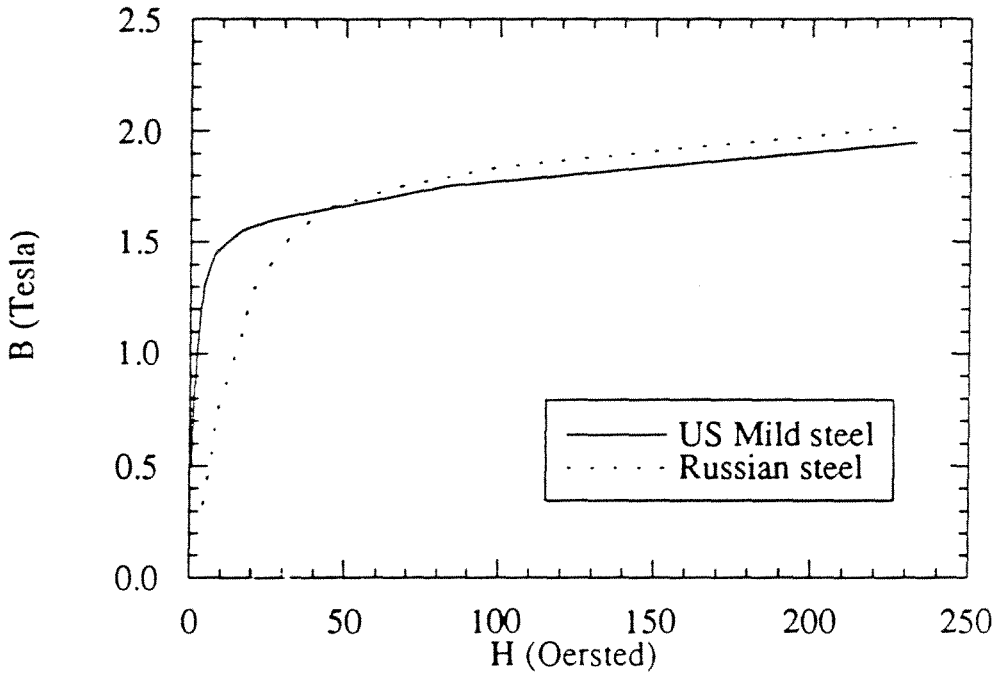

Fig. 2.4 Magnetic properties of irons used in the magnetic analysis

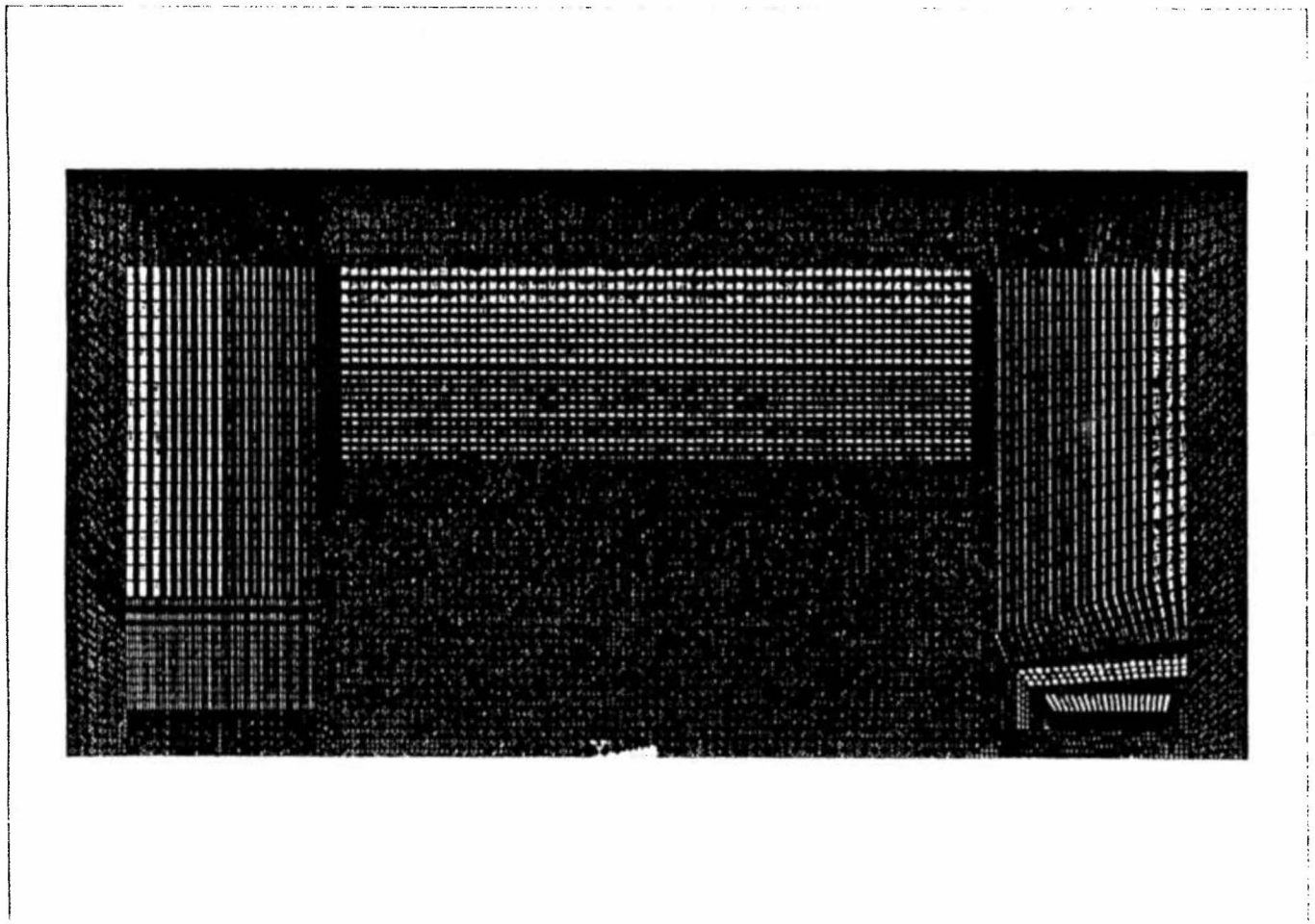

Fig. 2.5: Meshed model

SLAC AHO 2003-032B2f17

ANSYS 5.0 A
MAY 3 1995
13:09:46
PLOT NO. 1
AREAS
TYPE NUM

ZV =1
DIST=1.075
XF =0.5125
YF =0.098
A-ZM=90
EDGE

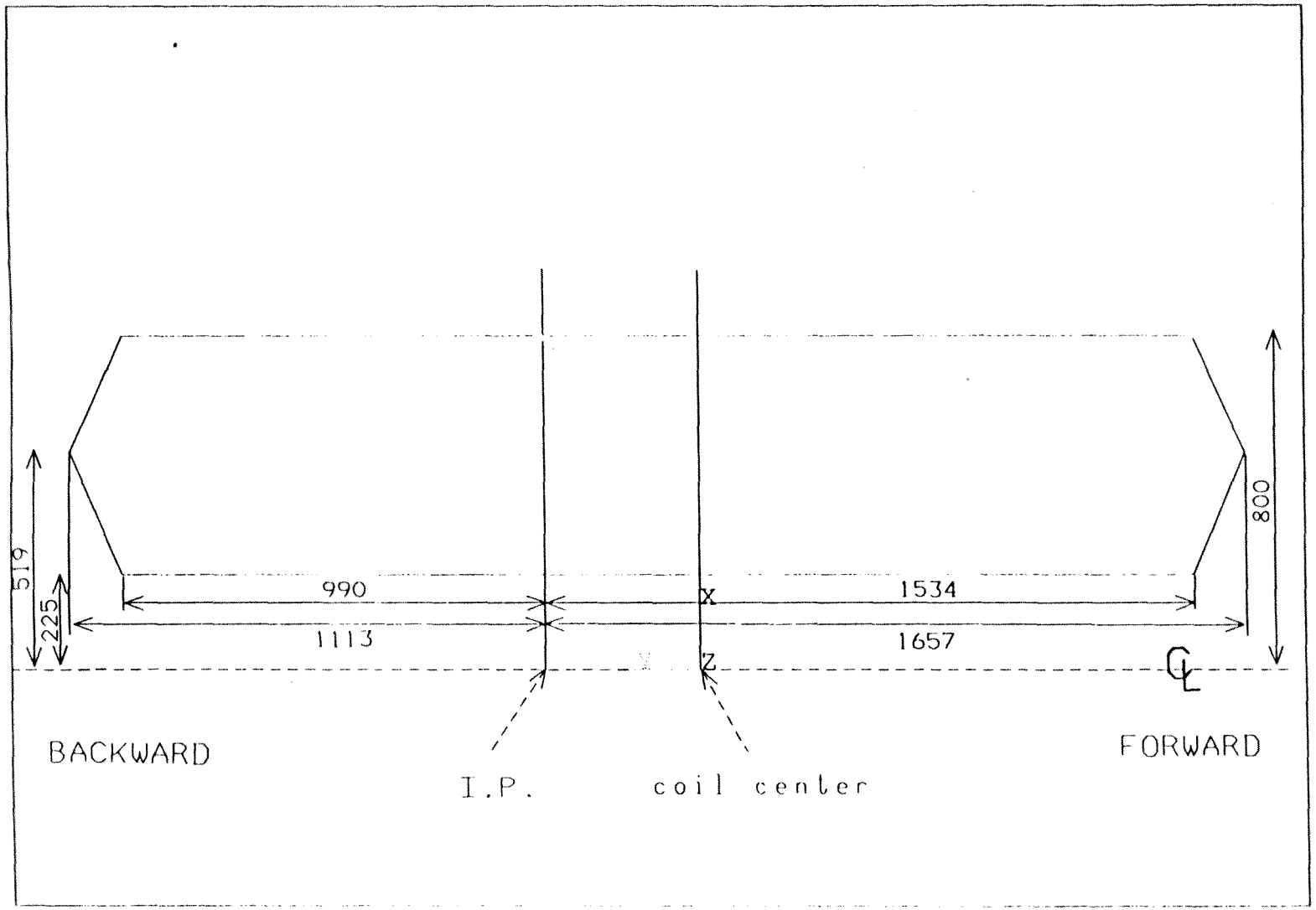

Fig. 2.6: Drift chamber

SLAC AHO 2003-032B2f17

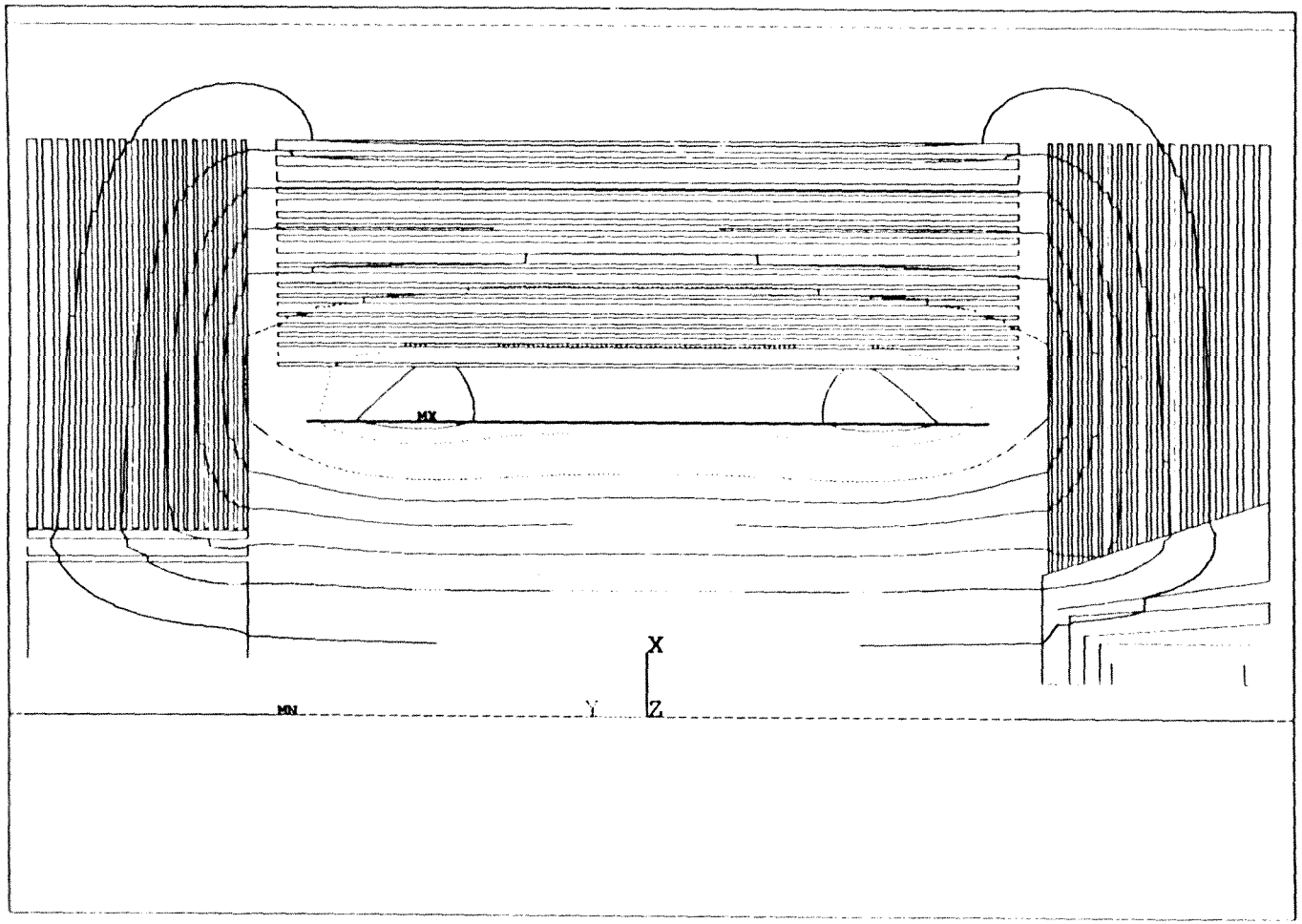

ANSYS 5.0 A
MAY 26 1995
13:30:24
PLOT NO. 1
NODAL SOLUTION
STEP=2
SUB =1
TIME=2
R*AZ
RSYS=0
SMX =1.855
A =0.10307
B =0.309211
C =0.515351
D =0.721492
E =0.927632
F =1.134
G =1.340
I =1.752

AREAS
TYPE NUM

ZV =1
*DIST=2.298
*XF =1.292
*YF =-0.011016
A-ZM=90
EDGE

Fig. 2.7: Potential vector lines

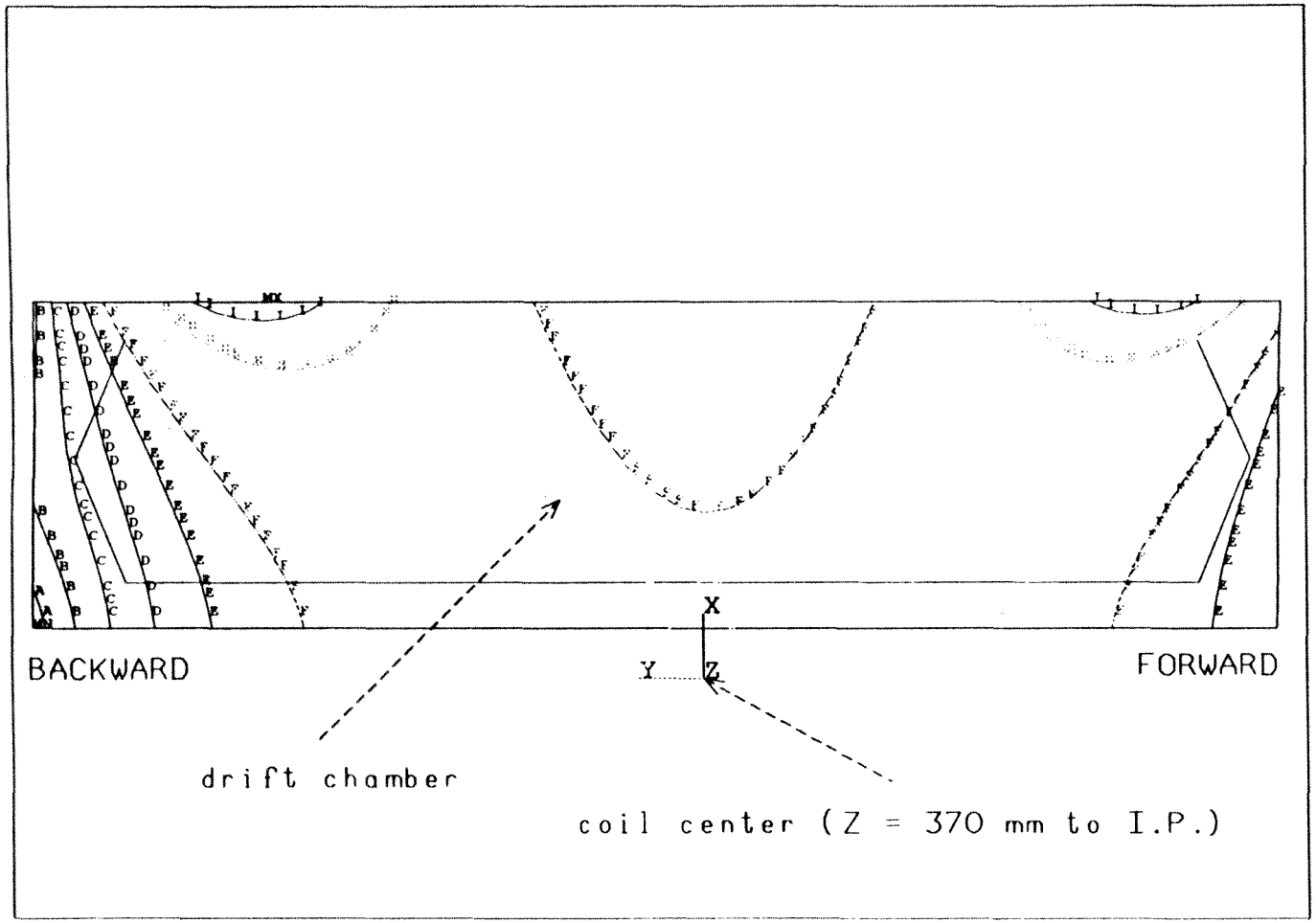

ANSYS 5.0 A
MAY 26 1995
12:11:40
PLOT NO. 1
NODAL SOLUTION
STEP=2
SUB =1
TIME=2
B0 = 1.4995 T
Bmn = 1.397 T
Bmx = 1.561 T
A = -6.2%
B = -5.0%
C = -3.8%
D = -2.6%
E = -1.4%
F = -0.2%

G = +2.2%
I = +3.5%

AREAS
TYPE NUM

ZV =1
*DIST=1.076
*XF =0.509128
*YF =0.105557
A-ZM=90
EDGE

Fig. 2.8: Field uniformity in the drift chamber

SLAC AHO 2003-032B2f17

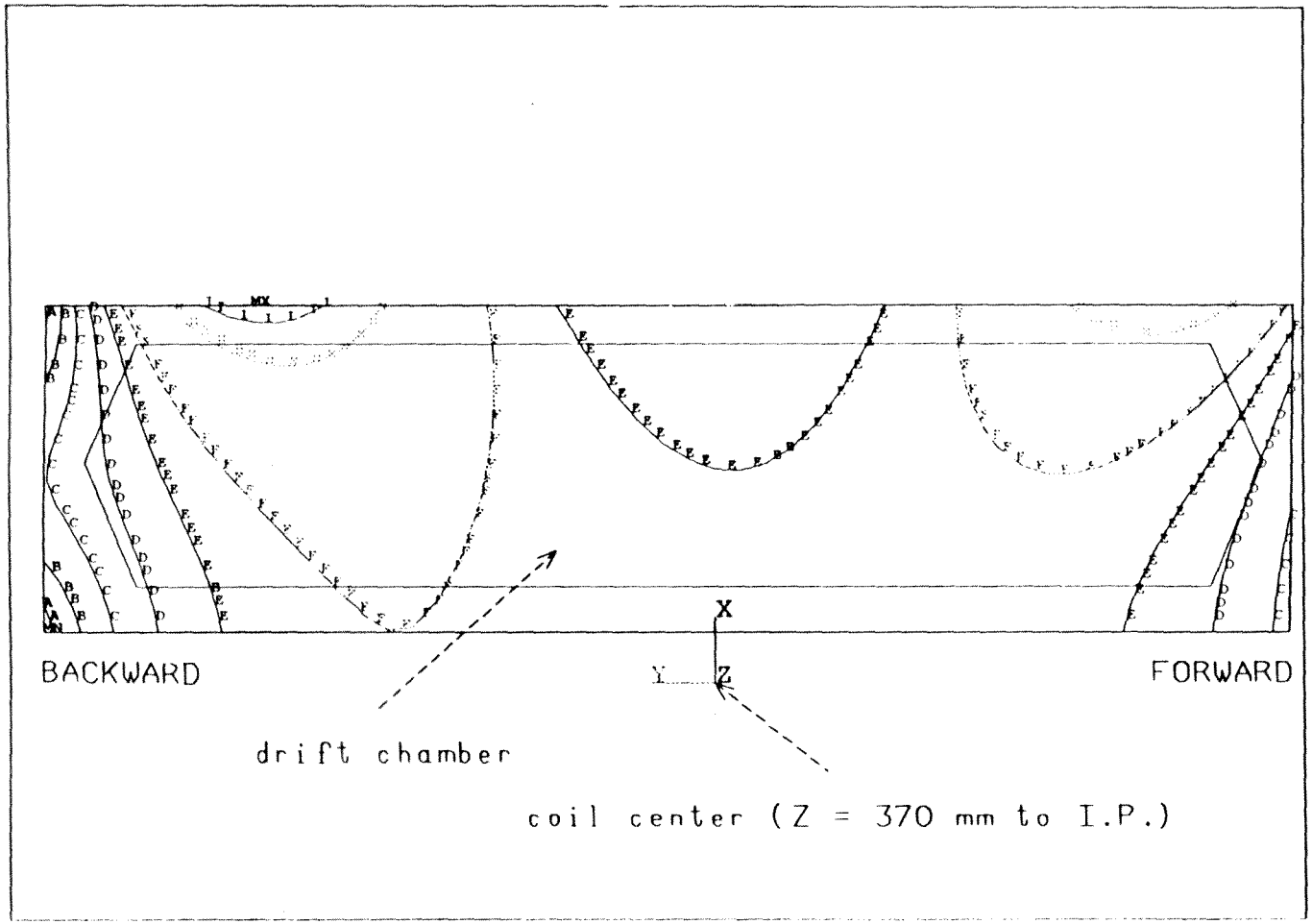

ANSYS 5.0 A
MAY 31 1995
10:35:45
PLOT NO. 1
NODAL SOLUTION
STEP=2
SUB =1
TIME=2
B0 = 1.5028 T
Bmn = 1.428 T
Bmx = 1.568 T
A = -4.4%
B = -3.4%
C = -2.4%
D = -1/3%
E = -0.3%
F = +0.7%
G = +2.8%
I = +3.9%

AREAS
TYPE NUM

ZV =1
*DIST=1.074
*XF =0.516071
*YF =0.141291
A-ZM=90
EDGE

Fig. 2.9: Field uniformity with backward plug shifted of 4 cm inward

SLAC AHO 2003-032B2f17

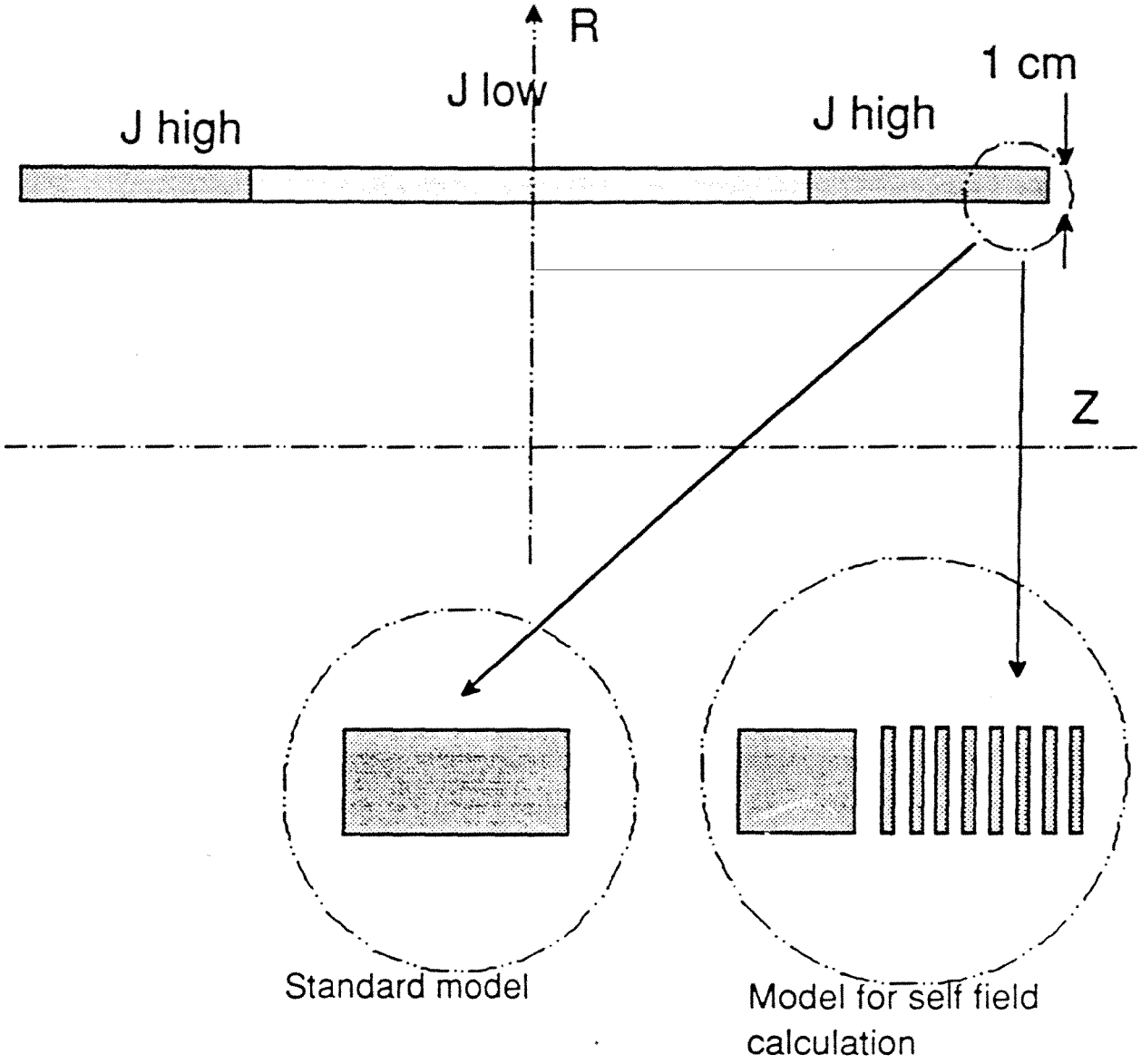

Fig.2.10 Model of solenoid for magnetic analysis

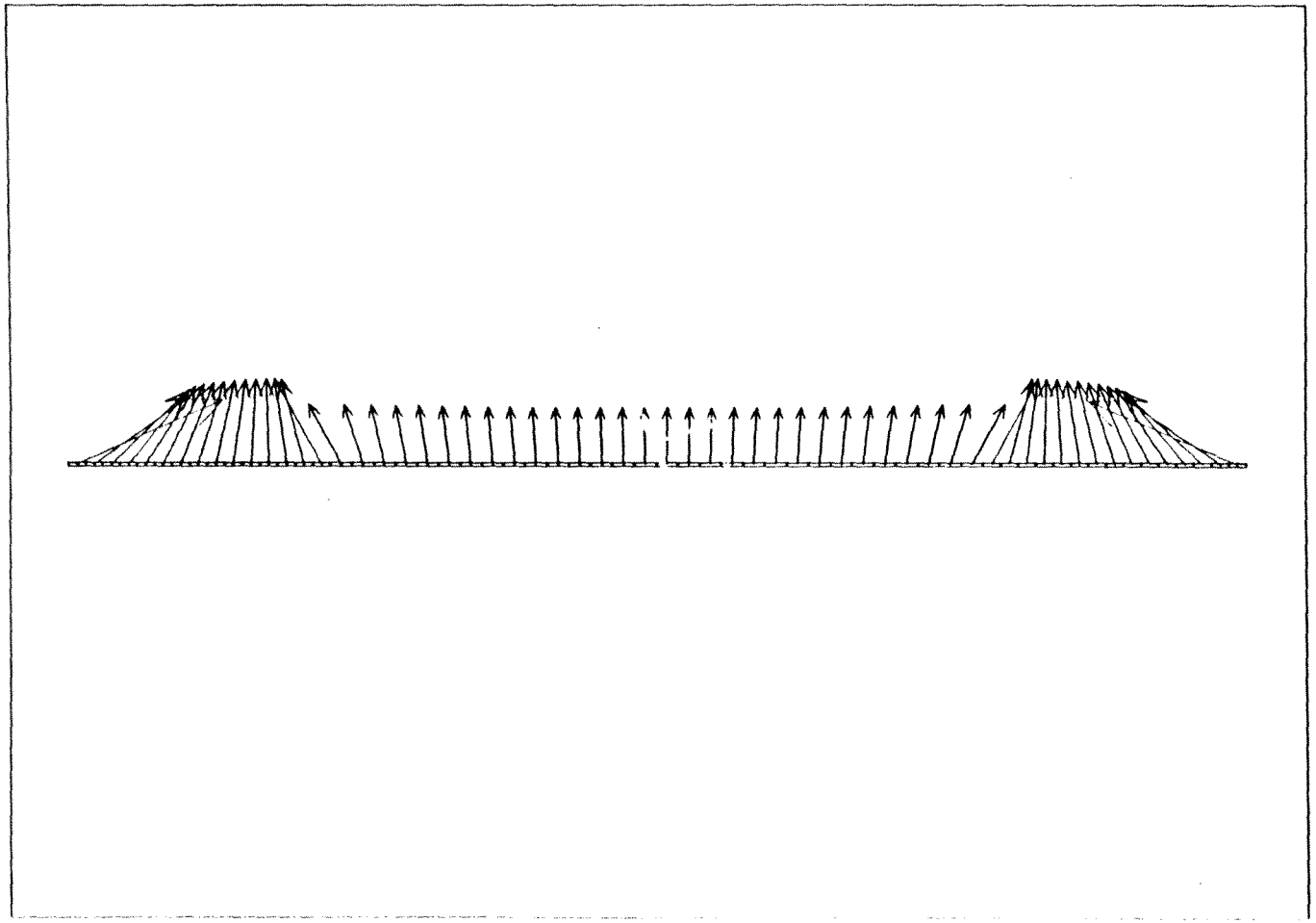

ANSYS 5.0 A
MAY 26 1995
16:02:12
PLOT NO. 1
VECTOR
STEP=2
SUB =1
TIME=2
FMAG
ELEM=46
MIN=484155
MAX=0.140E+07

484155
599015
713874
828734
943594
0.106E+07

0.125E+07
0.140E+07

Fig. 2.11: Forces on the coils

SLAC AHO 2003-032B2f17

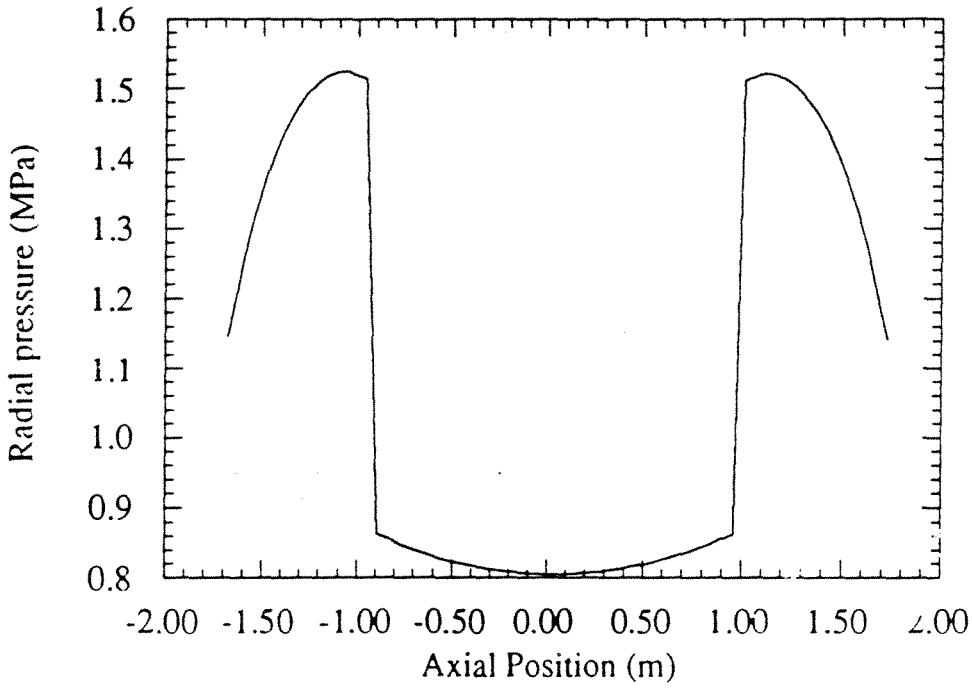

Fig 2.12 Radial magnetic pressure vs the axial position

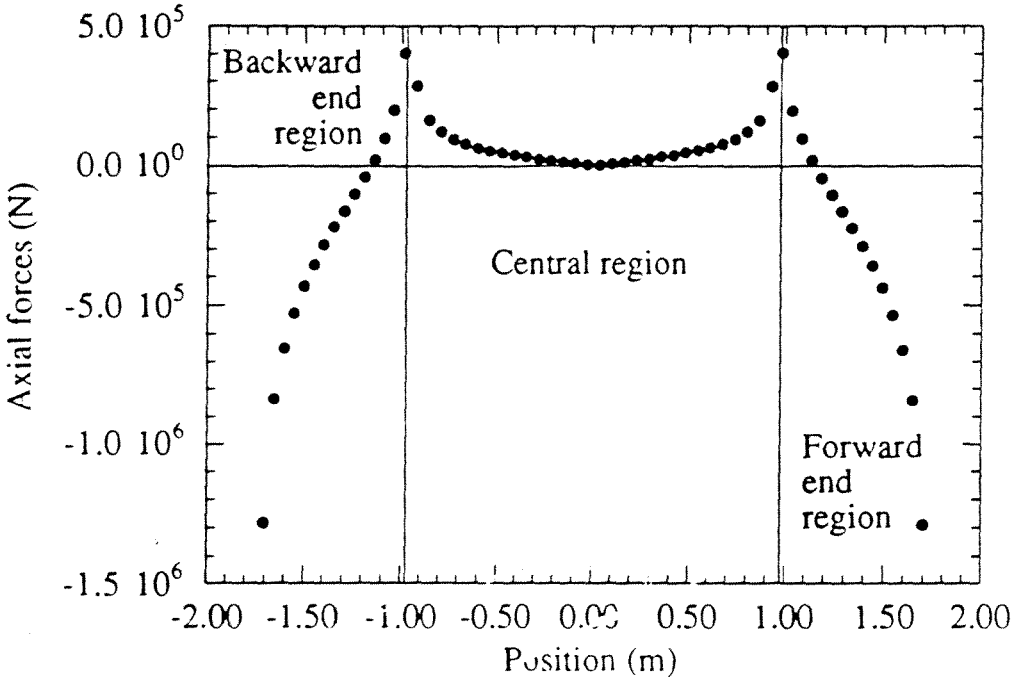

Fig. 2.13 Axial magnetic forces at the coil elements of the mesh

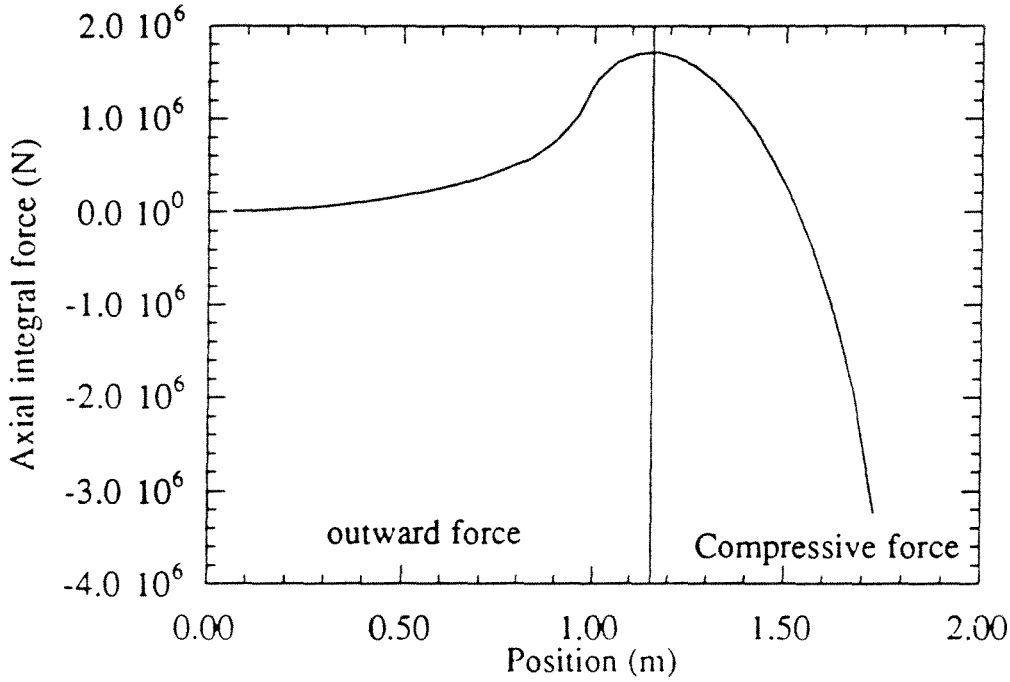

Fig.2.14 Integral axial force vs the axial position

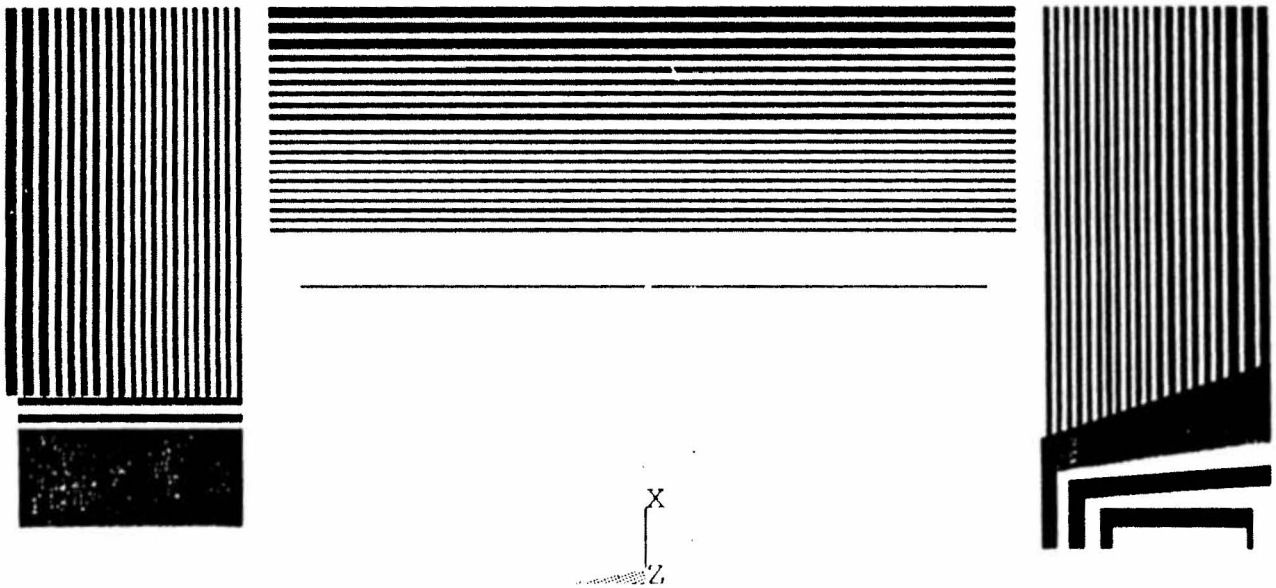

ANSYS 5.0 A
MAY 31 1995
15:12:58
PLOT NO. 1
AREAS
MAT NUM

ZV =1
DIST=3.85
XF =1.75
A-ZM=90
CENTROID HIDDEN

plates of 33 mm

SLAC AHO 2003-032B2f17

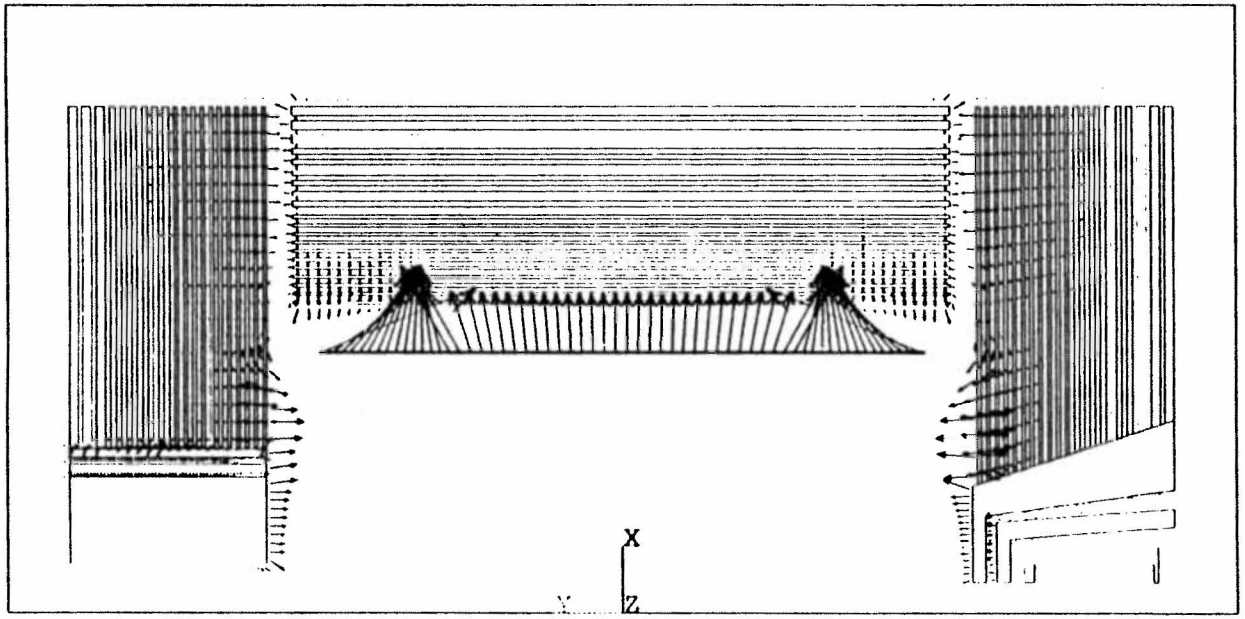

ANSYS 5.0 A
MAY 31 1995
11:40:50
PLOT NO. 1
VECTOR
STEP=2
SUB =1
TIME=2
FMAG
ELEM=46
MIN=0.228E-03
MAX=0.140E+07

0.228E-03
175379
350758
526137
701517
876896

0.140E+07

AREAS
TYPE NUM

ZV =1
DIST=3.85
XF =1.75
A-ZM=90
EDGE

Fig. 2.16: Magnetic forces

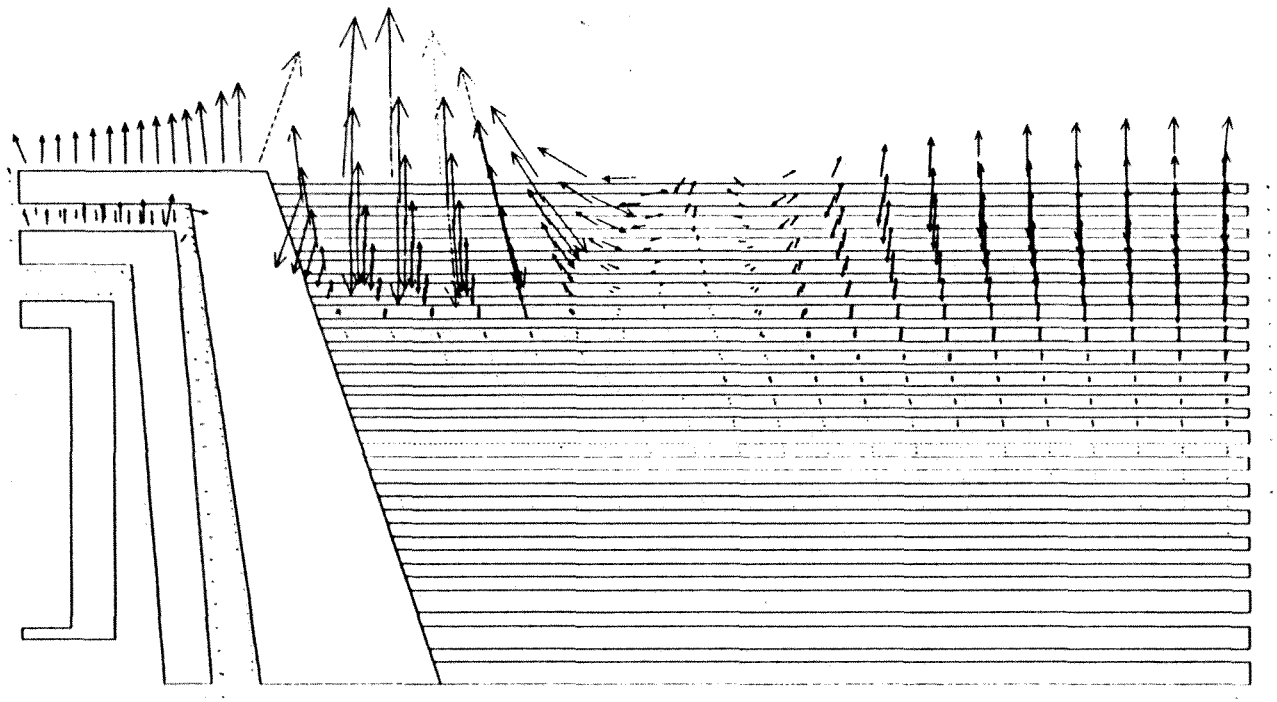

Fig. 2.18: Detail of magnetic force at the forward end-door

SLAC AHO 2003-032B2f17

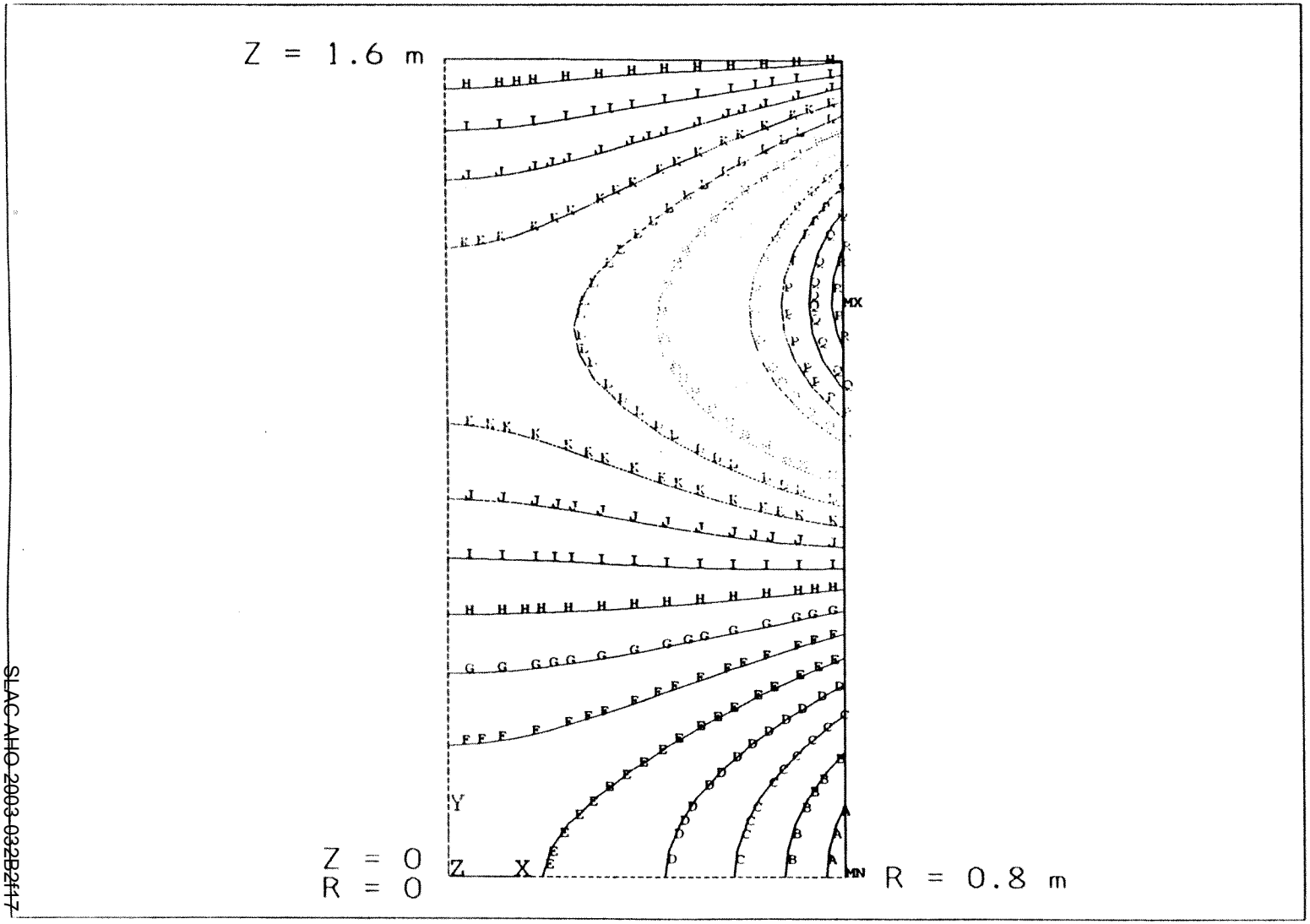

ANSYS 5.0 A
MAY 31 1995
16:29:13
PLOT NO. 1
NODAL SOLUTION
STEP=2
SUB =1
TIME=2
B0 = 1.5258 T
Bmn = 1.49 T
Bmx = 1.626 T
A = -2.1%
B = -1.6%
C = -1.1%
D = -0.6%
E = -0.0%
F = +0.4%
G = +0.9%
H = +1.4%
I = +1.8%
J = +2.4%
K = +2.9%
L = +3.4%
[illegible]
O = +4.9%
P = +5.4%
Q = +5.8%
R = +6.4%

Fig. 2.20: Field uniformity in the drift chamber obtained by simplified 2D model

SLAC-AHO-2003-032B2f17

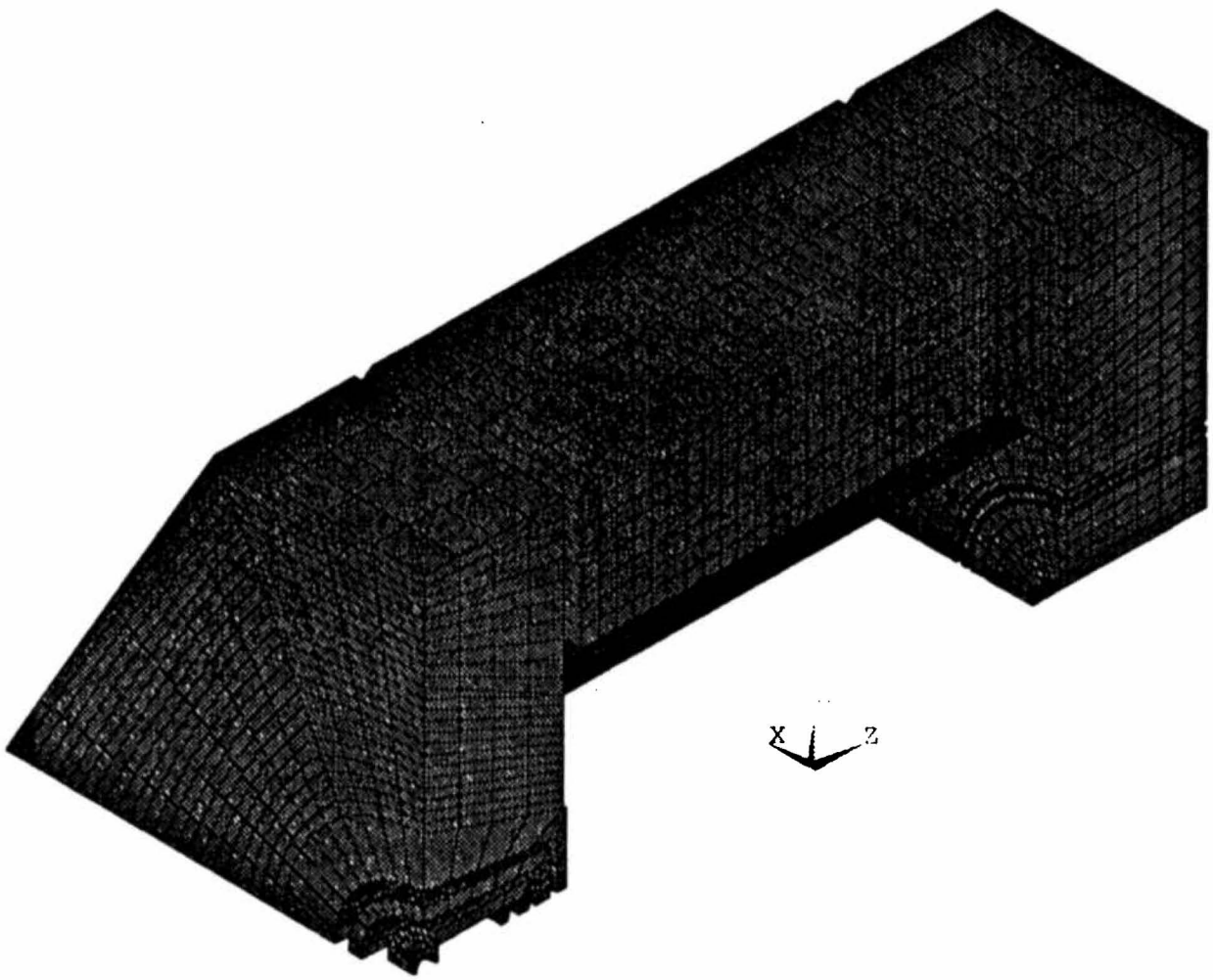

ANSYS 5.0 A
MAY 29 1995
14:49:33
PLOT NO. 1
ELEMENTS
MAT NUM

XV =-1
YV =1
ZV =-1
DIST=3.758
XF =1.686
YF =1.46
CENTROID HIDDEN

Fig. 2.21: Simplified model of the magnet

SLAC AHO 2003-032B2f17

after a copper covering (electro-deposition) of the aluminum, should have a resistance less than 5×10^{-10} Ω each, in order to limit the power dissipation to few mW.

SLAC AHO 2003-032B2f17

3.2 Electrical insulation

Electrical insulation is an extremely important aspect of solenoid design and manufacture. Two categories of insulation are required:

(i) ground plane insulation between the coil and support cylinder. The ground plane insulation must operate at relatively high voltages during quench conditions and will be subjected to strict QA controls. The design of quench protection systems is based on a maximum voltage to ground of 250V. The ground plane insulation will be made by a 1mm layer of glass fiber epoxy laminate which is bonded to the support cylinder before winding. The insulation will be fully tested at 2kV before winding.

(ii) turn to turn insulation: Conductors will be insulated with a double wrap of ~0.1mm glass tape during winding to give an insulation thickness of 0.2mm. The turn to turn insulation thickness will be 0.4mm and will be fully impregnated in the bonding process. The conductor must be insulated during the winding process.

Electrical tests will be carried out during winding to detect any failure of insulation. The tests will include continuous testing for turn to turn and turn to ground insulation.

3.3 Conductor stability

The BABAR Solenoid coil will be indirectly cooled using the technology established for detector magnets such as DELPHI, ALEPH, CDF etc. The reliable operation of these existing magnets has demonstrated that safe stability margins can be achieved using high purity, aluminum clad superconductors in a fully bonded, indirectly cooled coil structure.

3.3.1 Stability Modeling

Modeling Codes

Conductor stability has been estimated using modeling codes developed at RAL and INFN Genoa for the study of LHC Detector magnets (Ref. (1) ASC Paper). The concept of the stability model is shown in figure 3.4 which also outlines the terminology. The model is set up to represent a defined length of coil matrix (typically 10m) in the longitudinal direction. The model is divided into longitudinal elements and an initial heat pulse is applied to a specified conductor length for a specified duration.

SLAC AHO 2003-032B2f17

In all cases the stability is computed for an input heat pulse duration of 100msec. Figure 3.7 shows typical temperature profiles in the conductor at 100msec and 200msec.

Table 3.2 - BABAR Solenoid Stability Parameters

Model Parameters	
Conductor width	32mm
Conductor thickness	3.2mm
Insulation (turn/turn)	0.4mm
Shell thickness	30mm
Ground plane insulation	1mm
RRR Al	500
Peak field	2.5 Tesla
Design Current Ic(2.5T)	16kA
Operating Current	6.83kA
Current Sharing Temp	6.5K
Critical Temp	8.2K
Pulse Time	100 msec

The computed stability shows a strong dependence on the properties of the aluminum substrate. In the BABAR Solenoid this is one of the few parameters which can be adjusted with minimum impact on coil geometry and magnet performance. The only impact of changing RRR will be on the magnet cost although the effect of changing RRR 500 to 750 is expected to be small ~2-3% for the solenoid.

SLAC AHO 2003-032B2f17

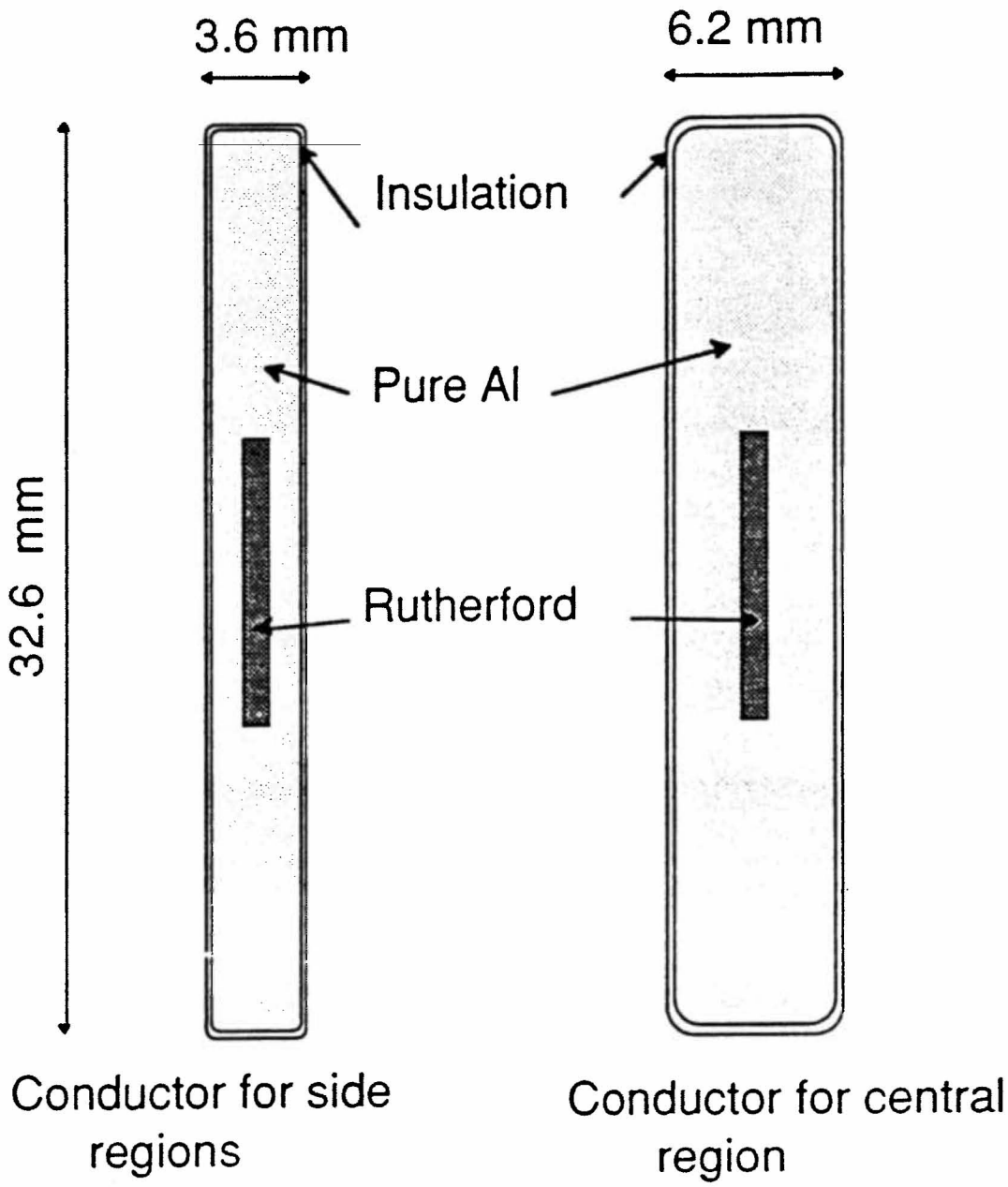

Fig.3.1 Cross section of the conductors

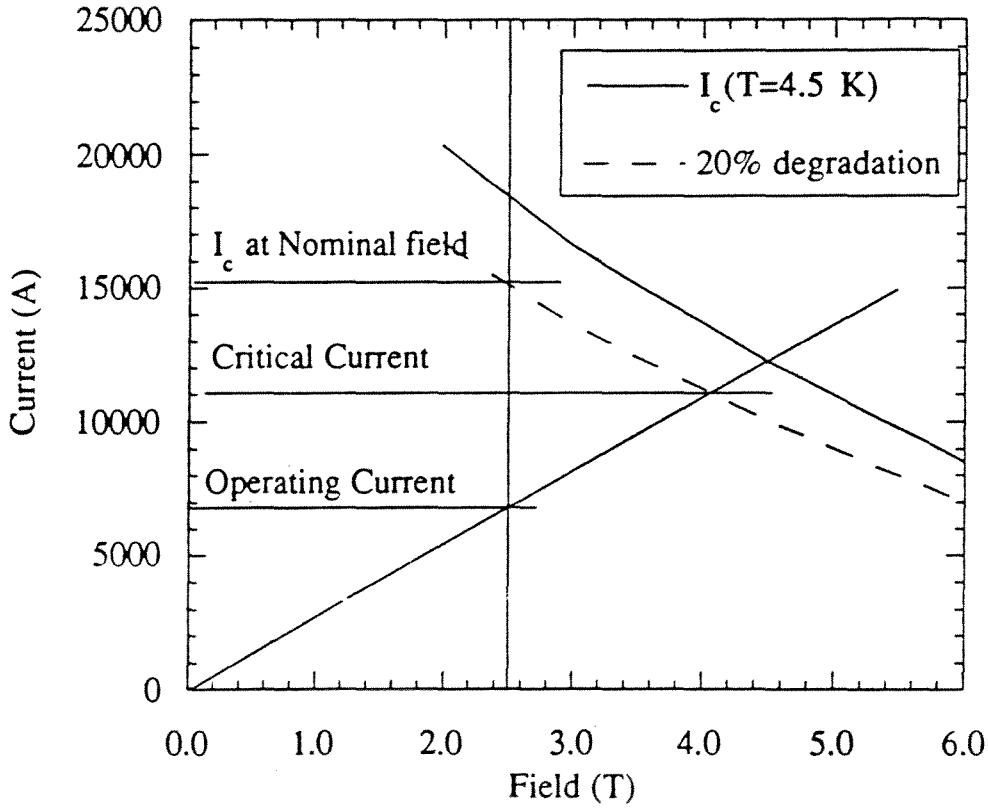

Fig. 3.3 Solenoid load line

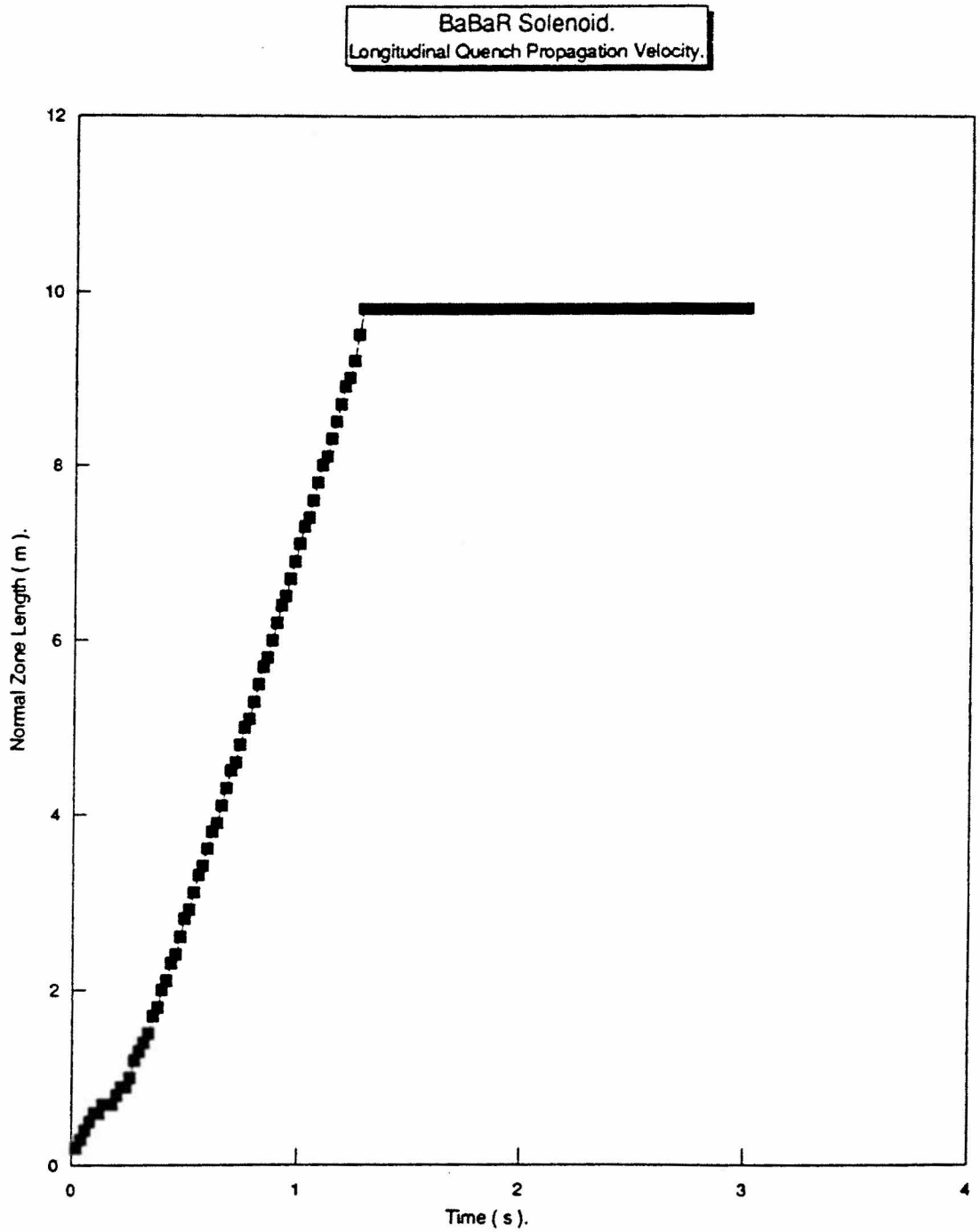

Figure 3.5 Rutherford Appleton Laboratory. File : D_QP_03.WK4.

RALTRAN5-5-1.FOR. BaBaR Solenoid.
Four time intervals shown. Graphs of temperature against element position for the conductors.

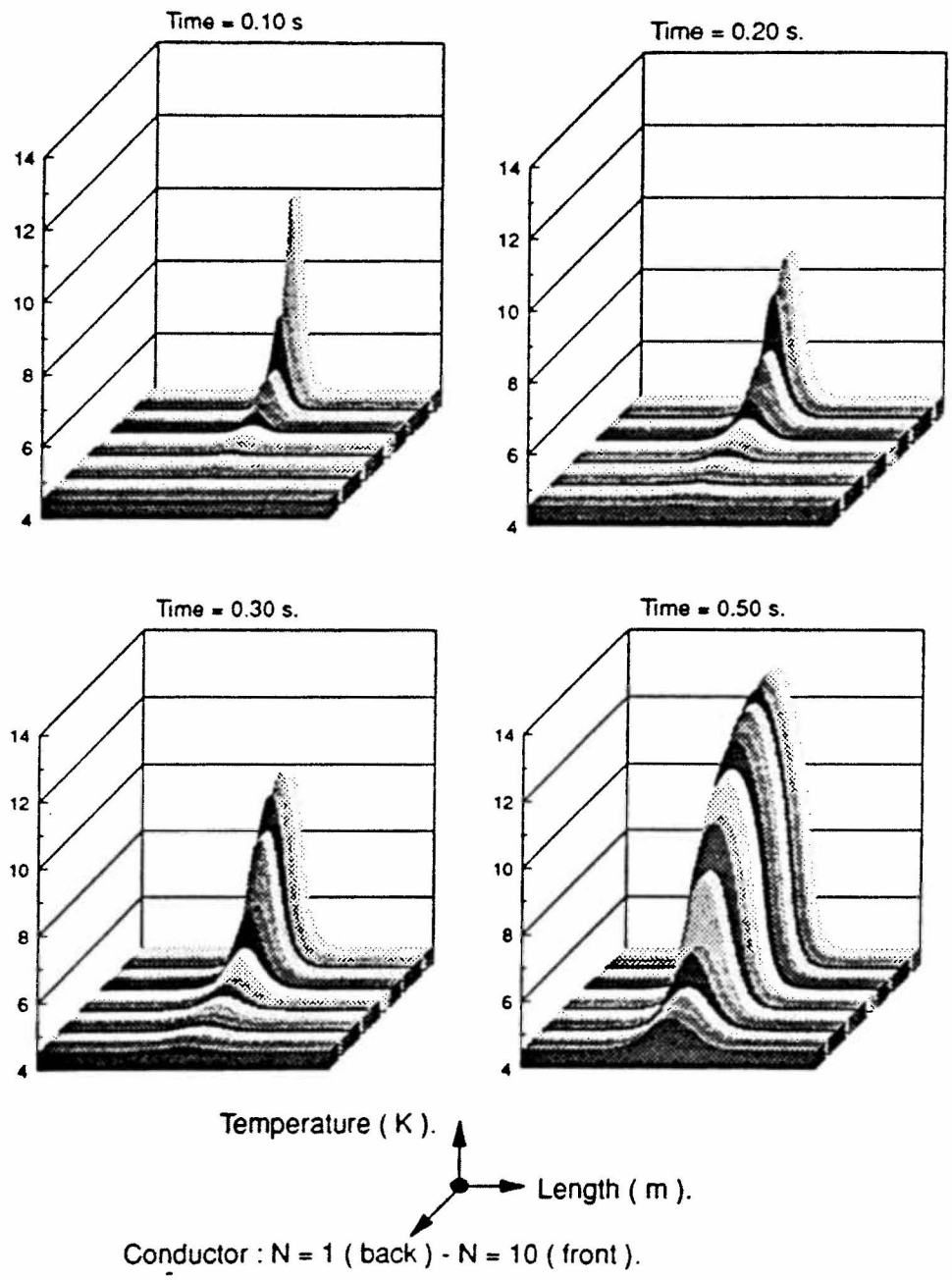

Figure 3.7 Rutherford Appleton Laboratory.

iii) The bonding between cylinder and winding can be critical for the axial shear stress. In fact due to the differential thermal contraction and to the axial magnetic loads, different loads are axially applied to winding and cylinder. In the present design the mechanical coupling between winding and cylinder is supposed to be given by epoxy resin impregnation. The mechanical design should minimize the shear stress at the cylinder-winding boundary

The thickness of the cylinder was designed on the basis of a simple 1D stress analysis, which approximates the solenoid to a series of concentric shells of different materials. This analysis was made looking at each step of the solenoid life as explained in the previous item (i). A 1D analysis was also used to study the effect of the axial forces. After designed the cylinder and the end flanges the stresses due to magnetic loads were verified using ANSYS code. Different models for the stress analysis were used as better explained later.

In order to have a first indication of the cylinder thickness, we can considered that the minimum thickness is given by:

$$\Delta R = \frac{PR}{\sigma_{max}}$$

where P= 1.53 MPa is the magnetic pressure, R is the inner radius and σ_{max} the maximum allowable circumferential stress, which for Al alloy is 279 MPa (see APPENDIX B). Considering that the cylinder could be obtained by welding rolled plates, we have assumed as limit stress 160 MPa. ΔR_{min} results to be 15 mm. We have assumed a thickness of 30 mm, which both gives a high safety factors and reduces the elastic deformation of the pure aluminum as explained in the next section. The ends of the cylinder were further thickened for anchoring the supports.

4.3 Stress Calculations

This section is devoted to the stress analysis made in order to design the cold mass. The stress analysis was carried out through several steps:

I. The first part is related to a simple 1-D analysis to determine the circumferential stress at the winding due to the cooldown and to the magnetic loads.

II. A Finite Element analysis, with ANSYS code, was then performed to verify the stress due to the magnetic loads obtained by the 1-D analysis. A local model was used for this analysis, simulating very closely some parts of the winding.

III. A further 1 D analysis for thermal and magnetic axial loads was carried out.

SLAC AHO 2003-032B2f17

Table 4.1 Circumferential Stress for the end regions (MPa)

Layer	Constr.	Cool down	I Charge Al Elastic	I Charge Al Plastic	Discharge (Al Plastic)
Outer Cylinder	-	20	57	70	30
Insulation	-	-69	-49	-37	-67
Winding Pure Al	-	9.6	39	14	-14
Rutherford	-	-140	-76	-43	-140
Winding Pure Al	-	9.7	40	14	-14
Insulation	-	-69	-49	-36	-68

Table 4.2 Circumferential Stress for the central region (MPa)

Layer	Constr.	Cool down	I Charge Al Elastic	I Charge Al Plastic	Discharge (Al Plastic)
Outer Cylinder	-	17	36	45	21
Insulation	-	-71	-59	-37	-70
Winding Pure Al	-	6.7	25	14	-14
Rutherford	-	-147	-107	-64	-150
Winding Pure Al	-	6.7	25	14	-14
Insulation	-	-71	-59	-37	-70

(17 - 20 MPa) . Due both to the high differential thermal contraction between the Rutherford cable and the aluminum and to the low cross section of the Rutherford, the Rutherford cables take a lot of compression (150 MPa).

SLAC AHO 2003-032B2f17

aluminum of the winding is stresses over the elastic limit. Figures 4.5 and 4.6 shows the obtained stress distribution in the two regions considered. The resulting stresses of the outer cylinder are 20 % lower than predicted by 1D shell model, so that we can consider substantially correct the information coming from the 1D analysis .

4.3.3 1-D analysis For Axial Stress

In order to carry out a 1-D analysis for axial stress we considered the winding and the cylinder as two homogeneous structures mechanically coupled. As first step, it was necessary to define the average thermal and mechanically properties of the winding.

Winding thermal contraction The axial thermal contraction from 300 K down to 4.5 K of the winding a_w was calculated according to:

$$a_w = (a_{Al} D_{Al} + a_{ins} D_{ins}) / (D_{Al} + D_{ins})$$

were a_{Al} a_{ins} are the thermal contraction of Aluminum and Insulating material (fiber-glass epoxy transverse to the fibers in this case) and D_{Al} and D_{ins} are the radial thickness of the two materials. With a_{Al} =4.15 10^{-3}, a_{ins} =6 10^{-3}, D_{Al} = 3.2 mm or 5.8 mm and D_{ins} =0.4 mm, we obtained a_w =4.35 10^{-3} for the end regions and a_w =4.27 10^{-3} for the central region. Considering the axial length of the two regions the winding contracts a_{wtot} =4.3 10^{-3} , i.e. 0.53 mm more than the supporting cylinder.

Young moduli The axial Young modulus of the winding E_w is given by

$E_w = E_{Al} E_{ins} (D_{Al} + D_{ins}) / (D_{Al} E_{Ins} + D_{ins} E_{Al})$

Using E_{Al} (T=4.5 K)= 78 GPa and E_{Ins}(T=4.5 K)=15 GPa we found E_w =53 MPa for the end regions and 61 MPa for the central region.

Winding and cylinder thermal contraction. It is useful to calculate what is the total thermal contraction of winding and cylinder considered as coupled structures.

Let be E_W and E_C be the Young modulus of the winding and supporting cylinder and a_W and a_C the relative thermal contractions from 300 to 4.5K,. the thermal contraction of the two coupled structures is:

$$a_{tot}=(S_W E_W a_W + S_C E_C a_C)/(S_W E_W + S_C E_C)$$

Where S_W and S_C are the axial cross sections given by

$$S_W = 2 p \langle R_w \rangle DR_w$$

SLAC AHO 2003-032B2f17

impregnation using bolts to push inward the end flanges against the winding (as shown in fig. 4.7) . Nevertheless we do not think that the required pre-stress can be completely applied. In fact using metric M20 bolts in aluminum alloy, a maximum force of 20 kN can be reasonably applied. Using 64 bolts (as allowed by the circumferential allowed space) we can apply a force of about 1.3 MN. Looking at the end regions , this pre-stress reduces the shear stress of 4% . Generally speaking, the benefits of the pre-stress are taken by the complete winding-cylinder bonding. In some parts the shear stress will be strongly reduced, in other parts (as the ends) the shear stress will remain essentially the same.

4.3.4 Finite Element Analysis Of The Overall Magnetic Stress

In the previous sections we developed simple 1D analyses, for both axial and radial stress, carried out separately. In this section we show the results of a stress analysis for only magnetic load carried out by modeling the complete cold mass (winding + supporting cylinder), so that radial and axial stress are considered at the same time. Two different models were made using ANSYS code:

i) Shell model: In the first model the cold mass was idealized according to the shell model presented before. Fig.4.8 shows a detail of the model with the meshed regions. For this finite element analysis both the real stress-strain curve of pure aluminum and the simpler linear stress-strain curve were considered.

ii) Linear model with sub-model and very fine mesh: With the second approach the cold mass was idealized through two models: a "coarse" model , which modeled each turn but not the insulation and a fine sub-model which modeled the insulation too. The details of this model are given in Appendix F.

The results obtained for the circumferential stress confirmed the ones from the 1-D analysis and are shown in tale 4.3 .

SLAC AHO 2003-032B2f17

4.3.5 Overall Stress State In Cold Mass

In addition to the calculations above, we have performed a Finite Element analysis of the cold mass including the effect of gravity , magnetic offsets and supporting system. These calculations are described in more detail in APPENDIX C. This model (shown in figure 4.10) consists of a cylinder thickened at the ends and subject to the loads and supports described below. 4-Noded shell elements were used with the ANSYS program version 5.0. The windings were assumed to contribute to the stiffness and strength of the structure. Output studied included Von Mises equivalent stress and deflections. In all cases we were careful to look at both surfaces of the shell elements as well as at the center plane, in order to capture bending effects.

The support directions are shown in figure 4.11.

The most obvious features of the results is that the stress due to the magnetic pressure dominates, none of the other loads has a particularly large effect except for the axial magnetic force (loadcase 6). . Note that this axial force is the force acting on each individual conductor, as distinct from the net axial forces of 20t and 10t due to misalignment and asymmetry. The stress value of 39 MPa corresponds broadly with the value for the simple 1D analysis given above, remembering that this was a linear analysis which did not take account of the increase in stress in the outer shell when the conductor yields.

Table 4.3 Supports

Supports		
Type	Location and number	degrees of freedom
Axial	6, evenly distributed around one end of the coil, with two on the horizontal center plane	"Z"
Radial	4 each end, at +/1 45 degrees from the horizontal center plane	tangential movement = 0

SLAC AHO 2003-032B2f17

ii) The Aluminum stabilizer of the conductor is stressed over the elastic limit only at the first solenoid energization. In the following magnetic cycles the stabilizer works between the compressive and tensile elastic limits

iii) The axial stress can be easily transmitted from the winding to the cylinder at a low value of shear stress ranging from 1.1 MPa to 4.5 MPa, depending on the model used for calculation. These values are much lower than the attainable shear stress given by an epoxy gluing (20 MPa)

iv) The application of a moderate axial pre-stress (through a force of 1.3 MN) could help in reducing the shear stress at the winding-cylinder boundary.

v) An interesting comparison can be made between the mechanical behavior of BABAR solenoid and a working thin solenoid as CDF. The important parameter is the radial displacement due to the magnetic load. For BABAR this displacement is 1 mm maximum, as shown above. For CDF the designed radial displacement was 0.67 mm as described in the CDF solenoid technical design. Nevertheless for CDF the aluminum stabilizer was considered elastic up to high value of the stress (40 MPa). In our case, Table 4.1 shows that for elastic response of pure aluminum the magnetic loads would cause a maximum stress on supporting cylinder of 37 MPa, corresponding to a radial displacement of 0.69 mm, very close to the design result of CDF.

4.4 MANUFACTURING METHOD

In the previous section we have stressed the importance of a good bonding between winding and supporting cylinder. There are two ways to couple the two structures corresponding to two different manufacturing approaches.

i) The first approach consists in the shrink-fit technology: the winding is wound and impregnated onto a removable mandrel, then machined and enclosed inside the outer cylinder through a shrink-fit operation. In this case the coupling is given by the mechanical interference. Nevertheless the winding could move with respect the coil so that the application of axial preloads is recommended.

ii) The second approach is based on the inner winding. The conductor is wound directly inside the cylinder, the winding is then mechanically compacted and impregnated. In this case the bonding is given by the epoxy-adhesion. In both solutions it is possible that the winding axially moves with respect the cylinder causing heat dissipation and premature

SLAC AHO 2003-032B2f17

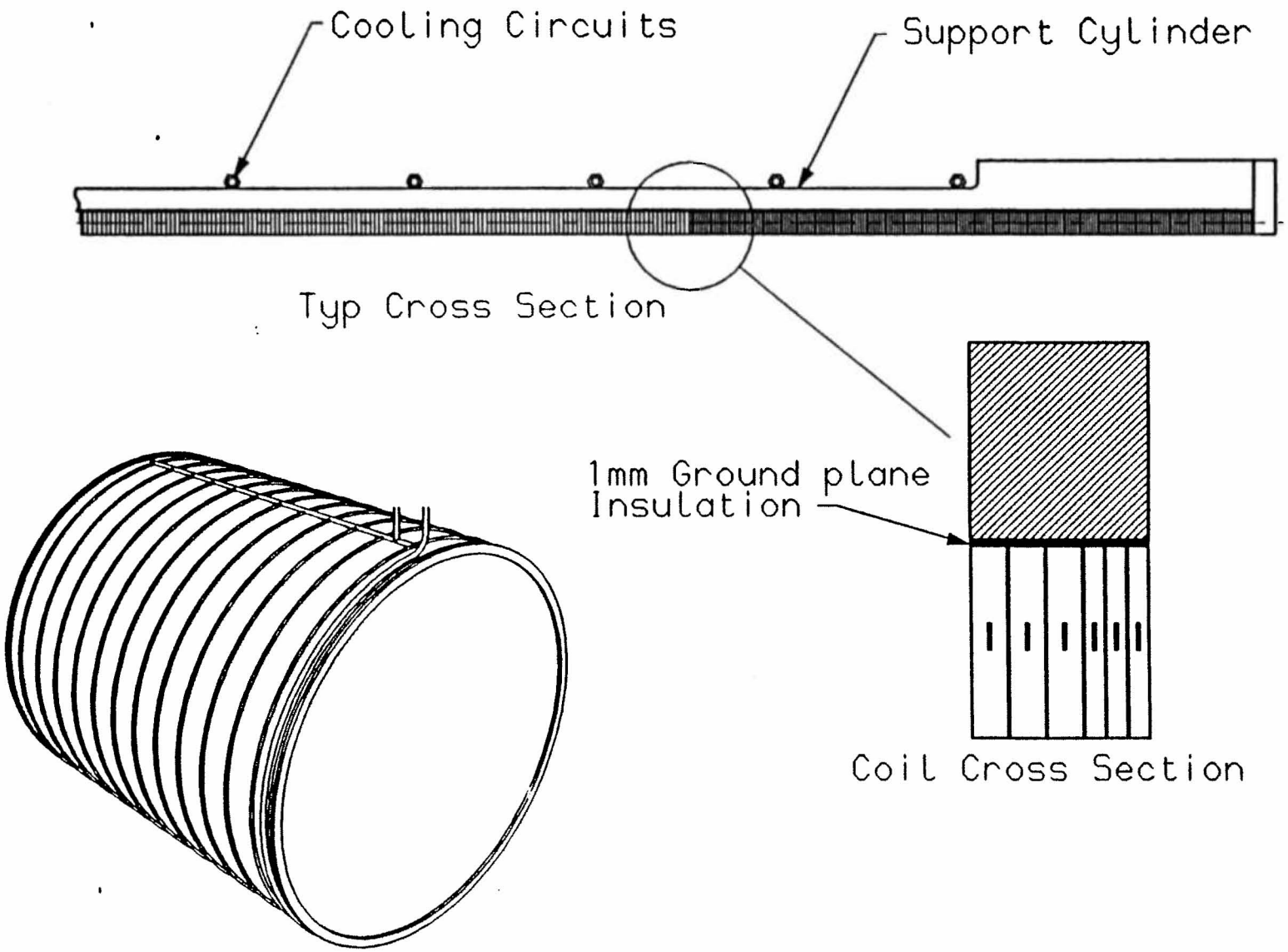

Fig 4.1 The Cold Mass

SLAC AHO 2003-032B2f17

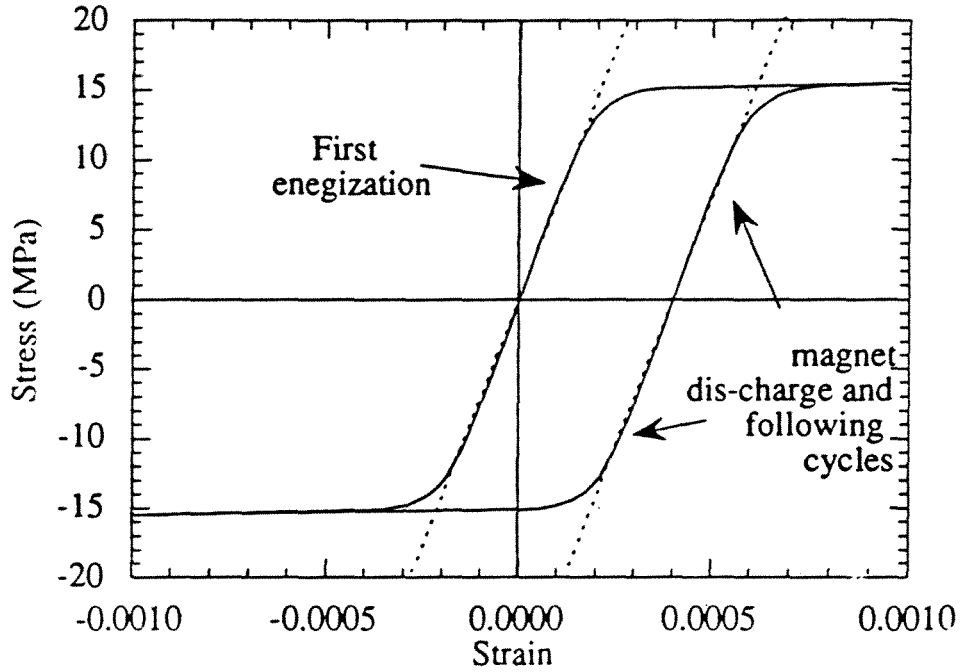

Fig. 4.3 Al pure stress-strain curve and operating conditions

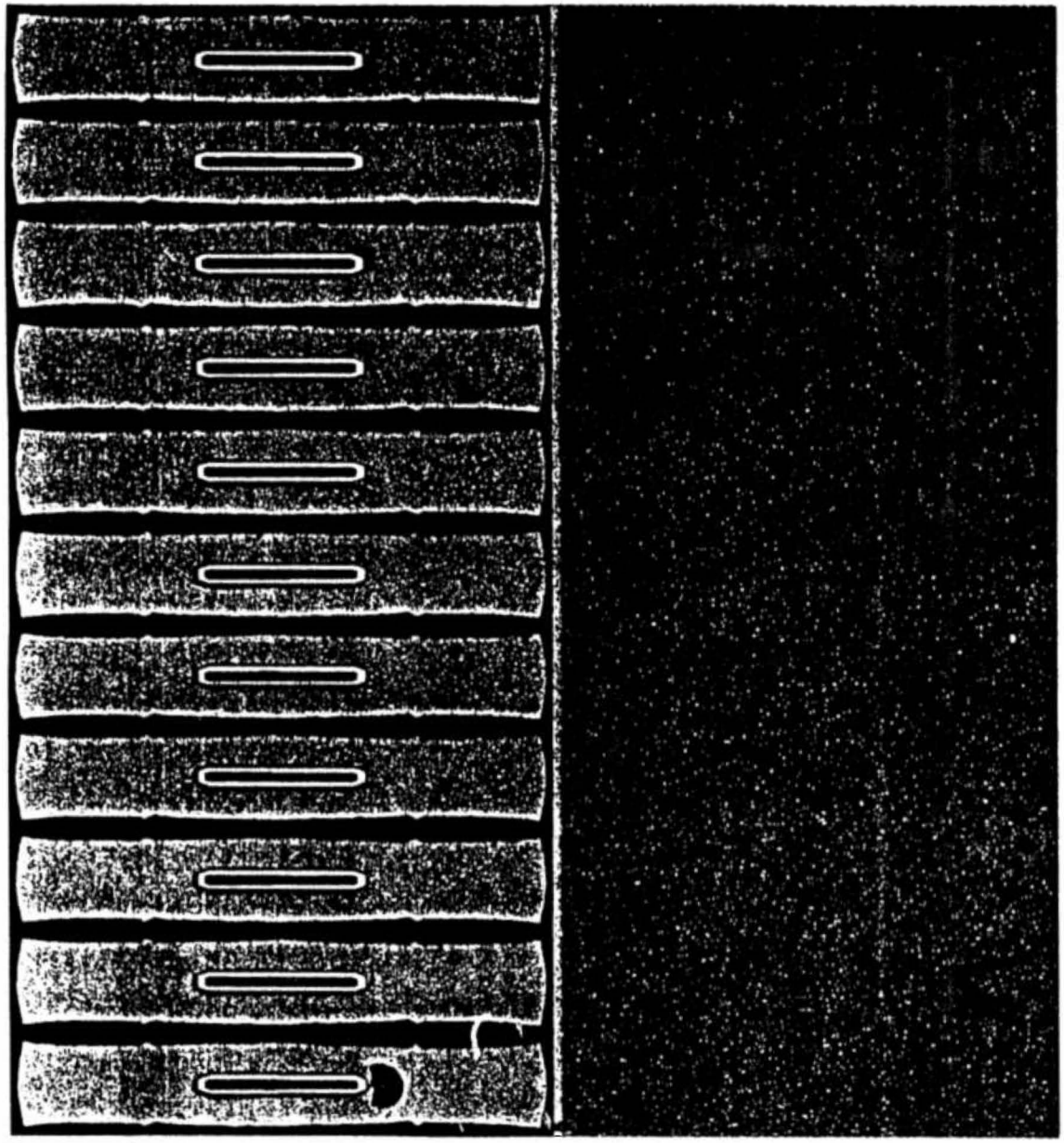

ANSYS 5.0 A
MAY 29 1995
14:13:50
PLOT NO. 1
NODAL SOLUTION
STEP=1
SUB =1
TIME=1
SZ (AVG)
RSYS=0
DMX =0.560E-03
SMN =0.462E+07
SMX =0.482E+08
0.462E+07
0.133E+08
0.220E+08
0.307E+08
0.394E+08
0.482E+08

Fig. 4.5: Circumferential stress in the central region

SLAC AHO 2003-032B2f17

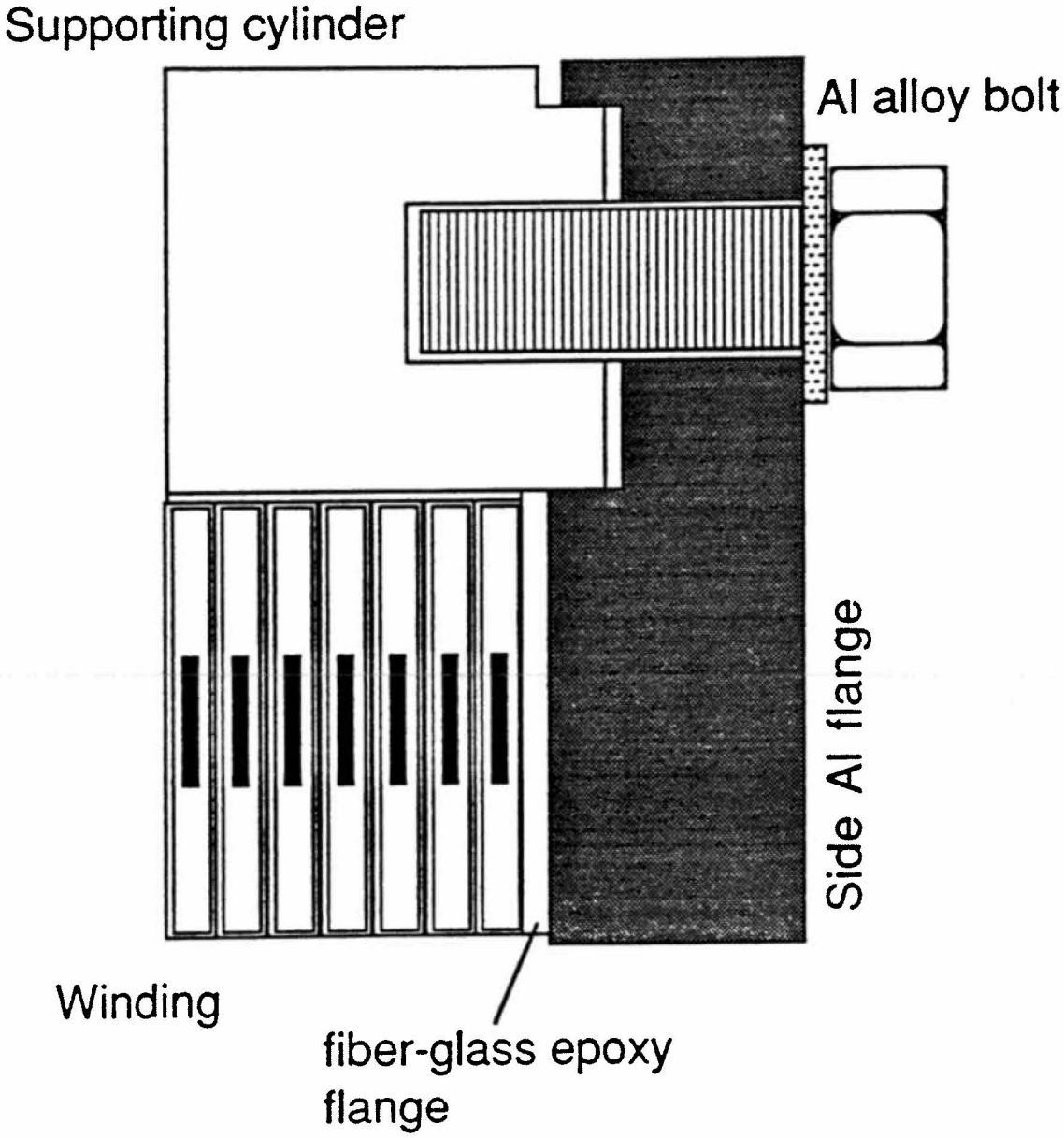

Fig. 4.7 Simple way to apply axial pre-stress to the winding

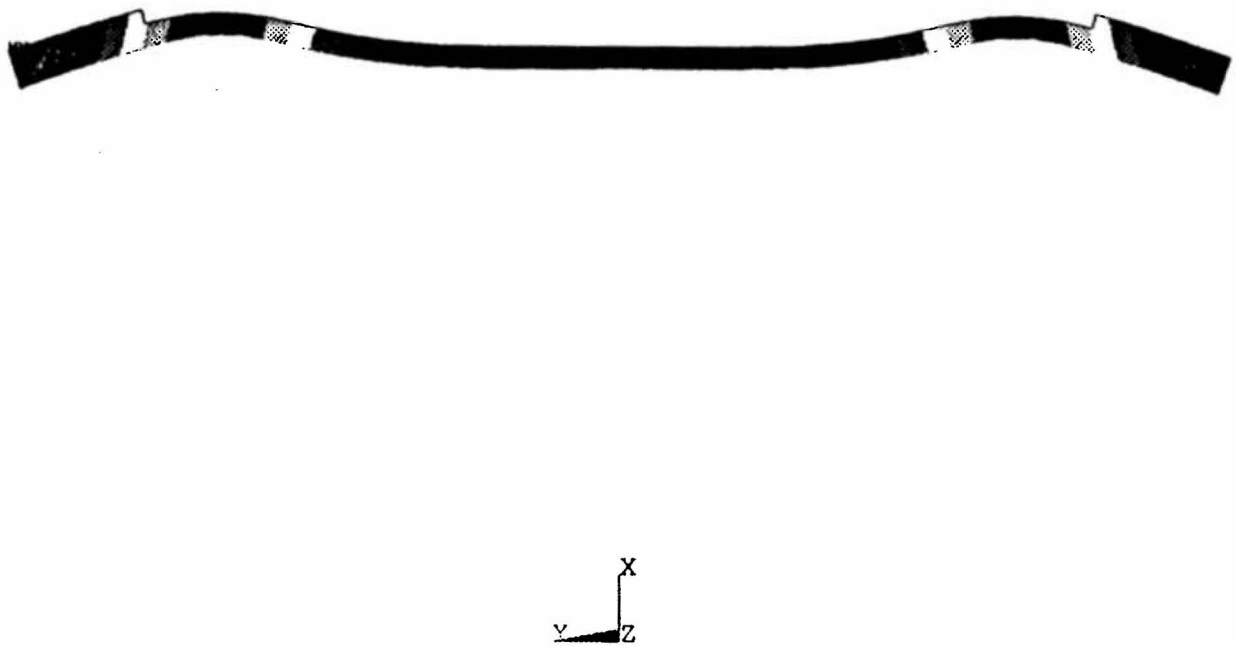

ANSYS 5.0 A
MAY 29 1995
16:57:36
PLOT NO. 1
NODAL SOLUTION
STEP=1
SUB =1
TIME=1
USUM
RSYS=0
DMX =0.001011
SMN =0.318E-03
SMX =0.001011

0.318E-03
0.395E-03
0.472E-03
0.549E-03
0.626E-03
0.703E-03
0.780E-03
0.857E-03
0.934E-03
0.001011

Fig. 4.9: Radial displacements due to magnetic load

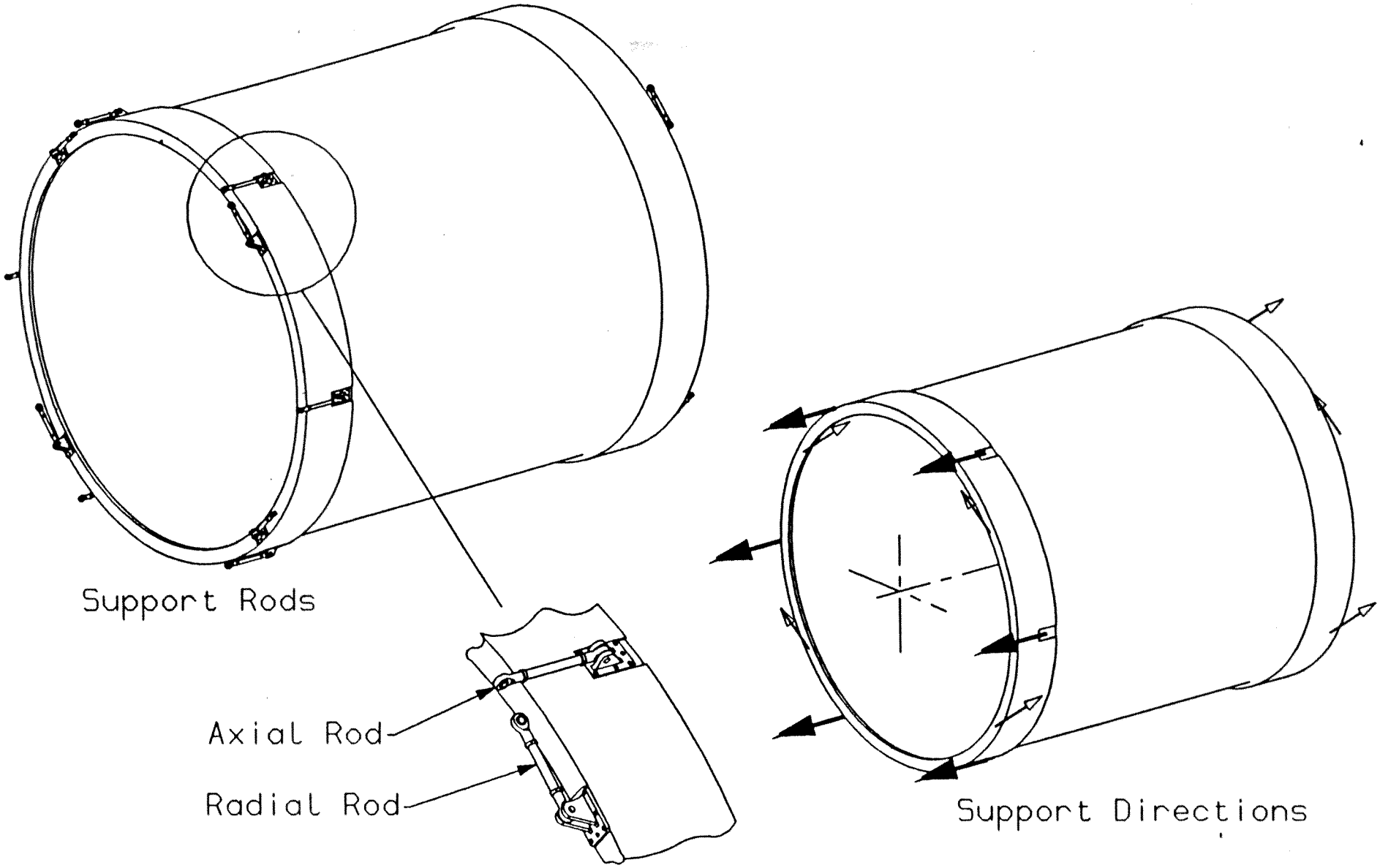

Fig 4.11 Support of the Cold Mass

SLAC AHO 2003-032B2f17

Table 5.1		
Model details		
Inner shell	Mean Diameter Thickness Length	1395mm 10mm 1875mm to center of end flange
Outer shell	Mean Diameter Thickness Length Thickened region	1695mm 30mm 1875mm to center of and flange 50mm thick for 200mm each end
End flanges	Thickness	50mm
Supports - axial	Four at one end, at ±30° to the vertical	"Z" - axial. See note below.
Supports - radial	One each end, at one side, on the horizontal center line	"X" - sideways. See note below.
Supports - vertical	Two each end, on the horizontal center line	"Y" - vertical

Note: There will in fact be Eight axial supports (four each end) and four radial supports (two each end), but they will be made so that they only act in one direction. See the description of the supports in the next section.

Table 5.2					
Load cases and results. All load cases included 1g downwards and vacuum loads.					
Case	Description	Additional loads	Max. deflection	Max. general stress	Max. local stress
1	Nominal	None	0.4	16	23.9
2	Earthquake - vertical	2g downwards	0.5	18	32.2
3a	Earthquake - sideways	1.2g +X direction	1.47	23	40.6
3b	Ditto - opposite direction	1.2g -X direction	1.72	20	58.6
4a	Earthquake - Axial Middle support	1.2g axial plus 60t load from detectors at middle radius of end flange	1.05	16	46.1
4b	Earthquake - Axial Inner support	1.2g axial plus 60t load from detectors at inner radius of end flange	1.43	25	42.1

The overall deflections are less than 2mm in all cases. This is acceptable in terms of the job the vacuum vessel has to do.

The stresses are in all cases less than 65MPa, which is the design stress for 5083 specified in the Pressure Vessel standard BS5500.

SLAC AHO 2003-032B2f17

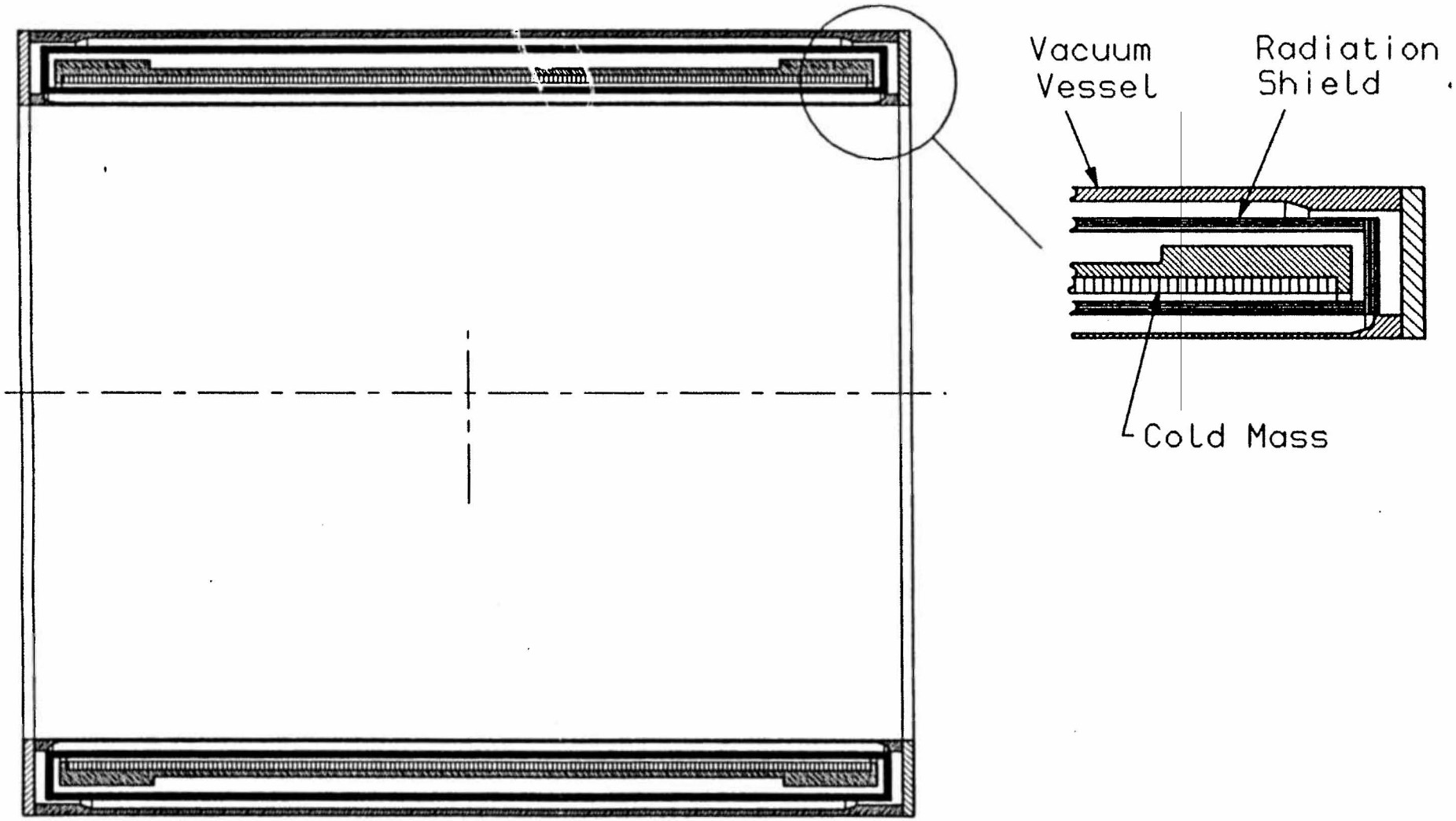

Fig 5.1 The Cryostat

SLAC AHO 2003-032B2f17

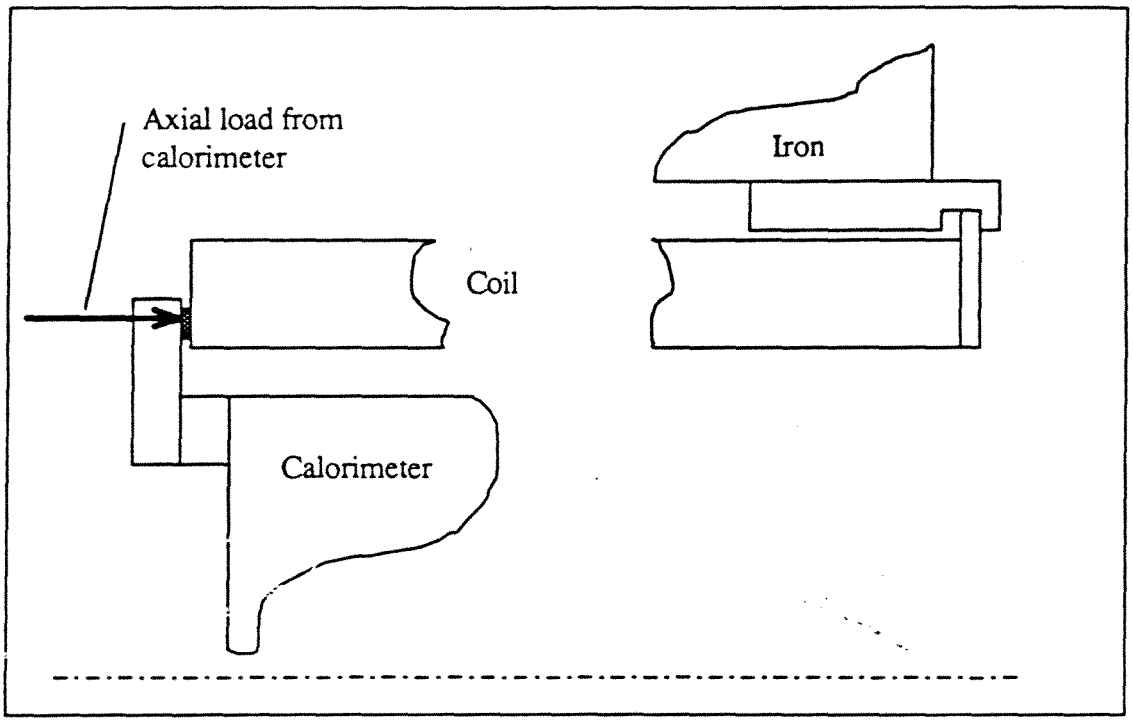

Figure 5.3 Outline scheme for axial support of inner detectors

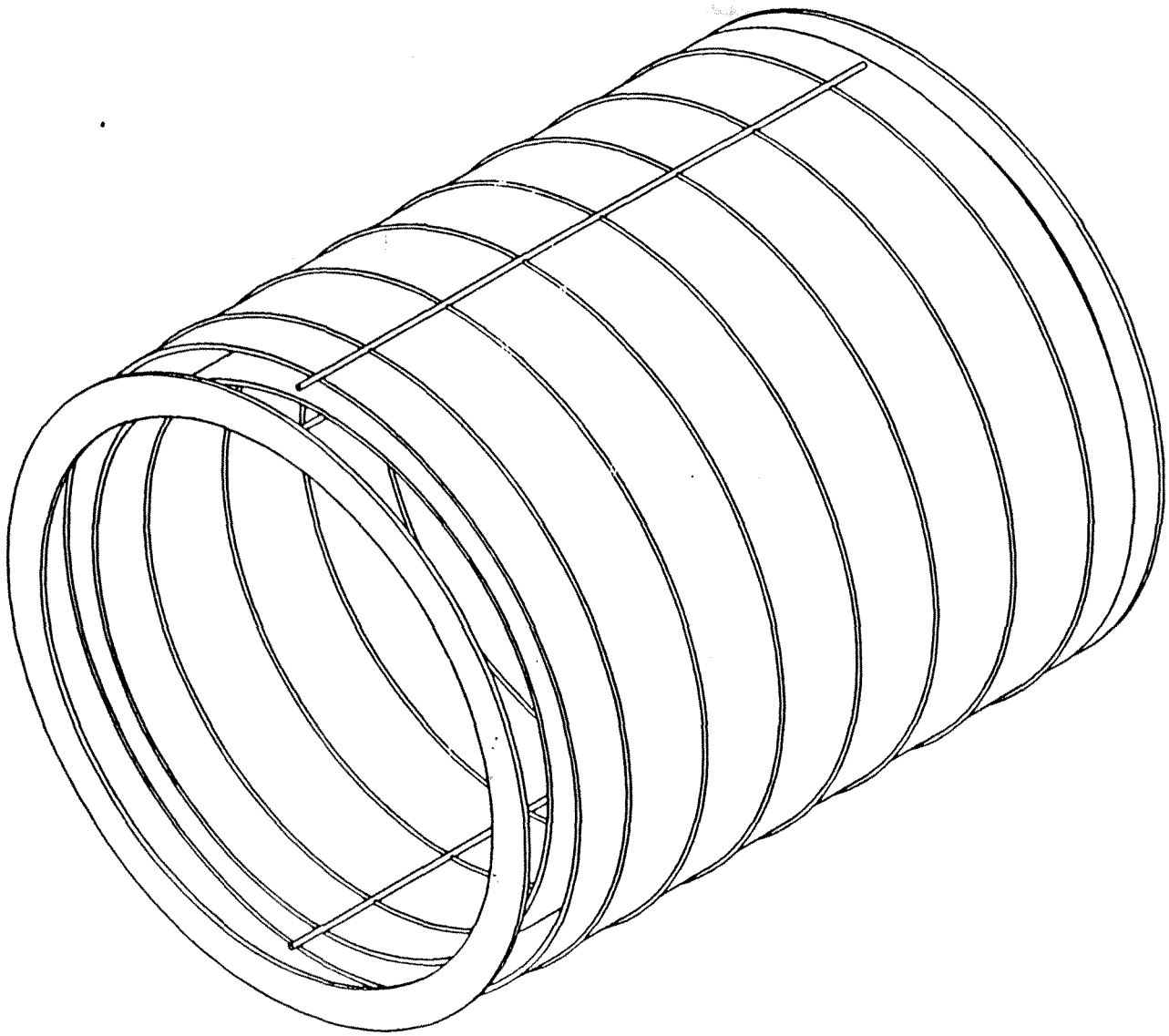

Fig 5.5Radiation Shield Schematic

SLAC AHO 2003-032B2f17

Other criteria:

- Earthquake loads are 1.2g sideways and 2g vertical. A fuller explanation of this is given in Appendix A.
- Alignment error of 2cm gives forces up to 20t. See section 2.5.
- Asymmetry of the flux return gives axial force of 10t. See section 2.5.

Table 6.1

	On cold mass (7 tonnes)	On cryostat (6.7 tonnes)	On detectors (50 tonnes)	Combined load on supports
Max. radial loads:				
g forces (1.2g)	8.4	8.0	60	
magnetic alignment errors	20			
Total	28.4	8	60	96.4t
Max. axial loads:				
g forces (1.2g)	8.4	8.0	60	
magnetic loads due to known geometry	10			
magnetic alignment errors	20			
Total	38.4	8	60	106.4t
Max. vertical loads:				
weight	7.0	6.7	50	
g forces (2g)	14.0	13.4	100	
magnetic alignment errors	20			
Total	41	20.1	150	211.1t

6.3 INTERNAL SUPPORTS (TIE RODS)

Inside the vacuum vessel, the cold mass is supported by six **axial tie rods** and eight **radial tie rods**. The concept is shown in figures 6.1 and 6.4. The six axial tie rods are positioned at one end of the cold mass, equi-spaced around the circumference. They take the axial forces, magnetic and earthquake. The eight radial tie rods are positioned four each end at 45° from the horizontal, aligned tangentially. They take the vertical and sideways forces, earthquake and magnetic.

6.3.1 Design Criteria

The design criteria we used were:

- **Strength.** The direct stress in each rod must be less than half the yield stress under normal loading, AND less than half the ultimate stress under earthquake loading. See also Appendix A)
- **Conduction.** The heat conduction over half the rod's length (assumed) must be acceptable between 80K and 4K. Total for all supports should be less than 10W.

SLAC AHO 2003-032B2f17

figure 6.5, in which vector diagrams are given showing how the loads add up. This analysis leads to the following maximum loads:

Tensile: 39t shared between four rods

Compressive: 29t shared between four rods.

The maximum nominal (non-earthquake) load happens when the magnetic alignment forces act at 45° (compare with case 2 in figure 6.5), and is given by

Max nominal loads: 20t + .707 × 7t = 25t shared between four rods

6.3.4 Sizes, Details Of Stresses, Heat Loads, Etc.

Applying the design criteria and loads given above, the following design was arrived at:

Table 6.2

	Units	Axial	Radial
Loads			
Nominal load - tensile	tonne	10	25.0
Nominal load - compressive	tonne	30	
Rods to resist nominal load		6	4
Quake load Tension	tonne	28.4	39.0
Compression	tonne	-38.4	-29.0
Rods to resist quake load		6	4
Material			
Material	Titanium alloy 6%Al, 4%V		
Ultimate stress	MPa	1000	
Yield stress	MPa	900	
Conductivity integral 80K to 4K	W/m	213	
Rod sizes			
Rod diameter - nominal. This is the diameter of the rod over all of its length except the ends, where it is turned down to M20.	mm	25	25
Rod length	mm	350	300
Rod diameter in thread root	mm	16.9 (M20)	16.9 (M20)
Stress, buckling			
Stress under Earthquake load in thread root			
Tension Compression	MPa	211 -285	434 -323
Factor of safety on ultimate stress under earthquake load		3.5 (compressive)	2.3 (tensile)
Factor of safety on buckling (using nominal diameter)		2.4	2.9
Thermal conductivity			
Rods in conductivity calculation		6	8
Total heat load over half the length of the rods	Watts	3.6	5.6

As the table shows, we have developed at a design which satisfies all the design criteria. The axial rods are closest to the stress limits with a factor of safety of 2.3 (we require at least 2.0) The radial

SLAC AHO 2003-032B2f17

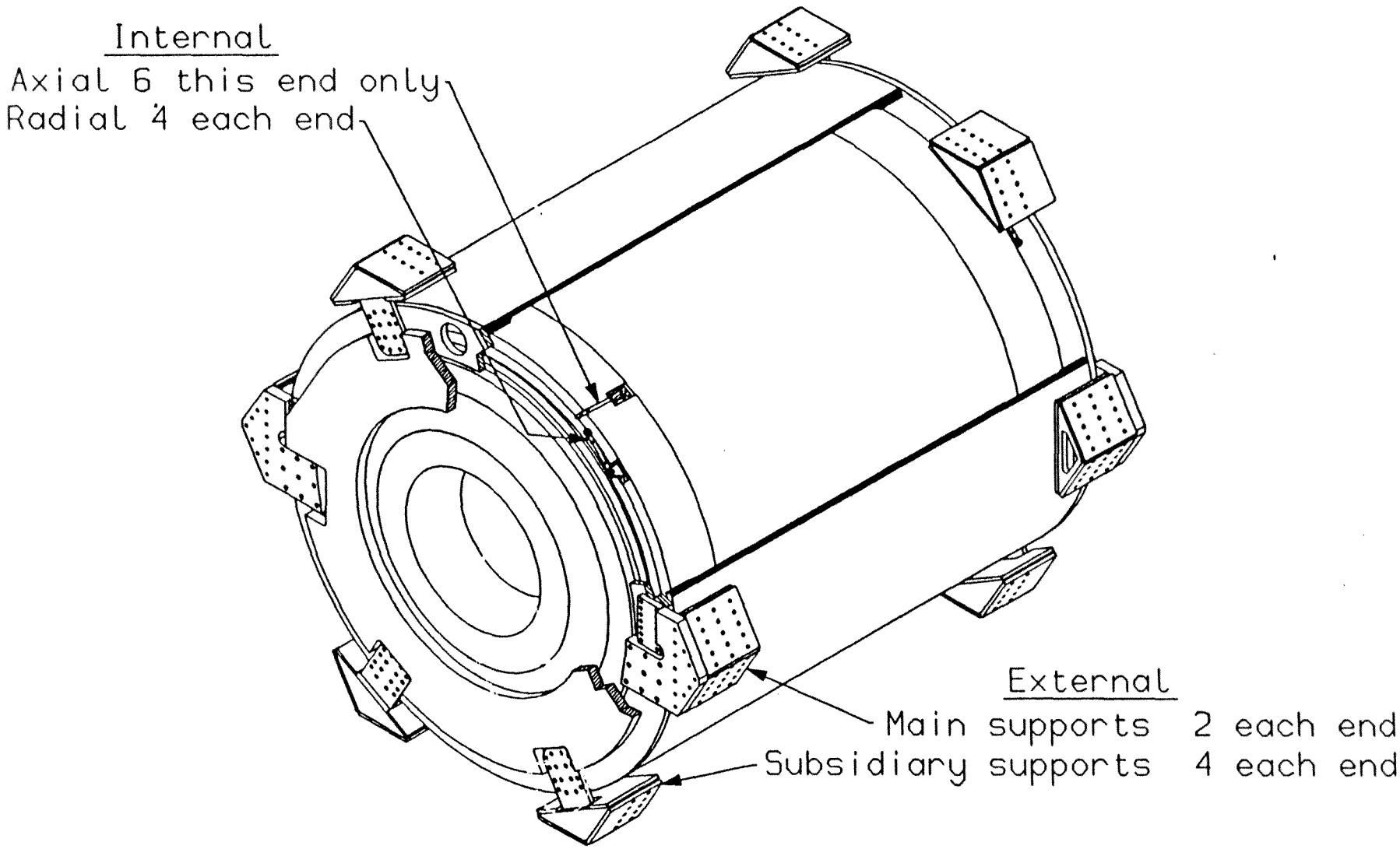

Fig 6.1 SUPPORTS OVERVIEW

SLAC AHO 2003-032B2f17

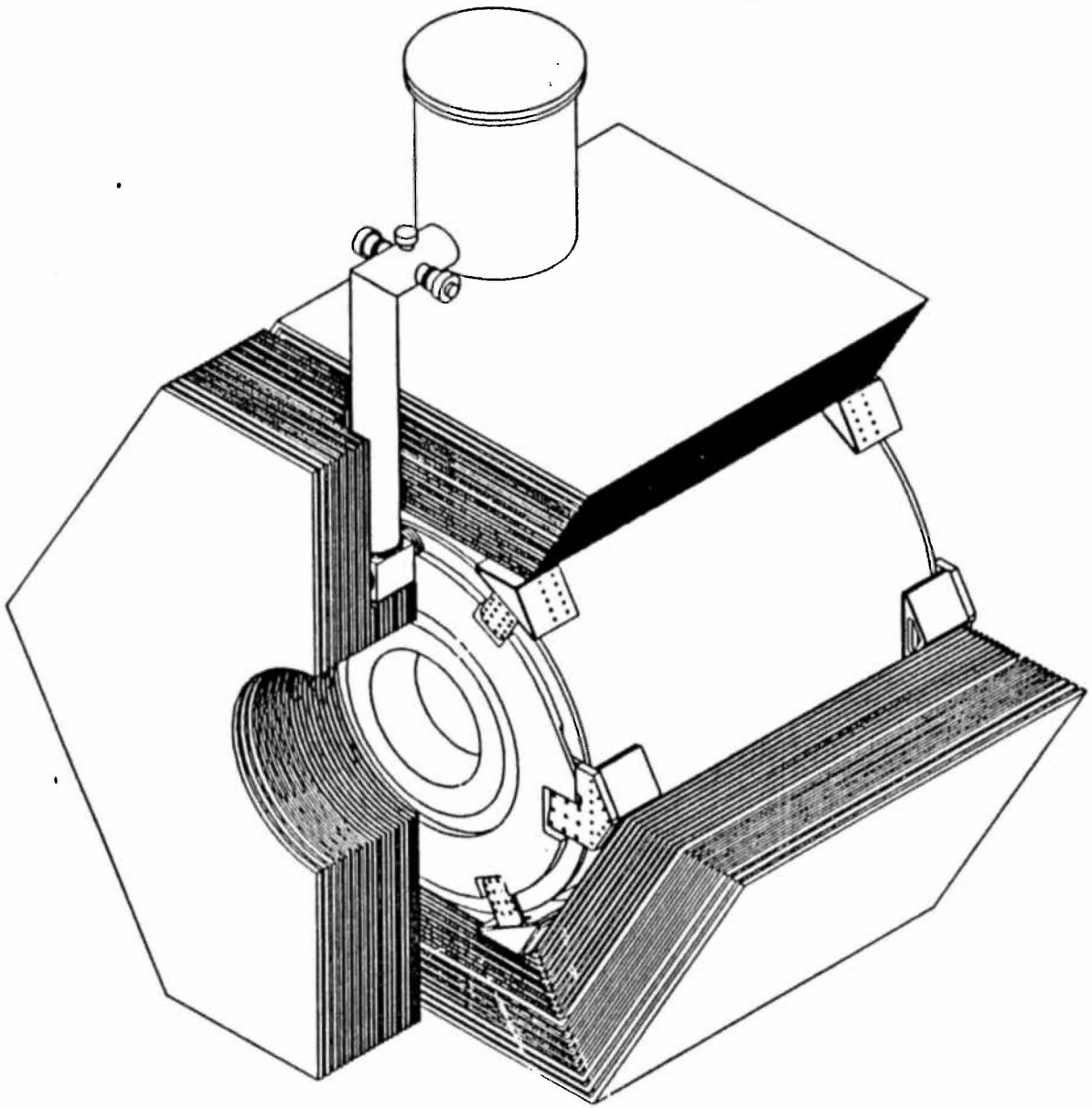

Fig 6.3 External Supports- Outline

SLAC AHO 2003-032B2f17

Figure 6.5 Forces in cold mass radial support rods

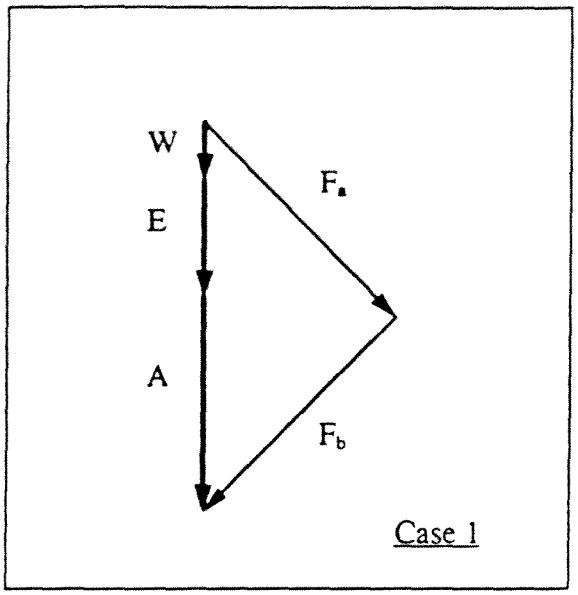

W = weight, 1g gives 7t
E = earthquake load, 2g gives 14t
A = Magnetic alignment error force, 20t
F_a = load in rods, set a (four rods)
F_b = load in rods, set b (four rods)

Case 1 - largest total load

$F_a = F_b = .707 \times (7+14+20)$
$= 29t$

Case 2 - largest load in a set of rods

$F_a = 14 + 20 + .707 \times 7$
$= 39t$

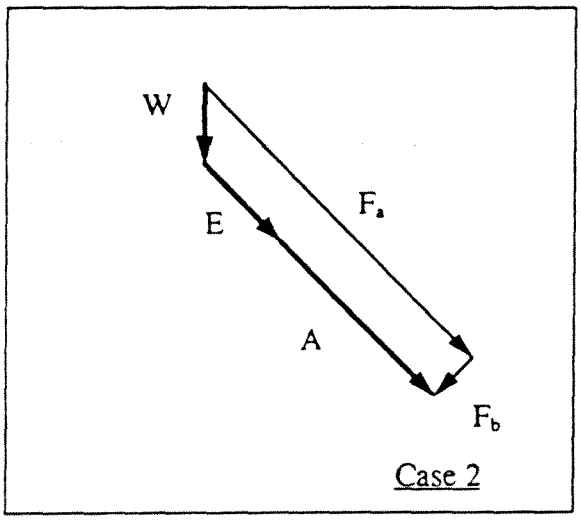

Case 3 - moving forces act sideways

$F_a = .707 \times (7+14+20) = 29t$
$F_b = .707 \times (7 - 14 - 20) = -19t$
(compressive)

Case 4 - largest compression force
(typical of several possible cases)

$F_b = .707 \times 7 - (14 + 20) = -29t$
(compressive)

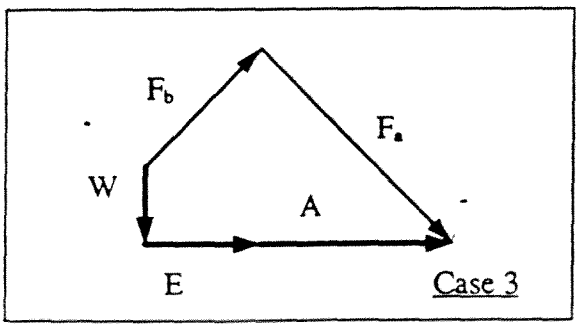

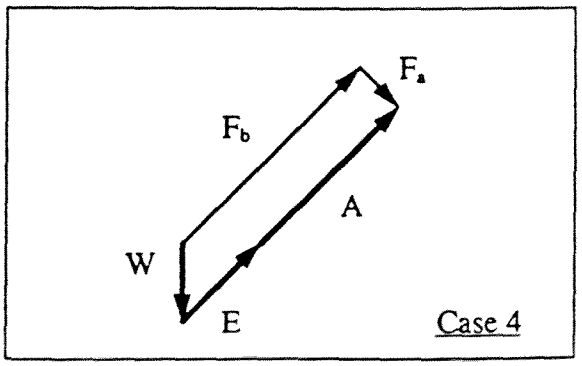

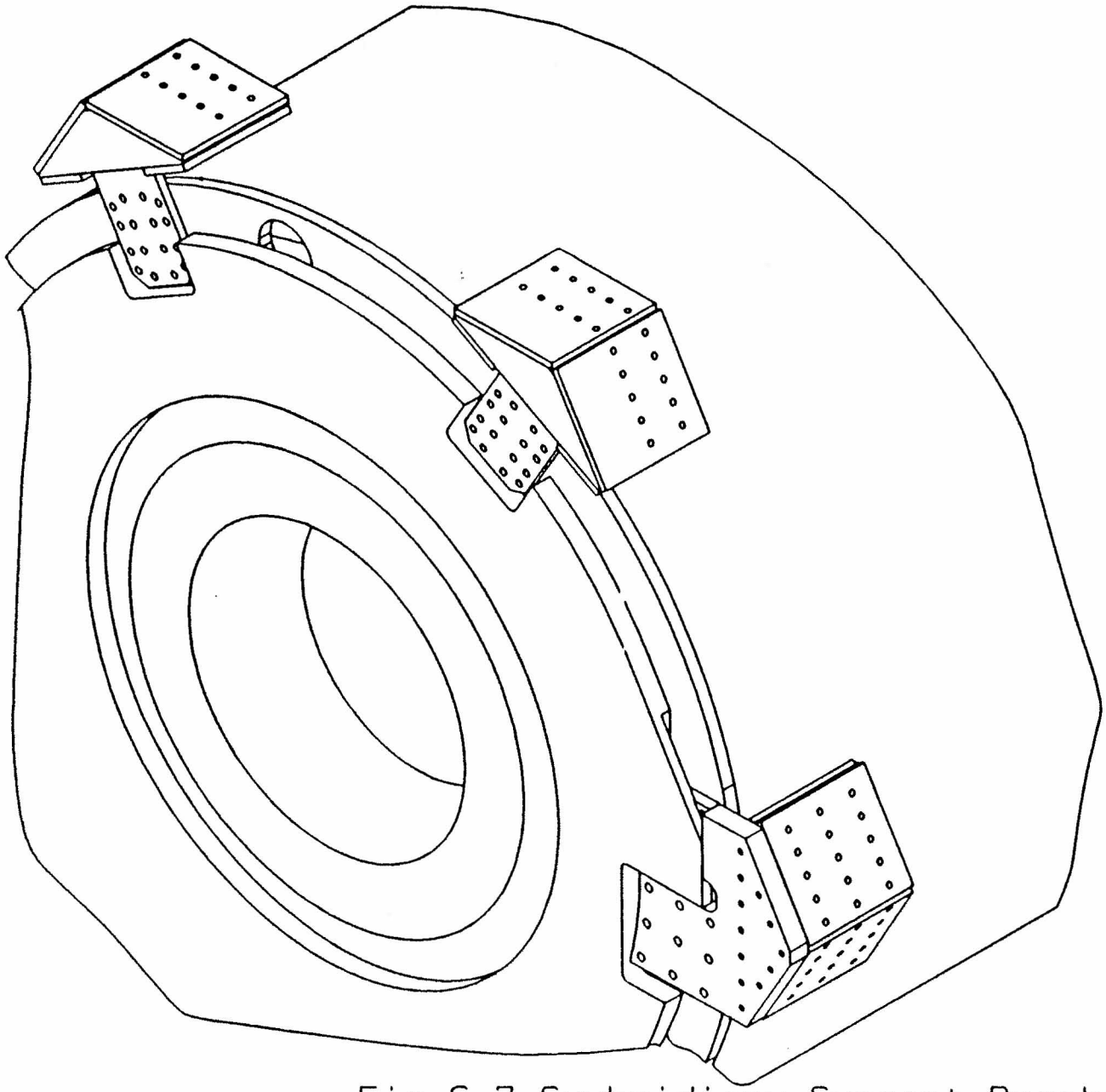

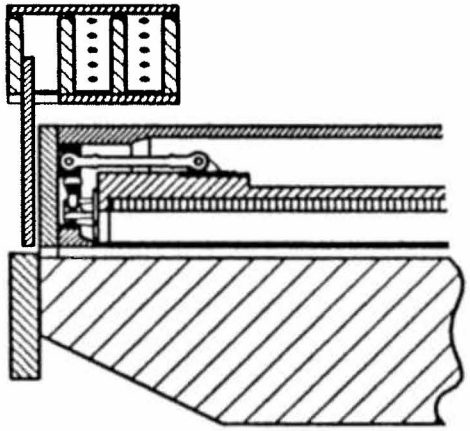

Typ Cross Section

Fig 6.7 Suubsidiary Support Brackets

SLAC AHO 2003-032B2f17

The turret valve box will be connected to the distribution valve box by two main flexible cryogenic transfer lines.

- Line 1 will contain the helium supply to the turret helium reservoir and is shielded by the gas return from the turret helium reservoir.
- Line 2 will contain the gas supply to the radiation shields and is shielded by the gas return from the shields

These lines exist and the cool down analysis has been tailored to use these lines.

Since the total liquid helium inventory in the coil / turret helium reservoir system is comparatively small in comparison to the capacity of the liquefier and its storage dewar, then to avoid unnecessary perturbation to the cryoplant the liquid will be vented to atmosphere in the event of a coil quench.

7.2.1 Cool down

Cool down of the coil cold mass and radiation shields from room temperature will be made by circulation of He gas. The gas may be supplied to the coil and the shield either directly from the refrigerator at the specified temperature in a controlled cool down or by mixing shield supply gas at approximately 40K from the cryoplant and 300K gas from the compressor system to cool down the shields and by mixing coil supply gas at approximately 4.5K from the cryoplant and 300K gas from the compressor system to cool down the coil. The gas mixing option recommended is that the mixing be carried out in the turret valve box since this minimizes the diameter of the cryogenic transfer lines.

Typical parameters for the cool down of the solenoid are given in Table 7.2. The full spreadsheet analysis is given in Appendix 1. A constant cool down rate is assumed during the cool down.

This analysis shows that with an initial mass flow rate of ~5gm/sec rising finally to ~10 gm/sec in the coil circuit the coil cold mass can be cooled to 5K in approximately 7 days. The corresponding mass flow for the shields is ~2 gm/sec rising to ~4 gm/sec. The cool down analysis is based on a maximum temperature difference across the shield and the coil of 40K in order to minimize thermal stresses. Cool down curves for the coil and shields are shown in Figure 7.11.

7.2.2 Operational Mode

After cool down the cryogenic system will be switched to operational mode where the coil is cooled by circulation of 2-phase liquid helium. The conceptual layout of the cold mass cooling circuit is shown in Figure 7.7. The design is based on the thermo-siphon technique established for ALEPH and CLEO II. The coil circuit will be fed from the turret dewar through a large bore manifold at the bottom of the force support cylinder. The cooling circuits are welded to the cylinder surface with a spacing of ~0.3m. The cooling circuits terminate in the upper manifold which connects to the turret helium reservoir through a phase separator.

The thermo-siphon cooling circuit will be designed for high flow rates to ensure a high quality factor for the helium - low vapor content. The design should allow for a minimum flow rate of ~30g/sec.

Typical parameters for the thermo-siphon circuit are given in Table 7.3.

The circuit will be equipped with pressure relief valves for safe operation during quench.

The turret helium reservoir will be designed to contain the minimum helium volume compatible with reliable operation. The total estimated volume of the coil and turret helium reservoir in real terms is < 80 litters.

7.2.3 Heat Loads

The estimated heat loads for the solenoid are given in Table 7.4. Eddy current heating in the support

SLAC AHO 2003-032B2f17

7.5 CRYOGENIC CONTROL

The cryogenic control system and must be capable of ensuring the safe working of the solenoid during cool down, normal operation and quench conditions. Details of the control interface and the operational protocols will need to be agreed between the solenoid manufacturer and SLAC.

7.6 FAULT CONDITIONS

7.6.1 Warm Up after a Fault Condition

Calculations show that above a radiation shield temperature of ~110K the radiation heat loads to the shield and the coil are equal. The radiation heat load is the dominant heat load so above this temperature the temperatures of the shield and the coil become locked together and warm up as one entity. This is illustrated in Figure 7.12.

Table 7.1. Parameters of cryogenic plant.

Normal running	
Shield	351 W at 60K
Coil	39 W at 4.5K
Current leads	0.75 g/s (22.5 litters/hr)
Cool down	
Peak compressor output	~14 g/s
Peak 40K mass flow rate	~4 g/s
Peak 4.5K mass flow rate	~10 g/s
Rated power at 4.5K	**141 W**

Table 7.2. Parameters governing cool down of solenoid.

System	
Cool down time	~7 days
Peak demand from compressors	~14 g/s
Radiation shields	
Cold mass	1000 kg
Peak 40K demand	~4 g/s
Coil	
Cold mass	7000 kg
Peak 4.5K gas demand	~10 g/s

Table 7.3. Thermo-siphon parameters

Operational driving head	~3 m
Operational driving pressure	353 Pa
Diameter of turret chimney lines	25 mm I.D. ~30 mm O.D.
Diameter of manifolds	45 mm I.D. ~50 mm O.D.
Diameter of coil cooling circuits	10 mm I.D.

SLAC AHO 2003-032B2f17

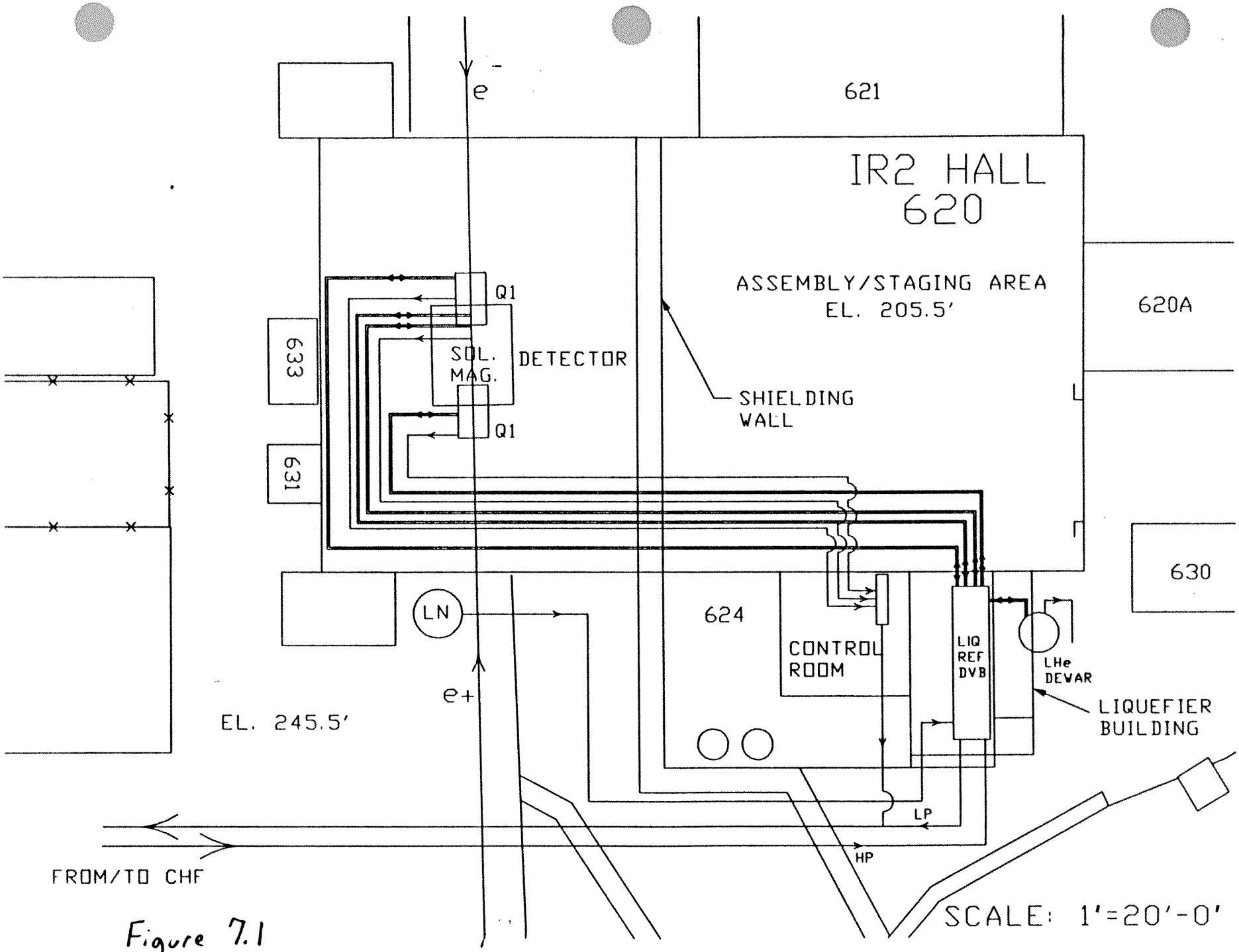
e-
621
IR2 HALL
620
ASSEMBLY/STAGING AREA
EL. 205.5'
620A
Q1
633
SOL.
MAG.
DETECTOR
SHIELDING
WALL
Q1
631
630
LN
624
CONTROL
ROOM
LIQ
REF
DVB
LHe
DEWAR
LIQUEFIER
BUILDING
e+
EL. 245.5'
LP
HP
FROM/TO CHF
SCALE: 1'=20'-0'

Figure 7.1

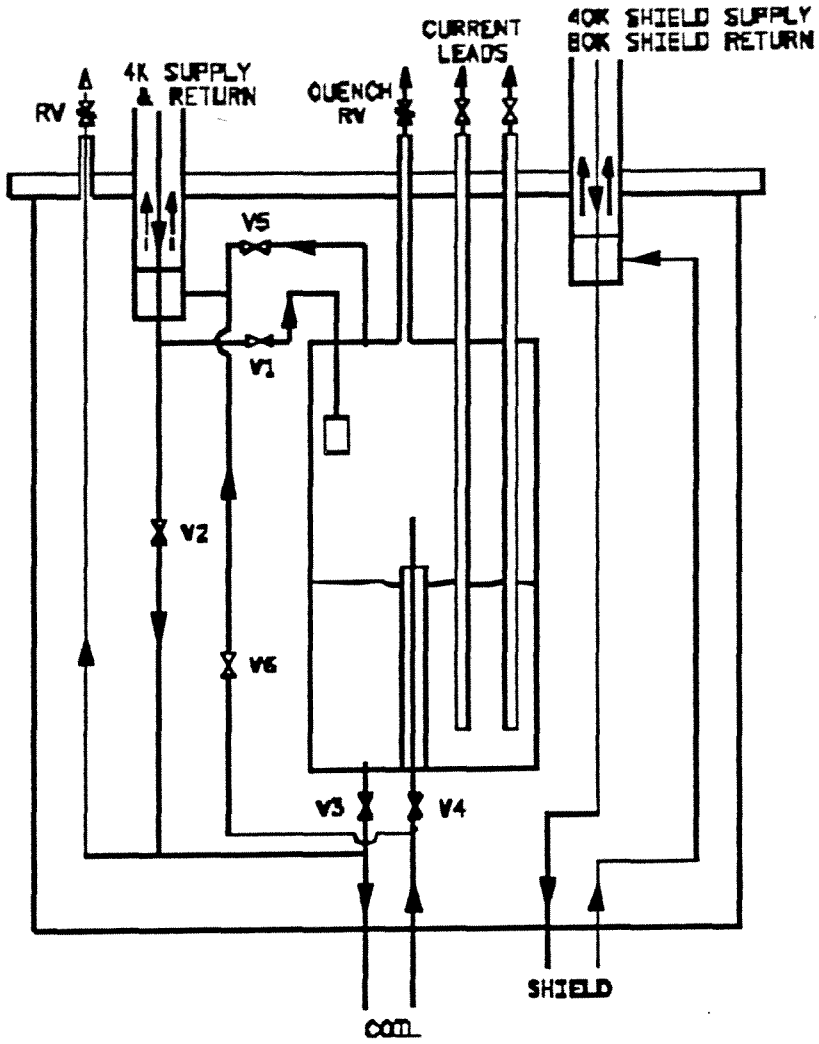

COOLDOWN
Controlled cooldown is achieved by passing progressively colder gas via the flexible 4K supply/return line from the refrigerator valve box until the coil is at a suitable temperature for LHe cooldown and fill, e.g. 40K. V2, and V6 are open; V1, V3, V4 and V5 are closed.

The coil shields are cooled down simultaneously to 40K in a similar fashion.

NORMAL OPERATION
During normal operation and LHe cooldown and fill V1, V3, V4 and V5 are open, V2 and V6 are closed.

Figure 7.3
Circuit for Controlled Solenoid Cooldown by the Refrigerator

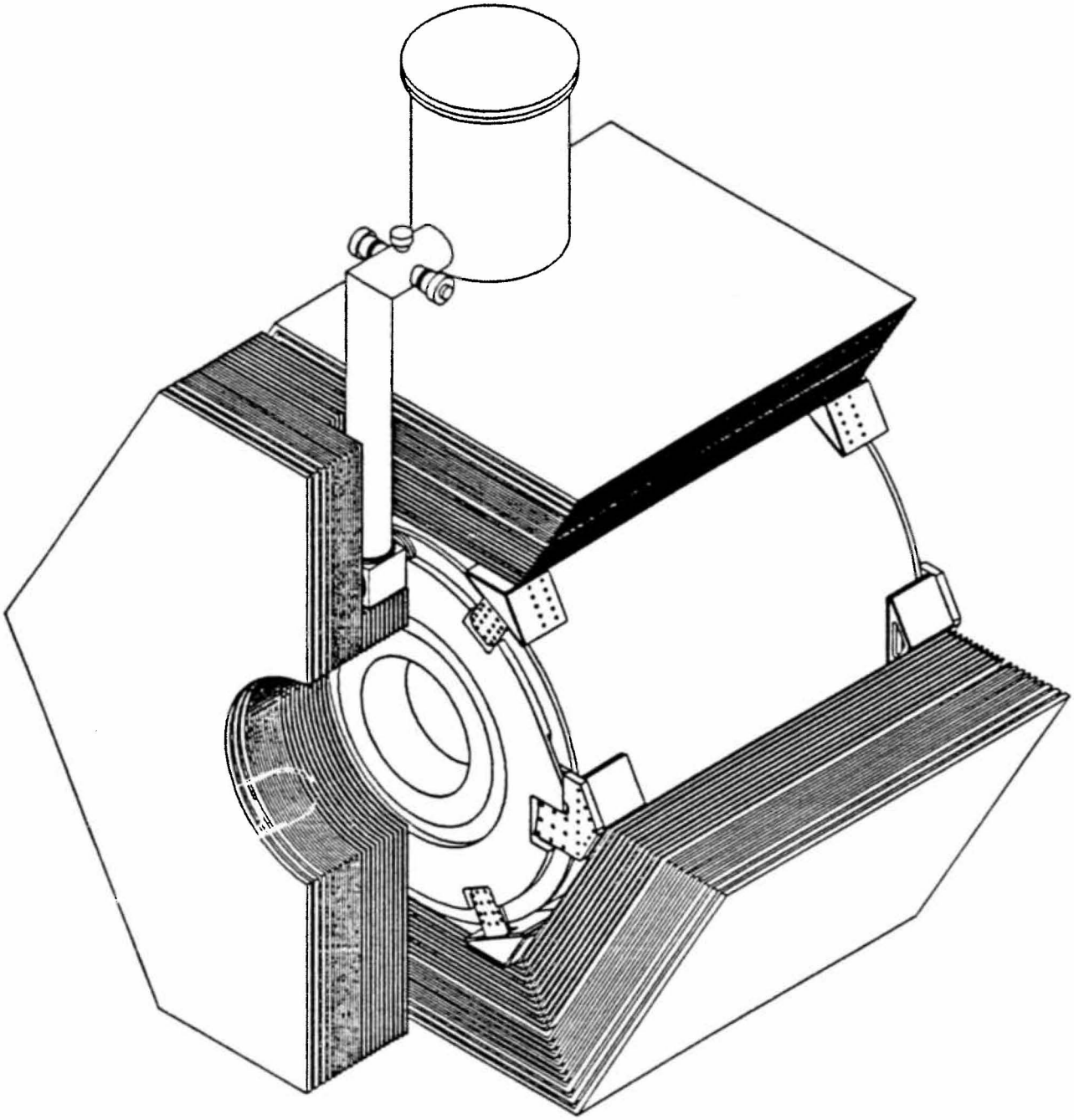

Fig 7.5

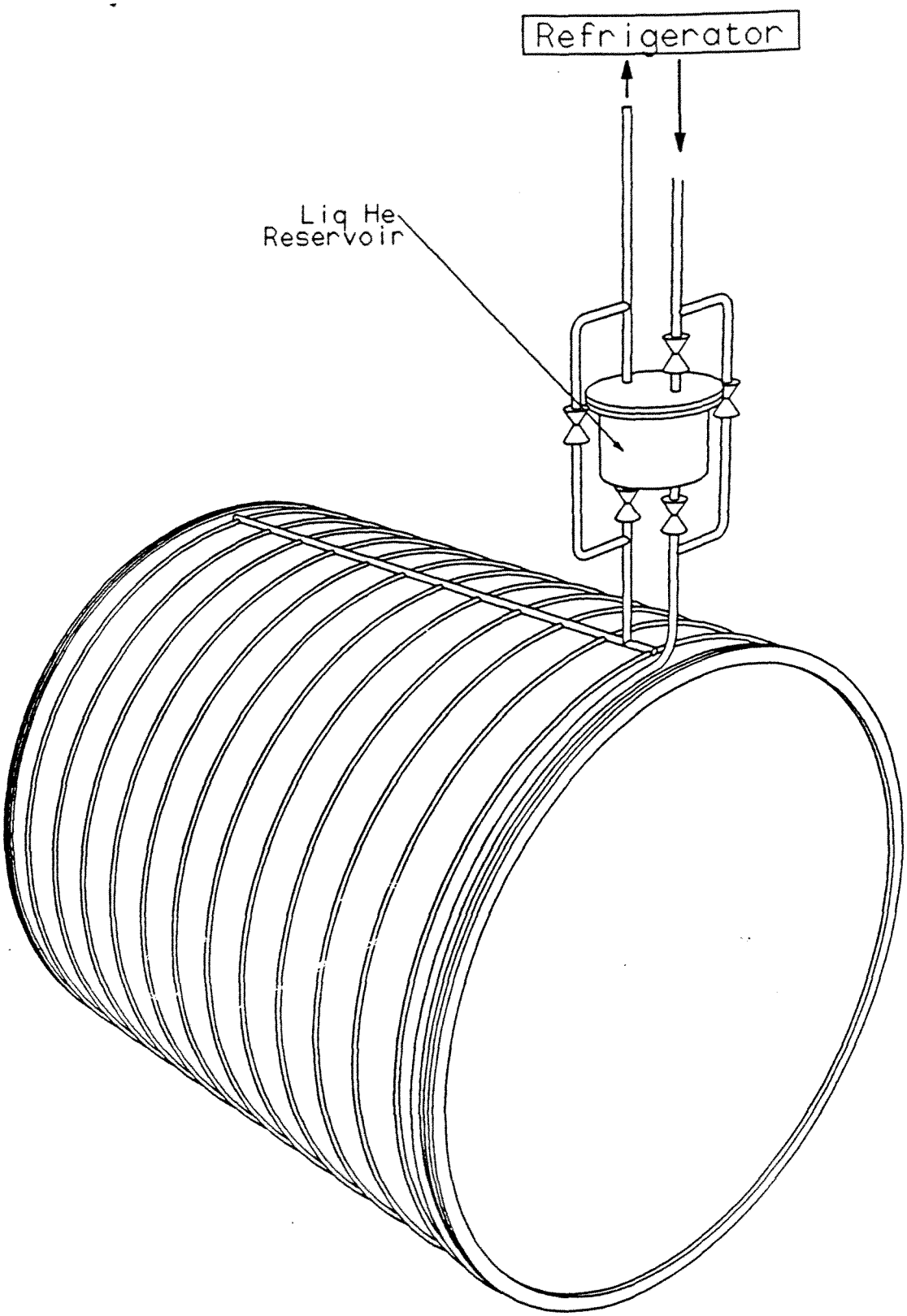

Cold Mass Cooling Concept

Fig 7.7

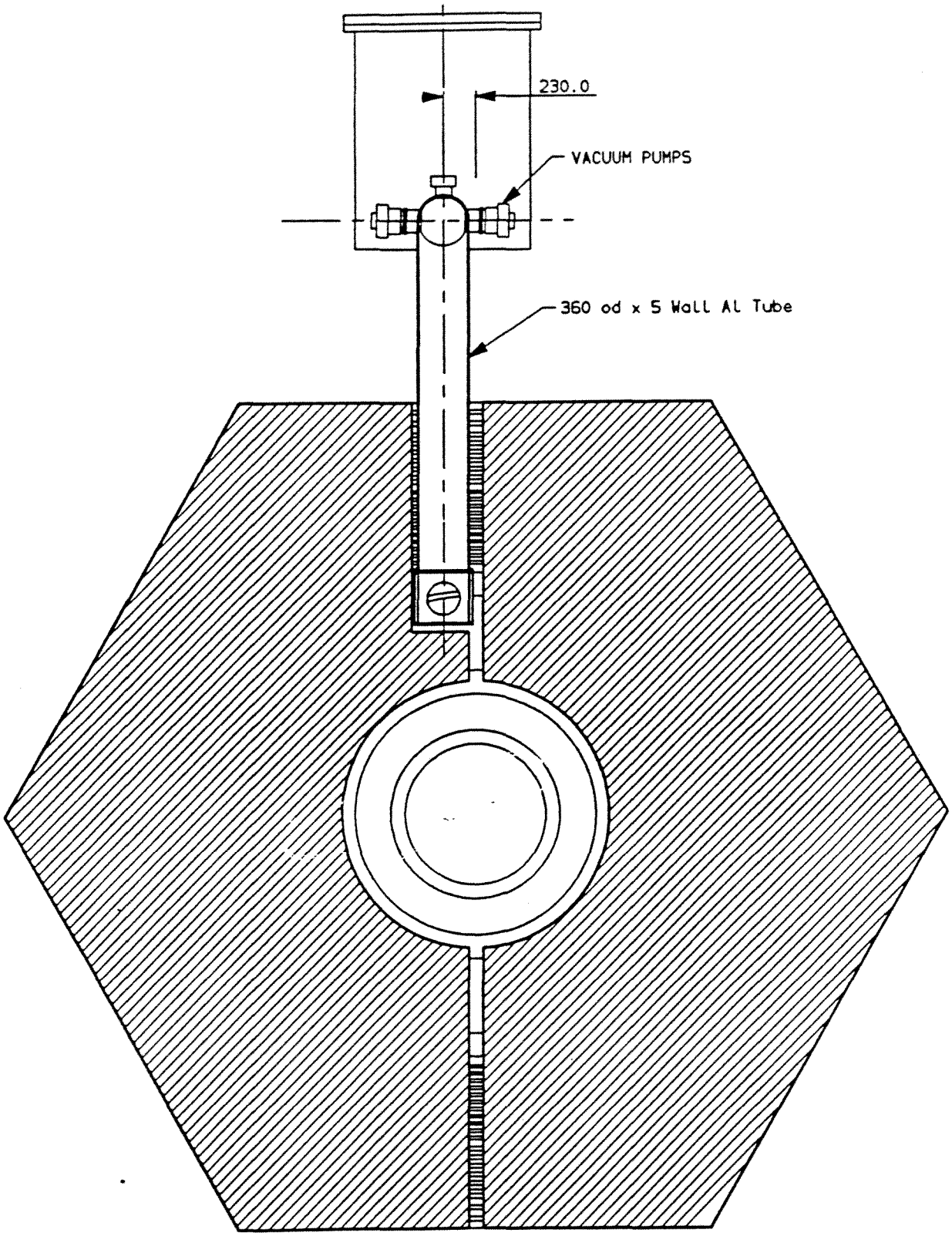

Fig 7.9

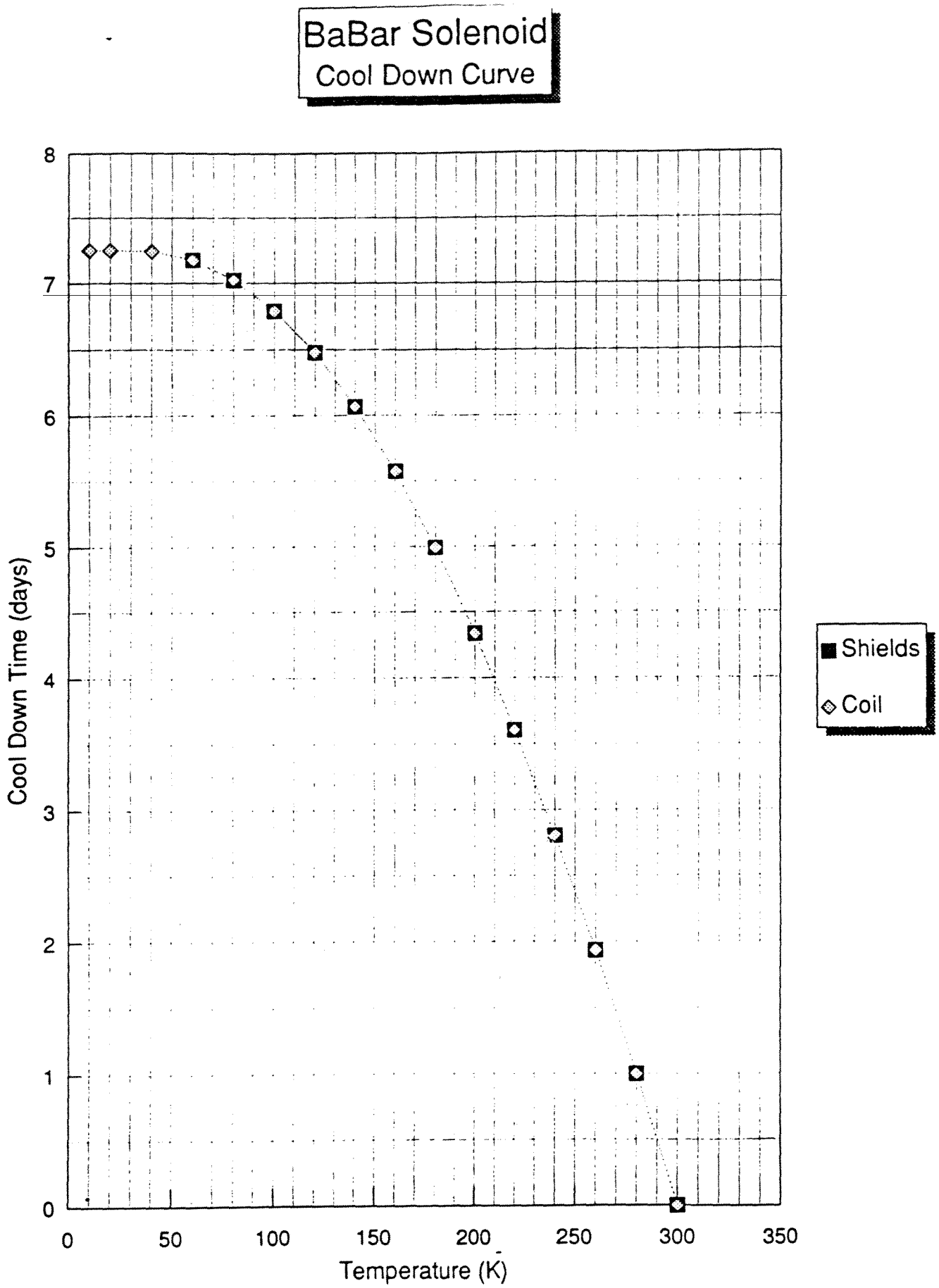
BaBar Solenoid
Cool Down Curve
Cool Down Time (days)
Temperature (K)
0
1
2
3
4
5
6
7
8
0
50
100
150
200
250
300
350
Shields
Coil

Figure 7.11.

BABAR SOLENOID CRYOGENIC DESIGN STUDY

COOL DOWN

Temperature differential during cool down (coil and shields) 40 K

RADIATION SHIELDS

Mass of shields	1.970 tonnes	1970	kg	
Total surface area		75.35	sq.m.	
Radiation heat flux		4	W/sq.m.	
Total radiation heat load at base temperature		301	W	
Radiation factor, R		3.7E-08	W/K^-4	
Heat load due to conduction at base temperature		50	W	Guess
Total heat load at base temperature		351	W	
Specific heat of helium gas		5190	J/kg	
Ambient temperature		300	K	
Average base temperature		60	K	
Temperature of incoming cold gas		40	K	
Temperature of outgoing cold gas at base temperature		80	K	
Mass flow rate at base temperature		1.7	g/s	

Mass flow rate used for shields is the mass flow rate used for the coils multiplied by the ratio of the cold masses.

COOL DOWN USING A MASS FLOW RATE OF 1.93 G/S AT AMBIENT CORRECTED FOR TEMPERATURE EFFECTS AT LOWER TEMPERATURES

Temp. (K)	C (Al) (J/kg./K)	Integ. kdT St.St. (W/m)	Heat Radiation (W)	Load Conduction (W)	Mass Flow Rate (g/s)	Gas Cooling Power (W)	Total Cooling Power (W)	Cool Down Rate (K/hr)	Cool Down Time for 20K (hr)
300	902	3060	0	0	1.93	401	401	0.81	
280	896	2740	0	0	2.02	419	419	0.86	24.0
260	869	2460	0	0	2.12	440	440	0.93	22.5
240	849	2180	0	0	2.23	464	464	1.00	20.8
220	826	1910	0	0	2.36	490	490	1.08	19.2
200	797	1660	0	0	2.51	521	521	1.20	17.6
180	760	1410	0	0	2.68	557	557	1.34	15.8
160	713	1170	0	0	2.89	600	600	1.54	13.9
140	654	939	0	0	3.14	652	652	1.82	11.9
120	580	726	0	0	3.43	712	712	2.24	9.8
100	481	528	0	0	3.86	802	802	3.05	7.6
80	357	349	0	0	3.86	802	802	4.10	5.6
60	214	198	0	0	3.86	802	802	6.85	3.7

Cool Down Time	172.3	hr	7.2 days
Cool Down Time to 100K	163.0	hr	6.8 days
Cool Down Time from 100K	16.8	hr	

COOL DOWN USING A MASS FLOW RATE OF 5 G/S AT AMBIENT CORRECTED FOR TEMPERATURE EFFECTS AT LOWER TEMPERATURES

Mass flow rate of helium 5 g/s
Gas cooling power 1038 W

Temp. (K)	C (Al) (J/kg./K)	Integ. kdT St.St. (W/m)	Heat Radiation (W)	Load Conduction (W)	Mass Flow Rate (g/s)	Gas Cooling Power (W)	Total Cooling Power (W)	Cool Down Rate (K/hr)	Cool Down Time for 20K (hr)
300	902	3060	0	0	5.00	1038	1038	0.81	
280	896	2740	0	0	5.23	1086	1086	0.86	24.0
260	869	2460	0	0	5.49	1140	1140	0.93	22.5
240	849	2180	0	0	5.78	1200	1200	1.00	20.8
220	826	1910	0	0	6.11	1268	1268	1.08	19.2
200	797	1660	0	0	6.50	1349	1349	1.20	17.6
180	760	1410	0	0	6.94	1441	1441	1.34	15.8
160	713	1170	0	0	7.48	1553	1553	1.54	13.9
140	654	939	0	0	8.13	1688	1688	1.82	11.9
120	580	726	0	0	8.88	1843	1843	2.24	9.8
100	481	528	0	0	10.00	2076	2076	3.05	7.6
80	357	349	0	0	10.00	2076	2076	4.10	5.6
60	214	198	0	0	10.00	2076	2076	6.85	3.7
40	77.5	82	23.6	5.9	10.00	2076	2046	18.64	1.6
20	8.9	16	29.1	9.3	10.00	2076	2038	161.61	0.2
10	1.4	3	29.4	10.0	10.00	2076	999	503.49	0.0

Cool Down Time 174.1 hr 7.3 days
Cool Down Time to 100K 163.0 hr 6.8 days
Cool Down Time from 100K 18.6 hr

REFRIGERATOR SPECIFICATION

Radiation Shields 351.4 W
Coil 39 W at 4.5K
Current Leads 0.75 gm/sec. (22.5 litres / hr).

Cool Down

Peak Compressor Output 14.0 gm/sec.
Peak 40K Gas Mass Flow Rate 4.0 gm/sec.
Peak 4.5K Gas Mass Flow Rate 10.0 gm/sec.

Refrigerator - Rated Power at 4.5K 141 watts

CHAPTER 8

8 VACUUM SYSTEM

8.1 Design Criteria

When designing the vacuum pumping system for the BABAR Solenoid the following criteria have to be considered:

- The system will have a large volume.
- During the initial pump down, if the system has been let up to air and when the magnet is warm there will be a high background out-gassing load 98% of which consists of water vapor.
- When the magnet is cold this out-gassing load will be negligible.
- A coating of oil will have disastrous effects on the effectiveness of multilayer superinsulation.
- The system will need to be roughed down to a relatively low pressure before the high vacuum pumps can be brought on line.
- A base pressure of at least 1×10^{-4} mbar must be attained by the high vacuum pumps before cool down can commence (Reference 1).
- The vacuum pressure will rise when the warm up of any internal component occurs.
- The high vacuum pumping system used to pump the insulating vacuum of the cryostat down to a pressure of 1×10^{-4} mbar when the system is warm must produce the necessary pumping speed **at the vacuum vessel**. This means the pumps must be connected to vacuum vessel by a pumping line which does not seriously reduce the pumping speed of the pumps themselves. In general this means a short, large diameter pumping line must be used.
- When the magnet is cold and the magnetic field is on a pumping system with a lower pumping speed could be used as the out-gassing load will be negligible.

8.2 Choice of High Vacuum Pumps

Superconducting magnets used in particle detectors have traditionally used diffusion pumps and more recently turbomolecular pumps for the insulating high vacuum of the cryostat. It is proposed to use turbomolecular pumps since used correctly they can be regarded as oil free. SLAC will be receiving a large number of them from SSC and it is intended to use whatever meets the BaBar solenoid insulating vacuum specification.

SLAC AHO 2003-032B2f17

8.6 System Operation

Referring to Figure 8.3. valves designated MV are mechanical valves and those designated SV are solenoid controlled valves. Valves MV 11/22 are normally open and capped. Valves MV 21/22 are normally open. All the solenoid controlled valves are closed when not powered. Gauges designated TC are thermocouple gauges measuring in the range 10 - 0.02 mbar and those designated PEN are Penning gauges measuring in the range $< 1 \times 10^{-3}$ mbar.

The operational sequence is as follows:

1. Rotary pumps RP 1 and RP 2 are started.
2. When the pressures on gauges TC 12/22 read less than 0.1 mbar and if the pressure on gauge TC 31 reads greater than 0.1 mbar valves SV 13/23 open and roughing down of the vacuum vessel commences.
3. When the pressures on gauge TC 31 reads less than 0.1 mbar valves SV 13/23 close and then valves SV 12/22 open.
4. When the pressures on gauges TC 12/22 read less than 0.1 mbar turbomolecular pumps TP1 and TP2 start.
5. When TP1 and TP2 reach full operational speed gate valves SV 11/21 open.
6. When the pressure measured on PEN 31 reads less than 1×10^{-4} mbar cool down can start.
7. Finally when the pressure measured on PEN 31 reads less than 1×10^{-7} mbar after cool down has started one of the valves SV 11/21 can be closed and its corresponding turbomolecular pump and backing valve can be switched off and closed respectively. The vent valve will open automatically to let the turbomolecular pump up to a predetermined pressure to prevent oil migration to the top of the pump nearest the pumping line.

8.7 Turret Valve Box

The turret valve will be connected directly to the solenoid vacuum vessel forming a common system. Under this scheme the turret valve box will not require a separate vacuum pumping system.

8.8 Transfer Lines

It is proposed that the vacuum insulation space of each of the flexible transfer lines has its own pump out port and if deemed necessary their own dedicated pumping systems. These transfer lines are the most exposed components and need to have self contained vacuum pumping systems to ensure they do not affect the safety of the magnet system.

8.9 Relief Valve

The purpose of the relief valve on the vacuum system common to the solenoid and the turret dewar is to relieve any pressure rise which might occur if a rupture occurs in the internal cryogenic system thus leading to a potentially high pressure. It is a large bore device designed to open at a differential pressure of more than ~100 mbar. Its location is shown in Figures 8.4. and 8.5.

8.10 Control System

The control system will have two modes automatic and manual.

The automatic mode will run through the sequences detailed in Section 8.6. It will be able to pick up

SLAC AHO 2003-032B2f17

8.12 Tables

Table 8.1 - System parameters of the vacuum system.	
Working volume	11 cubic meters
Surface area of multilayer insulation	2262 square meters
Surface area of aluminum alloy	300 square meters
Water vapor fraction in out-gassing load	98%
Working pressure	$< 10^{-7}$ mbar
Cool down commencement pressure	$< 10^{-4}$ mbar (See Ref. 1)
Vessel roughing pressure	< 0.1 mbar
Inner diameter of pumping line	210 mm
Internal diameter of outer pumping line with turbo pumps above the electronics platform.	~400 mm.
Length of pumping line with turbo pumps above the electronics platform.	3.4 m.
Internal diameter of outer pumping line with turbo pumps below the electronics platform.	~360 mm
Length of pumping line with turbo pumps below the electronics platform.	2.0 m
Pump down time to 1×10^{-4} mbar	200 hours

Table 8.2 - Parameters of the pumping system.	
Pumping speed of high vacuum pumps	2 X 470 litters/sec
Pumping speed of roughing pump	2 X 18 cubic meters/hr
Roughing time to 0.1 mbar. (Pump and purge 4 times)	5.5 hours
Nominal backing pressure	< 0.01 mbar
Critical backing pressure	~ 0.5 mbar
Maximum steady state turbo inlet pressure for effective use.	~ 0.05 mbar
Diameter of roughing line	40 mm
Diameter of backing line	40 mm
Length of roughing line	~5 meters
Length of backing line	~5 meters

SLAC AHO 2003-032B2f17

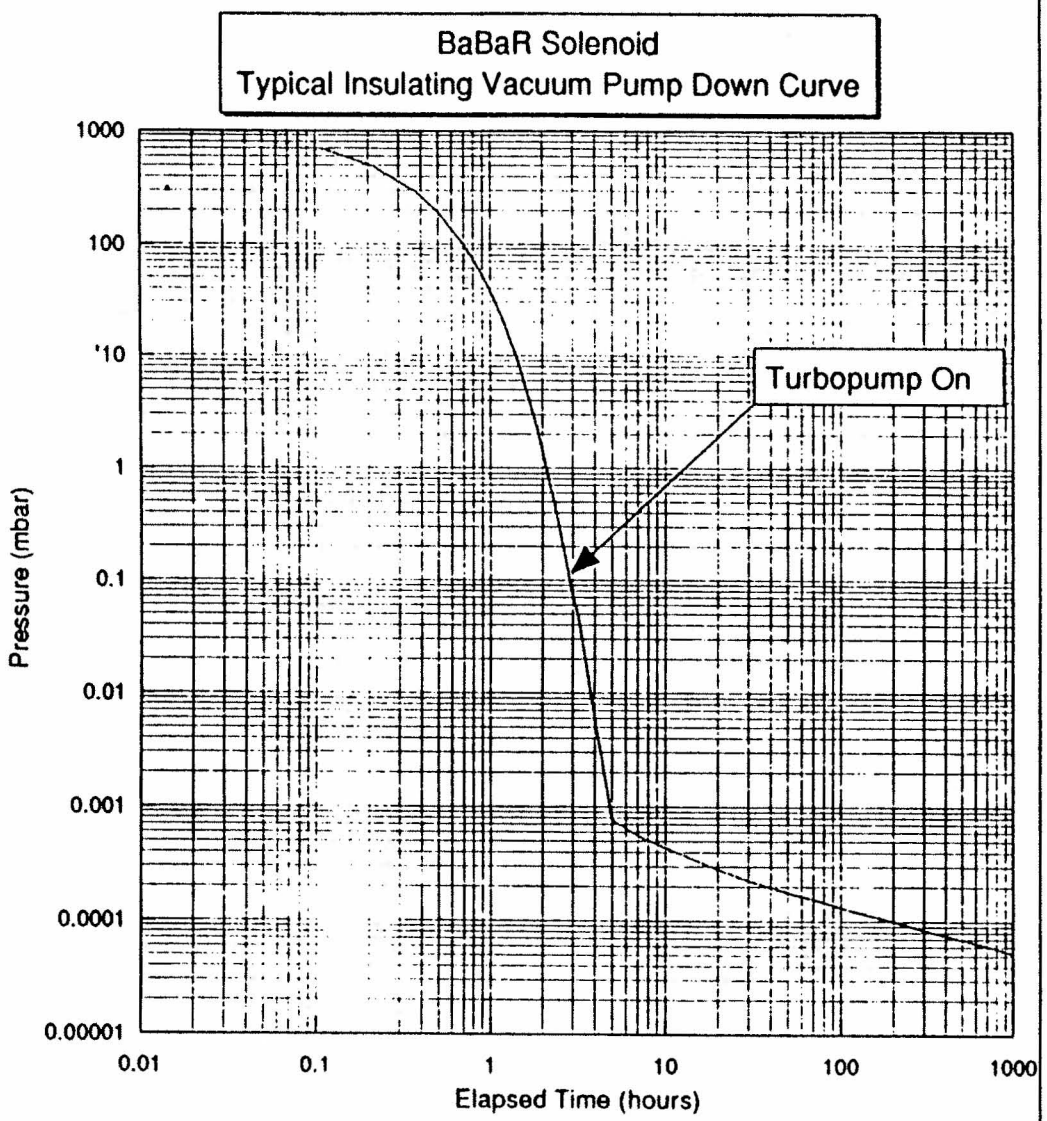
BaBaR Solenoid
Typical Insulating Vacuum Pump Down Curve
Turbopump On
Pressure (mbar)
1000
100
'10
1
0.1
0.01
0.001
0.0001
0.00001
0.01
0.1
1
10
100
1000
Elapsed Time (hours)

Figure 8.2.

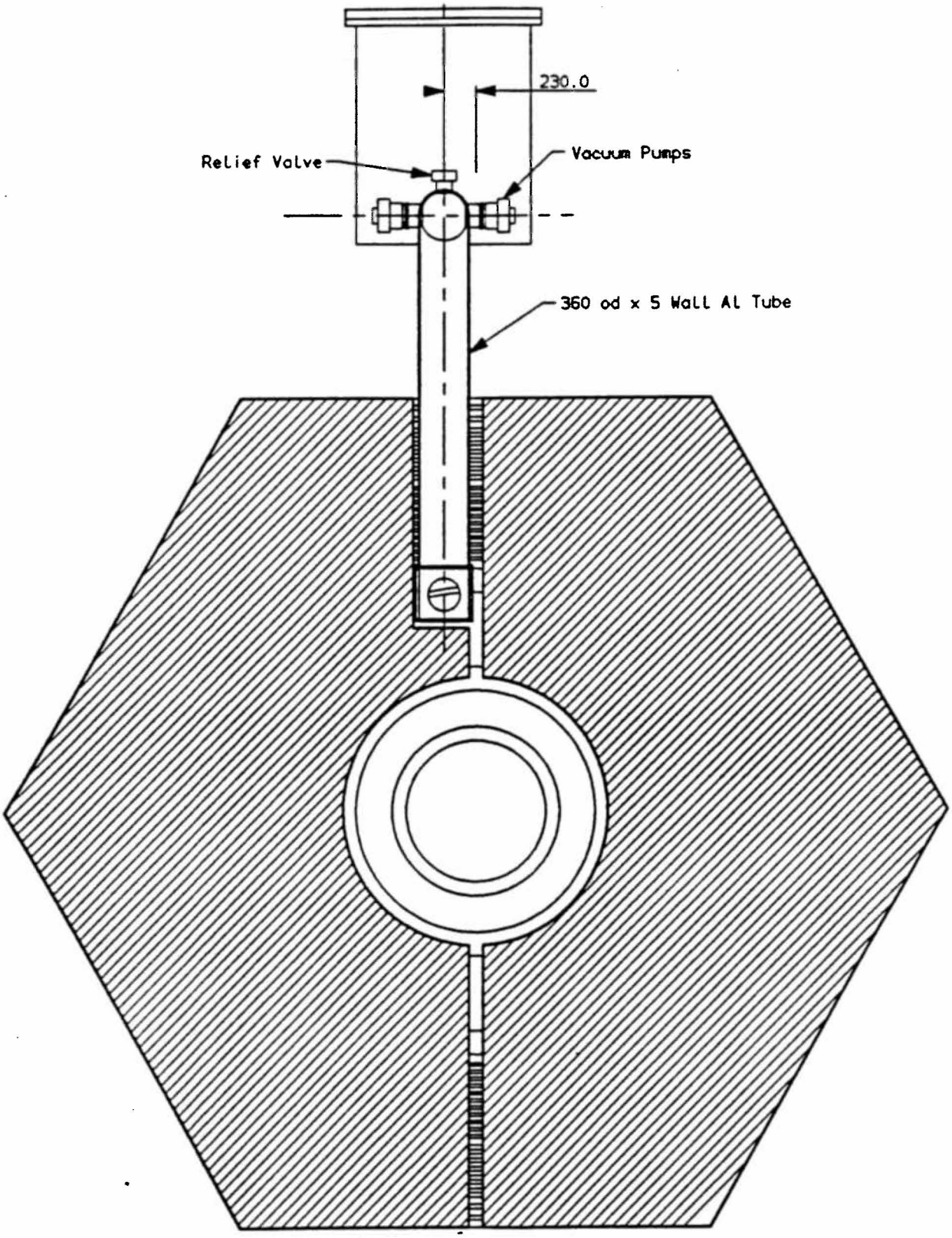

Fig 8.4

CHAPTER 9

9. DC POWERING AND QUENCH PROTECTION

9.1 CONCEPT

The DC power and quench protection concept is shown in figure 9.1.

The solenoid will be powered from a 7.5kA DC power supply with sufficient voltage capacity to ramp a full field in 30 minutes.

Two modes of discharge are incorporated in the circuit shown in figure 9.1.

1. Slow Dump Discharge Circuit

   Slow discharge - normal ramp down of the current - will be initiated by opening CB1. This will allow the solenoid to discharge through the diode/slow dump resistor combination. This passive type of circuit allows controlled ramp down of the solenoid current under power failure conditions i.e. loss of main power supply. Clearly it is also possible to ramp down the solenoid field by reversing the power supply but this would probably initiate a fast dump (quench) in the event of a mains power failure.

2. Fast Dump (Quench) Discharge Circuit

   Fast discharge will be initiated by opening the linked circuit breaker system CB2 allowing the solenoid to discharge through the fast dump resistor. Fast discharge parameters are given in Table 9.1. The fast discharge concept is based on two main criteria:

   i. A voltage limit of 500 volts across the solenoid during fast discharge. Center-tapping of the fast dump resistor will limit the voltage to ground to 250V. The center-tapped resistor will also allow the measurement of earth leakage currents as a safety and diagnostic tool.

   ii. The protection concept is based on an upper temperature limit of 100K for the cold mass under quench conditions. This limit will give a very good safety margin against peak temperature rise and thermally induced stresses at quench.

Fast discharge of the solenoid will be initiated by the quench detection system or by certain interlocks designed to protect the overall solenoid system.

SLAC AHO 2003-032B2f17

for aluminum with a resistivity ratio RRR = 500.

This highly conservative adiabatic approach yields hot spot temperatures which are within the design criteria.

9.2.2 Quench Analysis

A quench analysis of the BABAR solenoid has been made using a code developed for the DELPHI Solenoid design. The code models the thermal and inductive behavior of the solenoid in order to take into account the effects of the quench back and heat transfer to the support cylinder.

The code has been used to model a number of quench scenarios and demonstrate that the BABAR Solenoid is conservative.

9.2.2.1 Quench Code Outline

Normal Zone Propagation

In order to simplify the modeling the normal region growth is assumed to be one dimensional i.e. the initial normal zone is assumed to occupy the full coil circumference - this is a reasonable assumption for such a solenoid.

Thermal Model

It is assumed that the coil is thermally bonded to the force support cylinder.

For any coil element the temperature is described by the heat balance equation:

$$C(\theta)\,\frac{d\theta}{\partial t} = Gc - Hc$$

where $C(\theta)$ is heat capacity of the coil elements.
Gc is heat generation in the coil
Hc is heat transfer to the shell

For any shell element the temperature variation is described by the heat balance equation:

$$C\,\frac{d\theta}{\partial t} = Gs - Hs$$

where Gs is inductive heat generated in the shell
Hs is heat transferred to the coil

Cooling of the shell during a quench is neglected.

Electro-magnetic Model

The support shell is represented as a shorted secondary winding with close inductive coupling to the main coil. The dump resistor and shell resistance are assumed to be constant with temperature while for the coil conductor temperature dependence of resistivity is included fully.

Numerical Modeling

The electro-magnetic and thermal models are solved by numerical integration.

SLAC AHO 2003-032B2f17

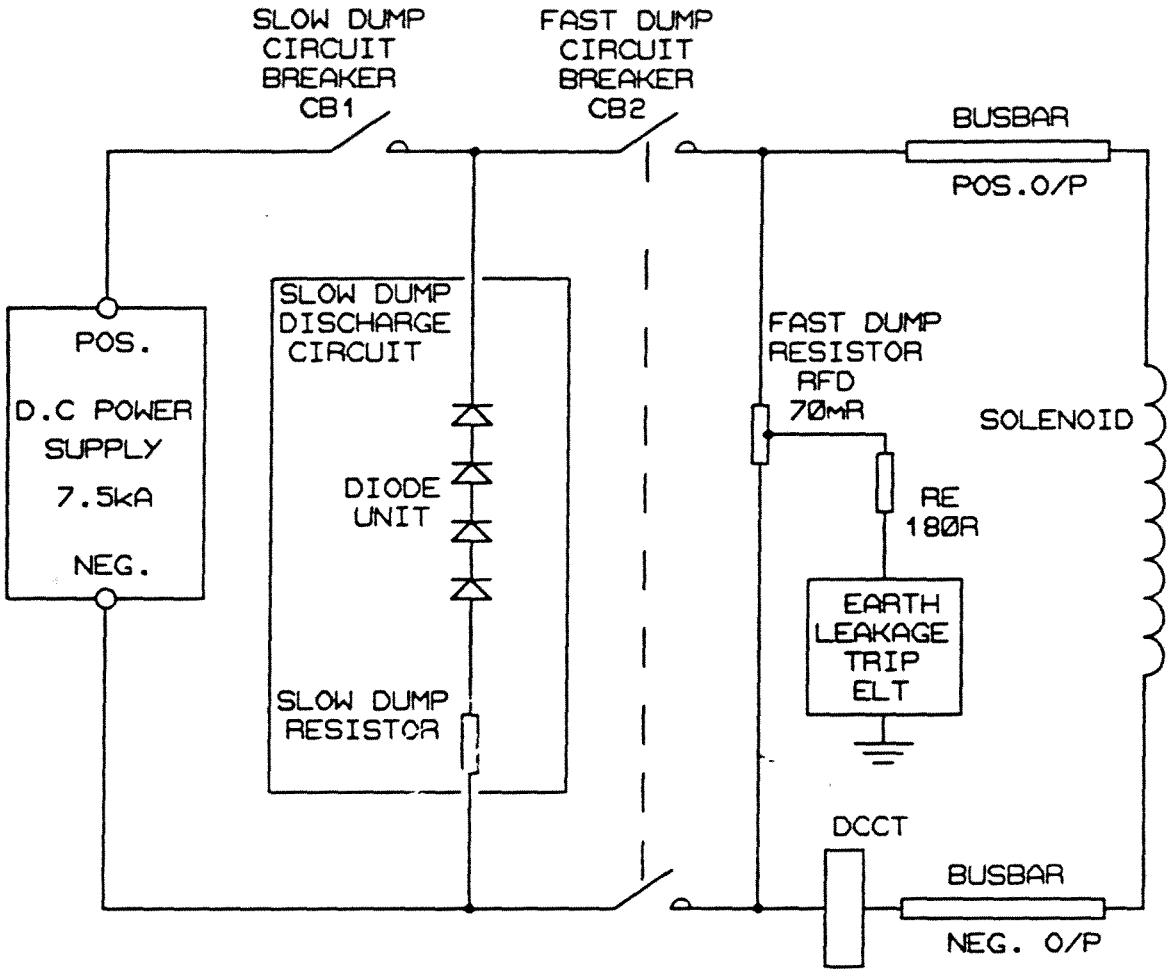

FIG. 9.1 D.C. POWER & QUENCH PROTECTION CONCEPT

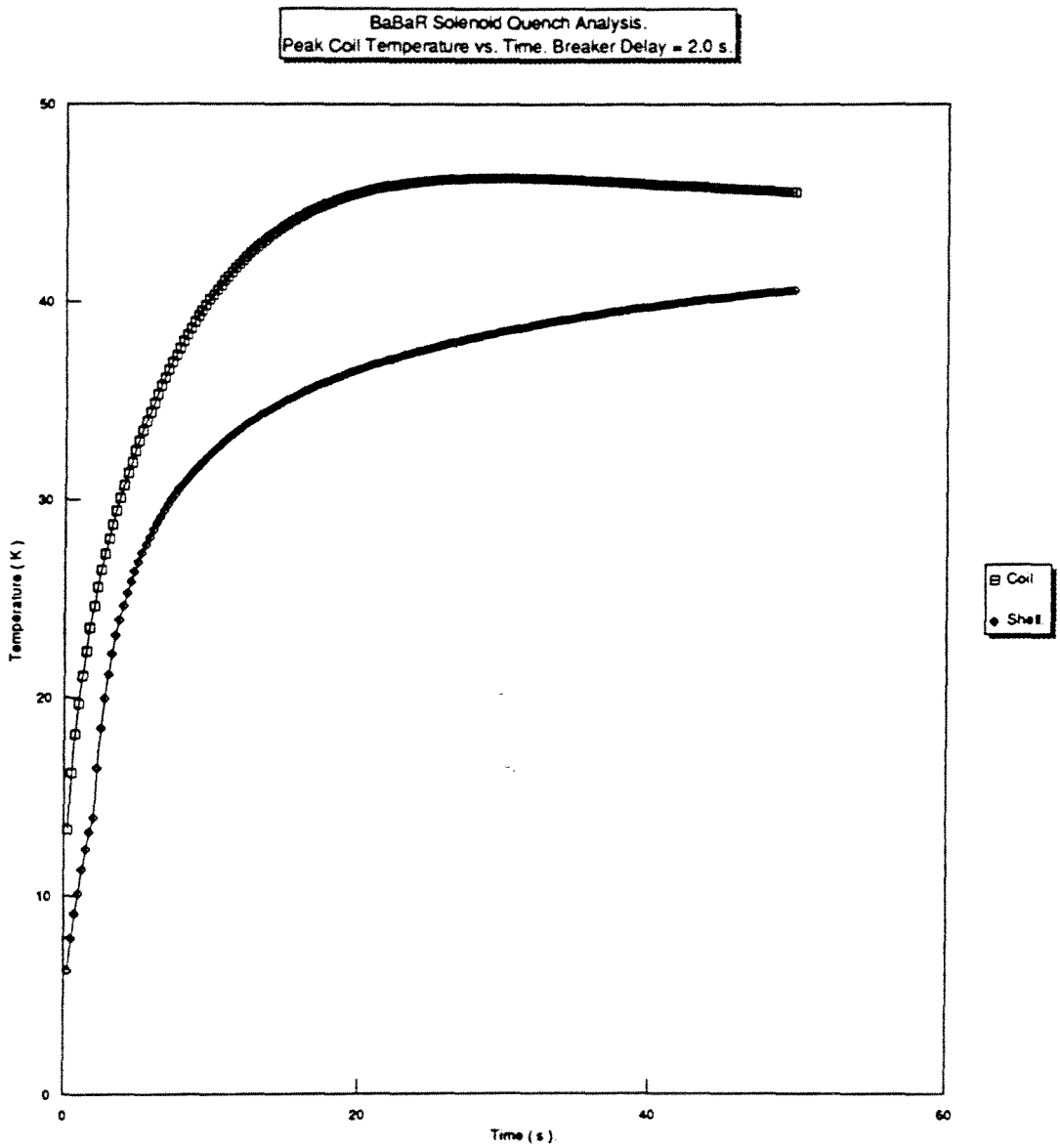

Figure 9.3 Rutherford Appleton Laboratory. File : FIG_9-3.WK4.

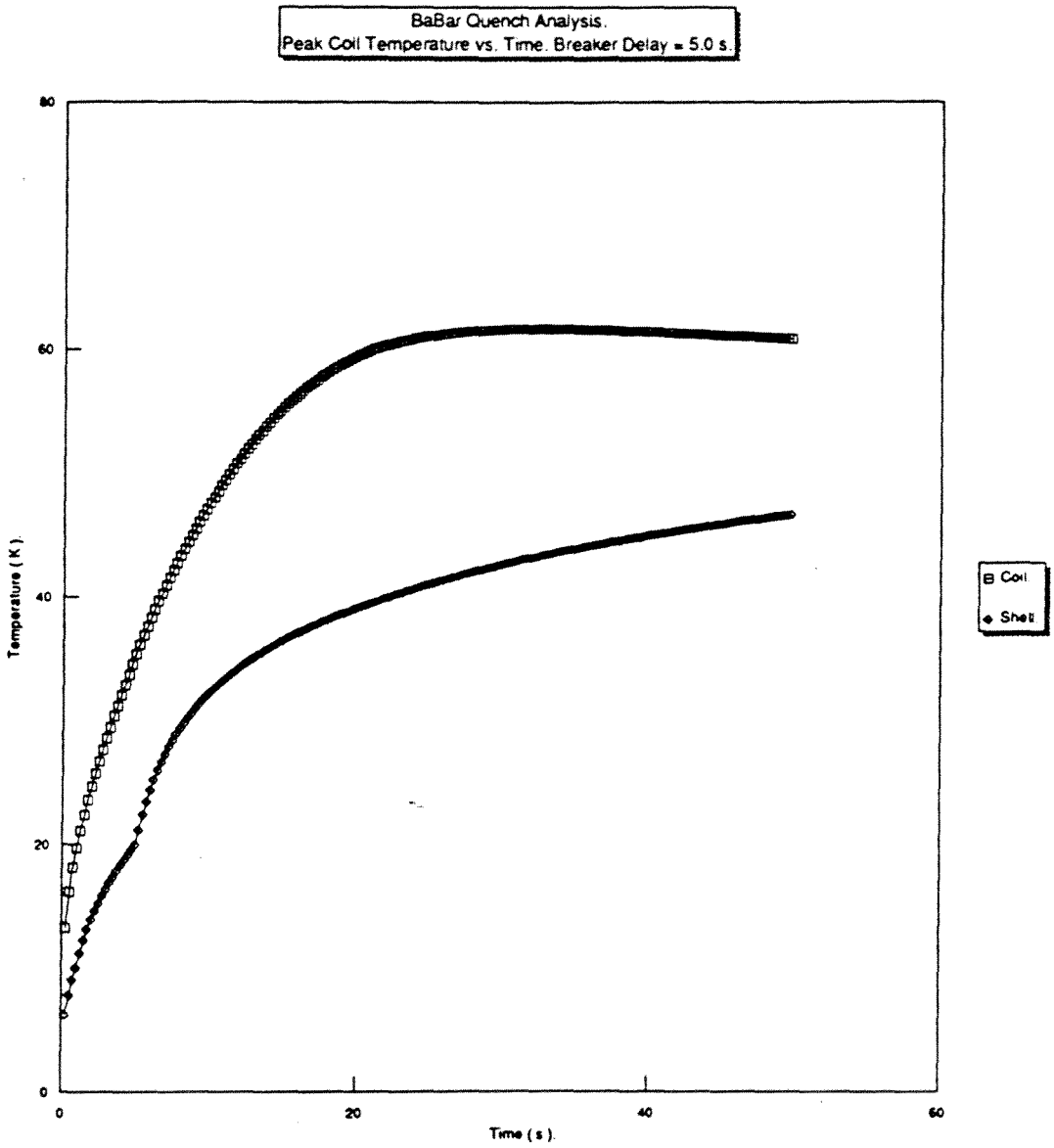

Figure 9.5 Rutherford Appleton Laboratory. File : FIG_9-5.WK4.

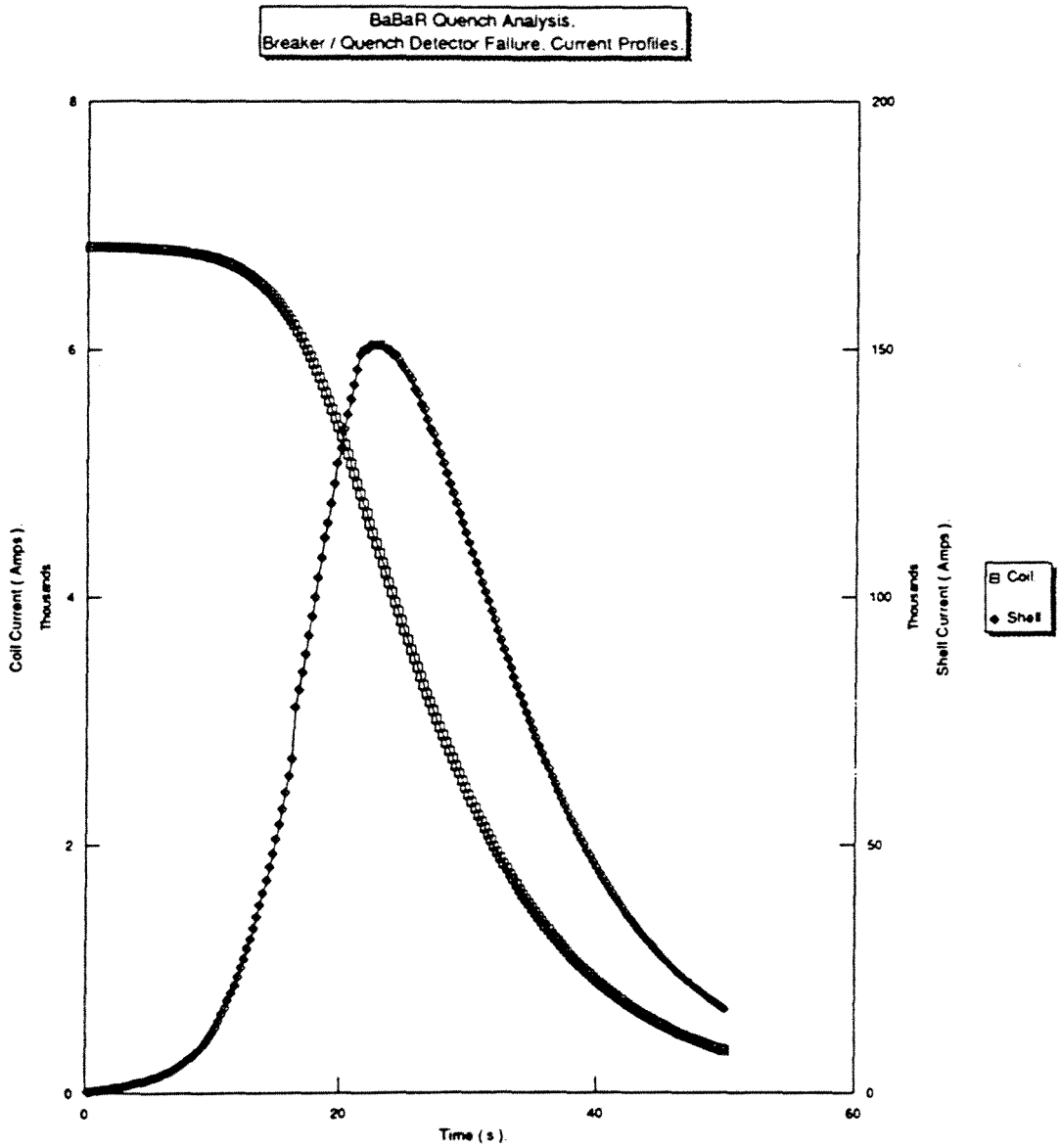

Figure 9.7 Rutherford Appleton Laboratory. File : FIG_9-7.WK4.

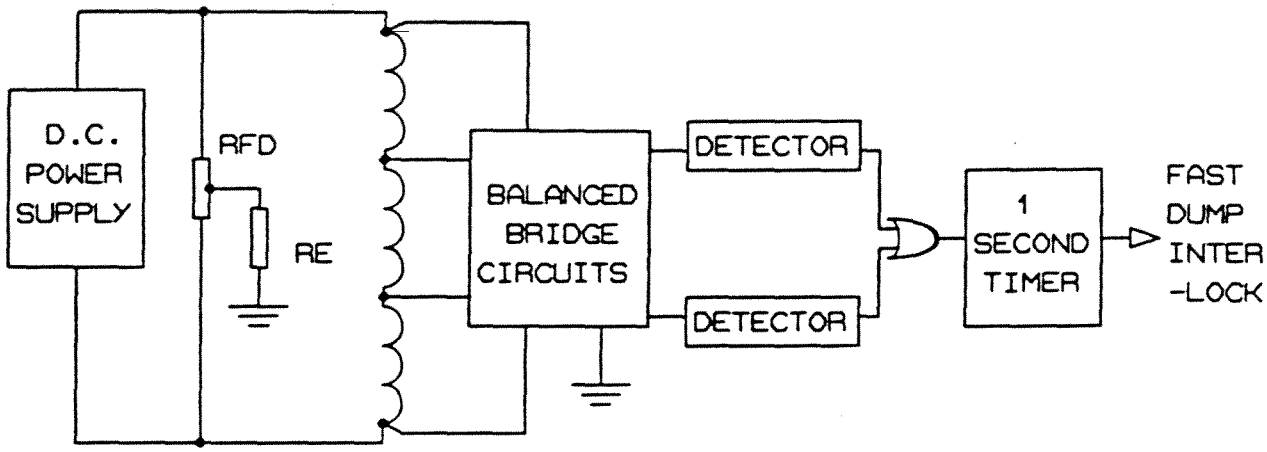

a) TAPPED WINDING BRIDGE LAYOUT

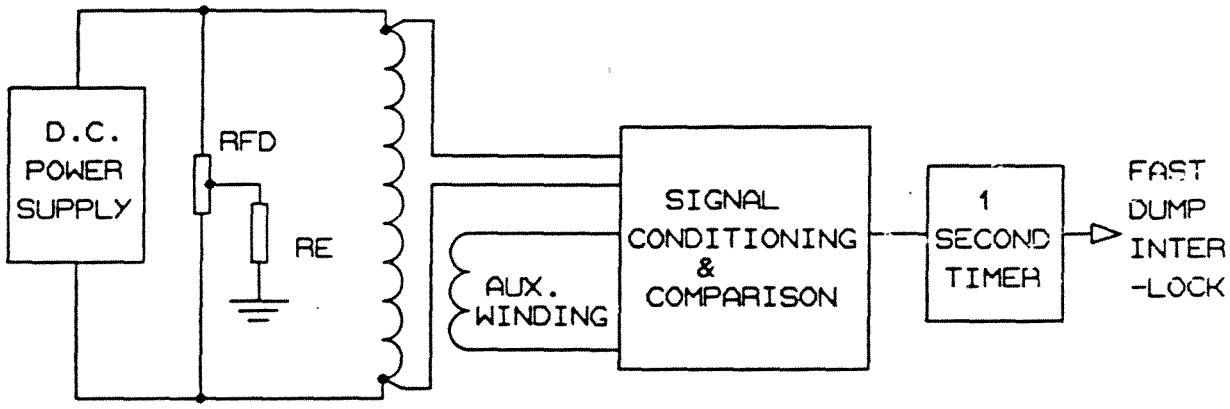

b) DIRECT MEASUREMENT WITH
RATE COMPENSATION

FIG. 9.9 QUENCH DETECTION SYSTEM

- outlet of cooling

This will allow full checking of coil temperatures during cooldown and operation. These transducers will be used for initial commissioning and diagnostics and a selected number ~4 will be logged during normal operation.

10.2.1.2 Radiation Shield Temperature

Temperature transducers will be installed on the radiation shields for commissioning, diagnostics and for control purposes.

The transducer package can be a single 1000Ω PRT.

Approximately 16 transducers will be installed on the radiation shield.

Temperature transducers will be installed as a package with protective covers and heat-sinking of leads.

10.2.2 Force/Loads

Forces/loads will be monitored using strain gauges. These will be applied to all cold mass supports and restraints - axial and lateral.

Force transducers will be used mainly in commissioning although certain transducers will be logged on a long-term basis and used for control purposes through links to interlocks.

10.2.3 Voltages/Currents

Solenoid current will be monitored using a DCCT and will be logged on a continuous basis.

Voltages will be measured on:
- current leads
- coil for protection/detection
- busbars

10.2.4 Cryogen Flow

Mass flow meters will be included in the cryogen system for monitoring and cooldown control. This will include mass flow rates for gaseous helium and pumped liquid helium.

Pressures - cryogenic systems will include pressure measurement for setting up and monitoring.

10.2.5 Magnetic Fields

The solenoid will be equipped with hall probes to measure and monitor fields within the structure.

10.2.6 Position Sensors

Position sensors may be included to accurately monitor the position of the cold mass and the solenoid.

10.3 TRANSDUCER LISTING

Table 10.1 gives an outline listing of the transducers, function and location.

10.4 MONITORING AND CONTROL

The control and monitoring system should be set up to allow adequate diagnostics at subsystem level for commissioning purposes.

SLAC AHO 2003-032B2f17

BARBAR SOLENOID
Instrumentation Listing

	Cryostat	Cold Mass	Cold Mass Supports	Axial Force Supports	Cold Mass Cooling Circuit	Radiation Shields	Current Leads	Bus Bars	Chimney	Turret Dewar	Totals
Temperature											
PRT 1000 Ohm		6			8	8	6		4	8	40
Carbon Resistor 220 Ohm		6			8		4		4	8	30
Temperature IC		1			1	1				2	5
Temperature Indicator		1			1	1					3
Differential Temperature IC		1			1	1					3
Forces											
Strain Gauge Bridge			8	6							14
Voltage											
Voltage Tapping		4					4	4	4	4	20
Voltage Indicator							2				2
Current											
Current IC							1				1
Cryogens											
Mass Flow IC					2	2	2				6
Pressure IC							1			1	2
Liquid Level										1	1
Carbon Resistor										10	10
SC Level Gauge										4	4
IC										2	2
Magnetic Field											
Hall Probes	10										10
Position											
Position Indicator	6	6									12

IC = Indicator/Controller

Table 10.1 gives an outline listing of the transducers, function and location.

SLAC AHO 2003-032B2f17

CHAPTER 11

11. INTERFACES

11.1 SPACE

The limiting volume occupied by the coil is that shown in figure 11.1, plus that occupied by the external supports and the chimney. Space is very tight in the vicinity of the four main support brackets, which may need redesigning once the earthquake criteria are more accurately defined. If large flanges are used on the inner detector, as we have assumed (figure 11.1), then it is not clear how the cabling from the inner detector will be routed out.

11.2 STRUCTURAL

The design of the external supports is linked to that of the iron yoke. For example, it would appear that the 1" thick plates in the regions where the main support brackets attach (see figure 6.1) are probably not sufficiently strong or stiff to support the earthquake loads. For this reason we have not used a lot of effort to analyze the design of the main brackets.

A suggested way forward would be to define the solenoid interface such that the solenoid includes the plates fastened to the end flange, but the rest of the support brackets are left as the responsibility of the BABAR team.

The interface between the inner detector end plates and the solenoid end flanges needs to be defined. We have looked at the way the axial load is passed into the solenoid (figure 5.3). Our calculations (section 5, table 5.2, cases 4a and 4b) suggest that the axial load may be put onto the vessel anywhere on the end flanges, provided it is reasonably well spread around the circumference.

We recommend that the design of the end plates for the inner detectors (figure 11.2) be progressed, as our simple calculations suggested there may be high stresses present.

11.3 ELECTRICAL/CONTROL

The detailed electrical and control interfaces remain to be defined. At this stage the interface between the solenoid and the ancillary equipment is at the top of the turret dewar.

The solenoid control system should incorporate the necessary interfaces to link the solenoid to the cryogenic electrical and vacuum systems.

11.4 CRYOGENICS

The physical interface of the solenoid to the BABAR cryogenics plant is defined at the top plate of the turret dewar for the purposes of their design study. In practice the interface will need to be carefully defined to take account of all operational and fault conditions - quench, power failure, refrigeration failure etc.

SLAC AHO 2003-032B2f17

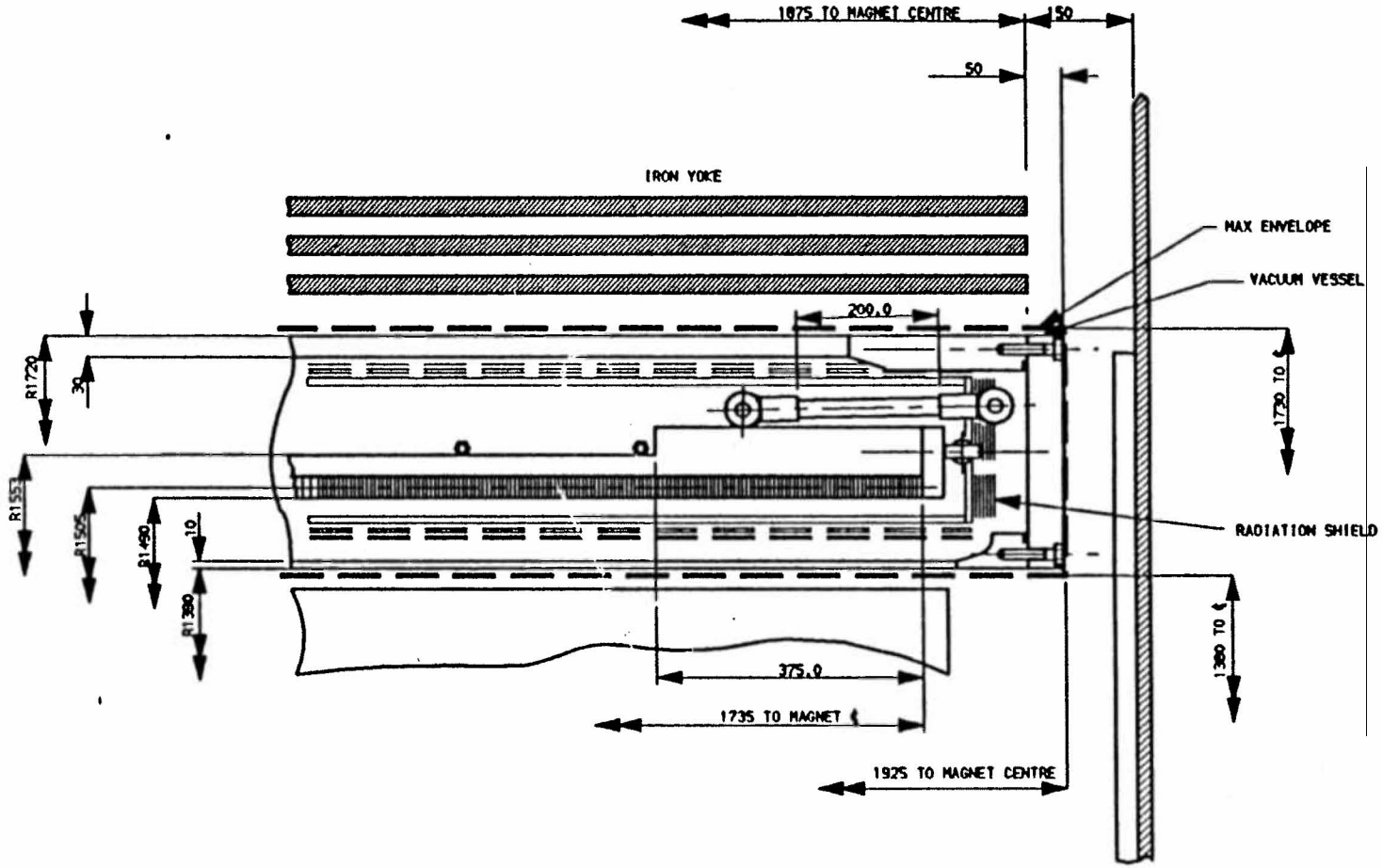

Fig 11.1 Interface Dimensions

SLAC AHO 2003-032B2f17

CHAPTER 12

12 ASSEMBLY, TRANSPORT AND INSTALLATION

12.1 ASSEMBLY OF THE COIL AND TESTS

The coil will be assembled inside the cryostat at the manufacturers and the electrical and hydraulic connections made at the chimney, so that the coil can be tested before shipping.

A complete cooldown will be carried out from room temperature to the operating temperature of 4.5K. The cooldown will allow checking of cooldown time, temperature control, heat loads and full operation of sensors.

A magnetic test will be performed at low field (30% of the operating current) to check superconductor operation, the joint resistance and the additional losses due to the energization.

12.2 TRANSPORT

Before delivering the magnet, after the tests at the factory, the end flanges could be dismounted to allow a hard connection of the cold mass to the cryostat walls. Depending on the transport facilities, the chimney could require to be dismounted too. In this case the electrical and hydraulic connection must be disconnected and protected against breakage.

SLAC AHO 2003-032B2f17

APPENDIX B

B. MATERIAL PROPERTIES

TABLE B.1 - Mechanical and physical properties of some aluminum alloys

Material	Temp K	Yield MPa	Tensile MPa	Elong. %	Weld-ability	Young GPa	Therm. Conduct. $Wm^{-1}K^{-1}$	Electr. Resist. μW cm
5083	295	235	335	15	Excell.	71.5	120	5.66
	77	274	455	31.5		80.2	55	3.32
	4	279	591	29		80.9	3.3	3.03
6061	295	291	309	16.5	Good	70.1		3.94
	77	337	402	23		77.2		1.66
	4	379	483	25.5		77.7		1.38
2219	295	371	466	11	readily	77.4	120	5.7
	77	440	568	14		85.1	56	
	4	484	659	15		85.7	3	2.9

SLAC AHO 2003-032B2f17

TABLE B.3 - RADIATION LENGTH

Component		Thickness (mm)	N I L
Cryostat Al inner wall		10	0.0255
Cryostat Al outer wall		30	0.0765
Al shields		20	0.051
Al stabilizer		32	0.0816
NbTi/Cu	min	-	-
	max	9	0.06
Al cylinder	min	30	0.0765
	max	70	0.1785
Insulation		2	-
Total	min		0.31
	max		0.47

SLAC AHO 2003-032B2f17

band 1	0.405m	1.73MPa
band 2	0.24425m	1.52MPa
band 3	0.24425m	1.4MPa
band 4	0.288m	0.859MPa
band 5	0.288m	0.7515MPa
band 6	0.288m	0.73MPa
band 7	0.288m	0.73MPa
band 8	0.288m	0.7515MPa
band 9	0.288m	0.859MPa
band 10	0.24425m	1.4MPa
band 11	0.24425m	1.52MPa
band 12	0.405m	1.73MPa

The other loads varied from case to case and are detailed below with the results.

C.3 RESULTS

Maximum displacements and Von Mises stresses are given for each case. The plots show the displacements and Von Mises stresses. They show the Von Mises stress at whichever surface of the element gives the largest stress. The largest stresses and displacements are due to the radial magnetic pressure. This is at a maximum near the ends of the coil, but because the ends of the support cylinder are thickened the maximum stress and displacements occur near this thickened region thus producing the patterns of the form shown in the plots.

i. Loadcase c1
This case had additional axial loads of 20 tonnes plus 1.2g.
Maximum displacement 0.86mm
Maximum Von Mises stress: 38.7MPa

ii. Loadcase c2
This case had additional sideways loads of 20 tonnes plus 1.2g.
Maximum displacement : 1.04mm
Maximum Von Mises stress : 39.6MPa

iii. Loadcase c3
This case had additional vertical loads of 20 tonnes plus 2g.
Maximum displacement : 1.13mm
Maximum Von Mises stress : 39.9MPa

iv. Loadcase c4
This case had additional vertical loads of 20 tonnes:
Maximum displacement : 1.02mm
Maximum Von Mises stress : 39.5MPa

v. Loadcase c5
This case had additional vertical loads of 2g plus 20 tonnes at 45° to the vertical:
Maximum displacement : 1.13mm
Maximum Von Mises stress : 39.9MPa

vi. Loadcase c6

SLAC AHO 2003-032B2f17

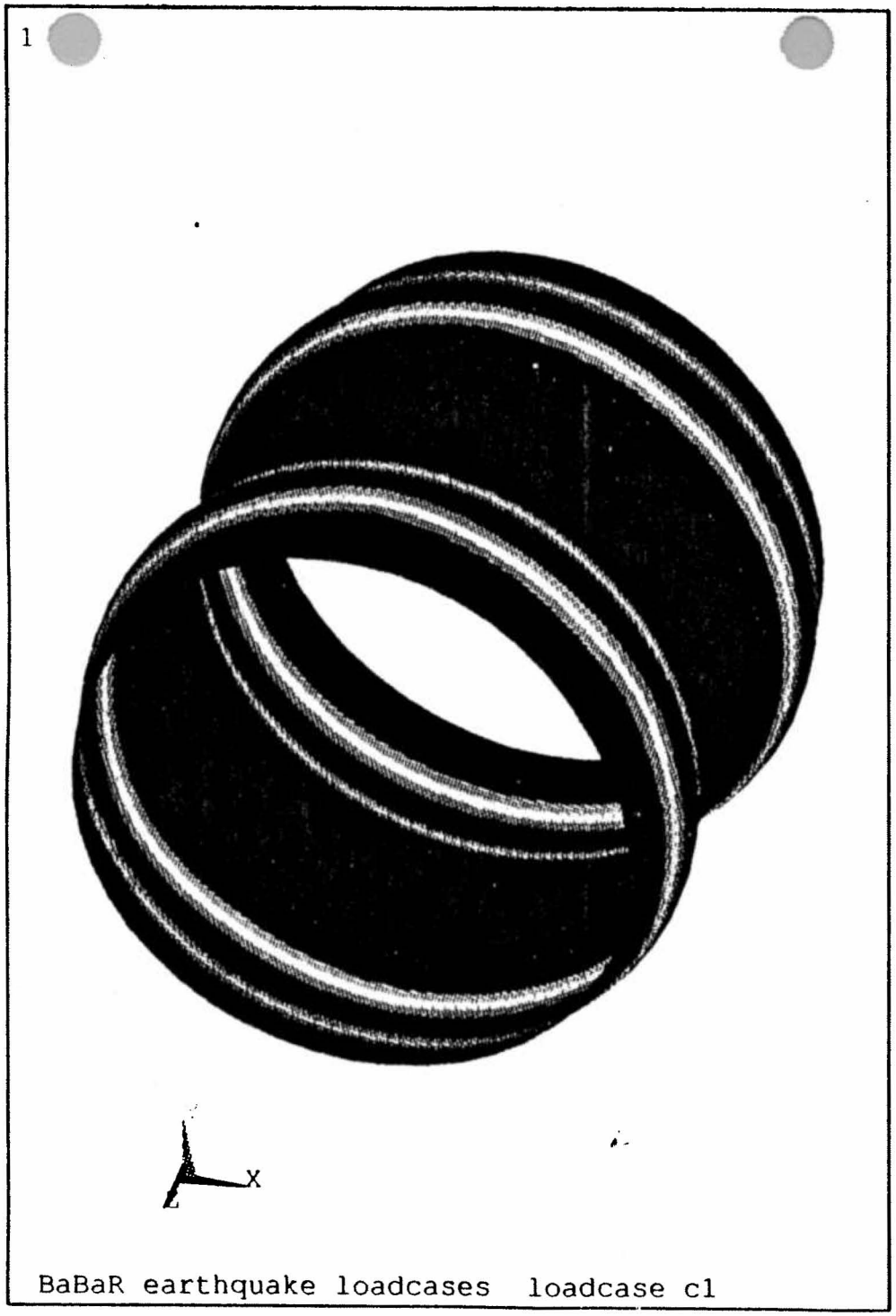

ANSYS 5.0 A
MAY 17 1995
13:59:23
PLOT NO. 1
ELEMENT SOLUTION
STEP=1
SUB =1
TIME=1
SEQV (NOAVG)
TOP
DMX =0.862E-03
SMN =0.136E+08
SMNB=0.114E+08
SMX =0.387E+08
SMXB=0.411E+08

0.136E+08
0.164E+08
0.192E+08
0.220E+08
0.248E+08
0.276E+08
0.304E+08
0.332E+08
0.359E+08
0.387E+08

APPENDIX C. Fig. C1

Stresses (Von Mises Equivalent) for Load Case 1. Max. value 38.7 MPa

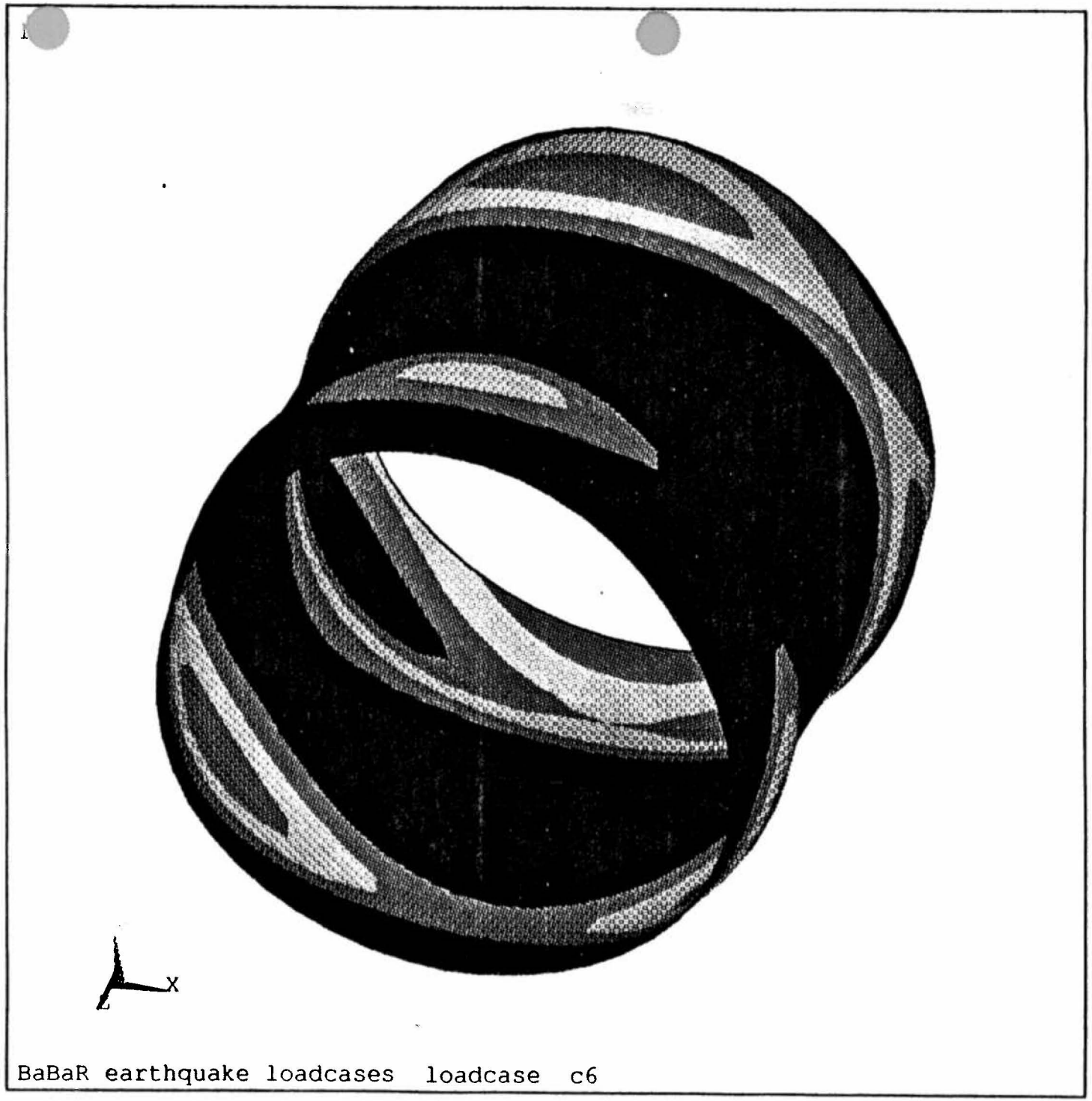

APPENDIX C. Fig. C3

Displacements (Vector Sum)

for Load Case 6.

Max. value 1.2mm.

SLAC AHO 2003-032B2f17

iii. Loadcase v3a
This case had additional sideways load of 1.2g in the +X direction.
Maximum displacement : 1.47mm
Maximum Von Mises stress : 40.6 MPa
The general level of Von Mises stress was less than 23MPa.

iv. Loadcase v3b
This case had additional sideways load of 1.2g in the -X direction.
Maximum displacement : 1.72mm
Maximum Von Mises stress : 58.6MPa
The general level of Von Mises stress was less than 20MPa.

v. Loadcase v4a
This case had an additional load of 60 tonnes distributed at the middle of the -Z end flange. The lumped masses were replaced by forces at six positions on the -Z end to simulate the axial load from the cold mass plus shield and forces were applied to simulate the weight of the cold mass plus shield at the eight positions corresponding to the support positions of the cold mass. It will be noticed that the displacements are asymmetrical with regard to left and right. This is seen most clearly in the plot of axial (Z) displacement. The reason for this can be seen in the next plot which shows a cross-section through the displaced and undisplaced structure. The constraints in X prevent the -X side of the structure from bending as much as the +X side.

Maximum displacement : 1.05mm
Maximum Von Mises stress : 46.1MPa
The general level of Von Mises stress was less than 16MPa

vi. Loadcase v4b
As case v4a except that the 60 tonnes was distributed at the inner edge of the end flange.

Maximum displacement : 1.43mm
Maximum Von Mises stress : 42.1MPa
The general level of Von Mises stress was less than 25MPa

D.1.3 Files

The files are stored in directories named /home/elnath/john/ansys/babar3/casei where i is the loadcase number.

SLAC AHO 2003-032B2f17

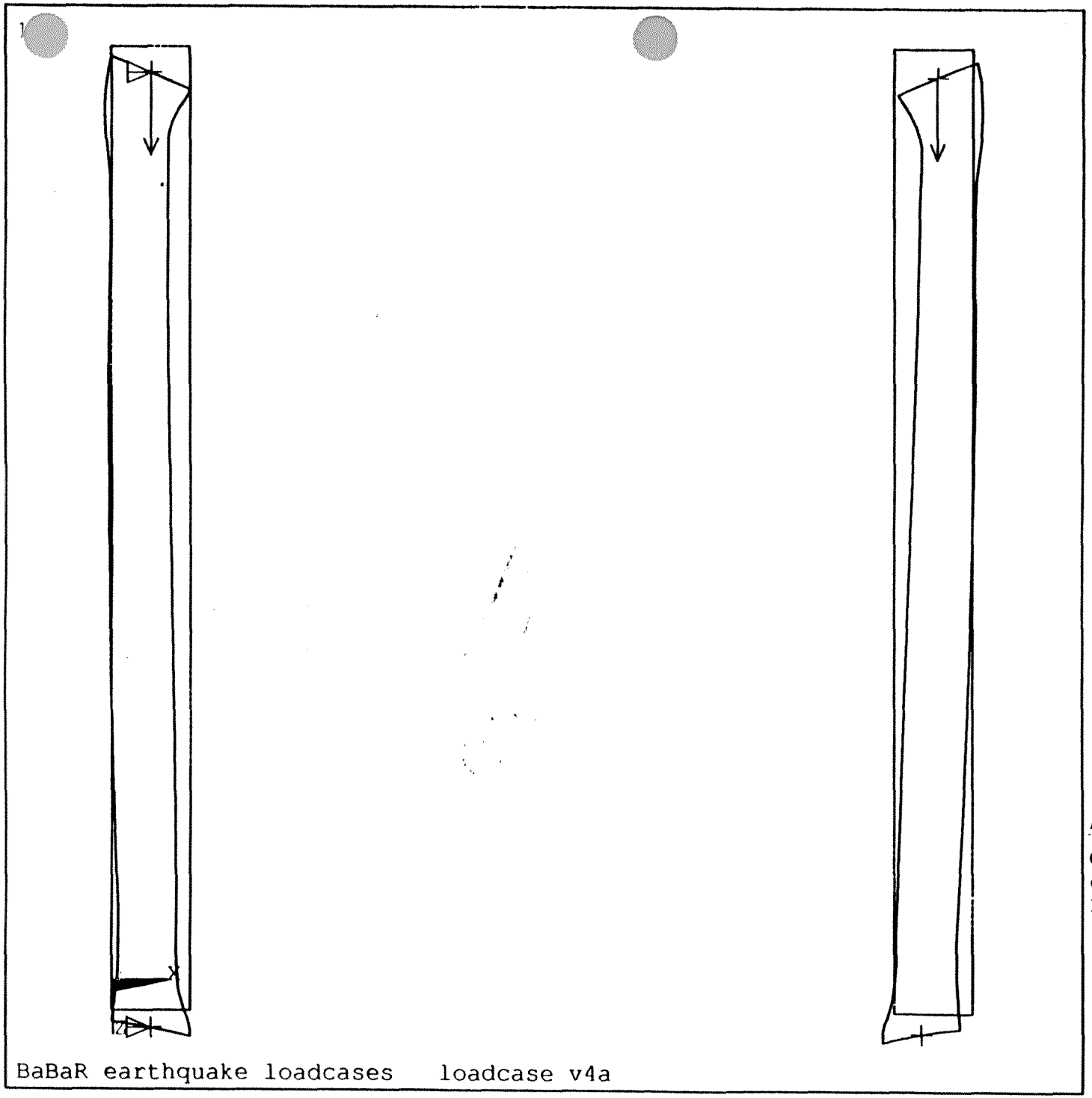

ANSYS 5.0
MAY 17 199
15:09:08
PLOT NO. 1
DISPLACEMENT
STEP=1
SUB =1
TIME=1
RSYS=0
DMX =0.001013
SEPC=24.355
U
F

DSCA=206.261
YV =1
DIST=2.133
XF =0.005386
YF =-0.001819
ZF =0.075775
PRECISE HIDDEN

APPENDIX D. Fig. D2

Cross Section showing form of displacements for Load Case 4a and 4b.

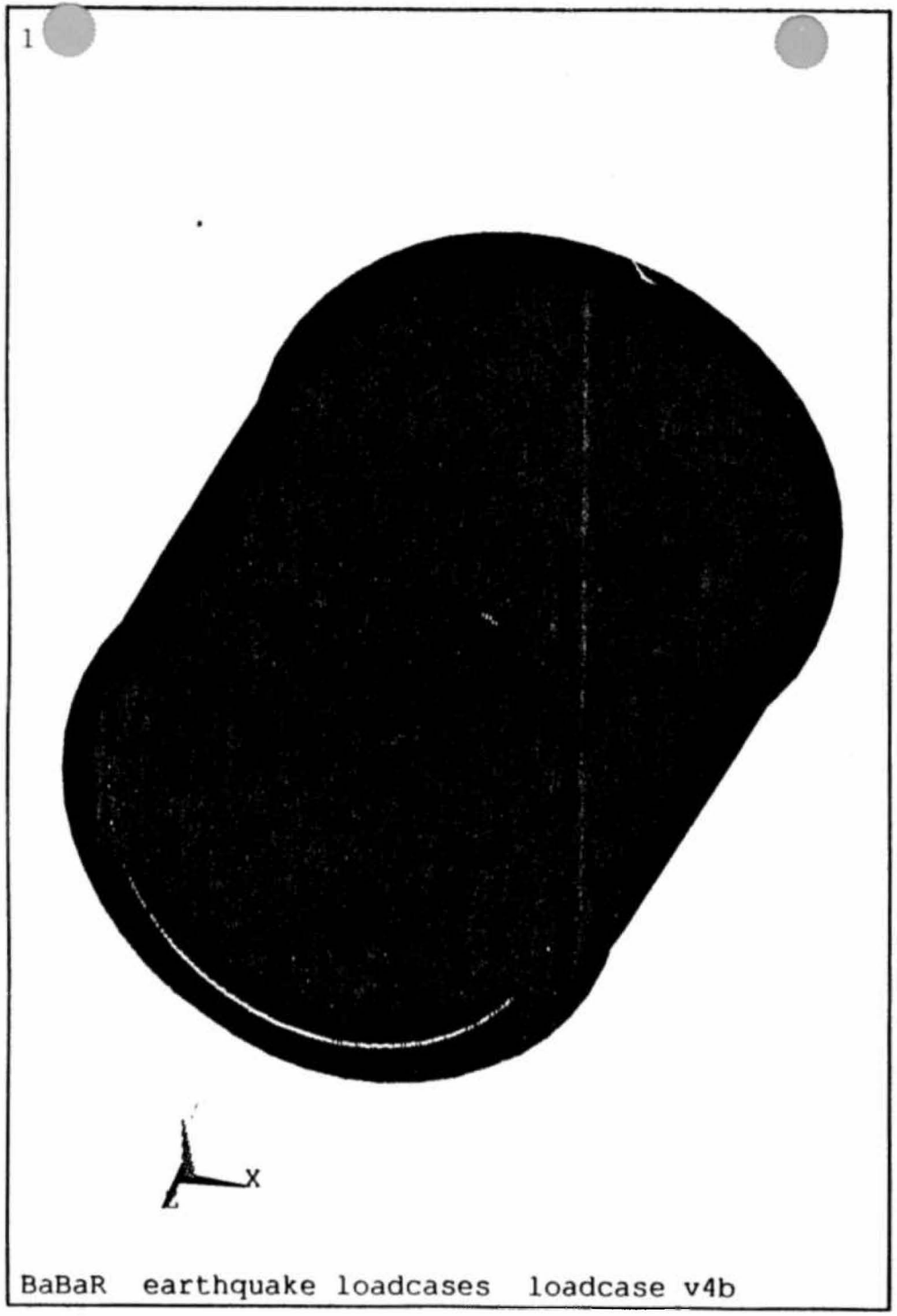

ANSYS 5.0
MAY 17 199
14:48:25
PLOT NO. 1
ELEMENT SOLUTION
STEP=1
SUB =1
TIME=1
SEQV (NOAVG)
BOTTOM
DMX =0.001428
SMN =0.205E+07
SMNB=-0.240E+08
SMX =0.421E+08
SMXB=0.690E+08

0.205E+07
0.649E+07
0.109E+08
0.154E+08
0.198E+08
0.243E+08
0.287E+08
0.332E+08
0.376E+08
0.421E+08

APPENDIX D. Fig. D4

Von Mises Stress
for Load Case 4B
Max. value 42 MPa

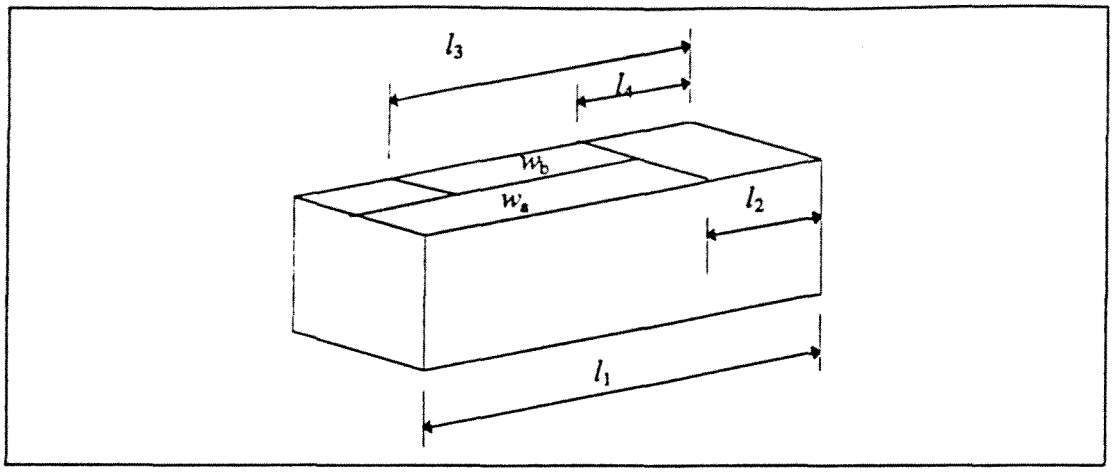

Giving:

$$M = \frac{W_a(l_1^2 - l_2^2)}{2} + \frac{W_b(l_3^2 - l_4^2)}{2}$$
$$= 65625 + 21213$$
$$= 8608 \times 10^3 \text{ N}$$

Stress is

$$\sigma = \frac{My}{I}$$
$$= \frac{86.8 \times 10^3 \times 0.35/2}{0.1 \times 0.35^3/12}$$
$$= 42.5 \text{ MPa}$$

$$\tau = \frac{F}{a}$$
$$= \frac{(37.5 + 14.6) \times 10^4}{0.35 \times 0.1}$$
$$= 14.9 \text{ MPa}$$

The stress level is perfectly acceptable for stainless steel.

APPENDIX F

F. BABAR Cold Mass - detailed analysis of the structure

This is reproduced from the RAL report number RAL/ASD/CME/MISC/012.

F.1 Introduction

A Finite Element analysis was made of the BABAR cold mass in order to determine in detail the stress distribution in the coil.

F.2 The Model

In order to calculate the stress distribution in the coil, particularly in the insulation , a very detailed FE model is required. It would not be feasible to model the entire structure in such detail so two models were made, one modeling each turn of the coil individually but not modeling separately the insulation or the conductors (the "coarse" model), and the other a submodel of the region of interest where both insulation and conductors were modeled in sufficient detail to allow accurate stress calculations to be made (the "fine" submodel). Because the structure has rotational symmetry about the axis and mirror symmetry about mid-axis an axisymmetric model of half the structure was made.

F.3 The Calculations

Appropriate forces and constraints were applied to the coarse model. The forces were the magnetic forces interpolated from the table shown below and applied to the center point of each coil and the constraints were those to provide the symmetry condition. This model was then run to calculate stresses and displacements. In particular the displacements of the coarse model at the positions corresponding to the boundaries of the fine submodel were calculated. The fine submodel was then run using the displacements from the coarse model as boundary conditions and with the same magnetic forces applied to the conductors in the submodel, this time the forces were distributed uniformly over the conductors.

F.4 Material Properties

For the fine model the relevant material properties were as follows:

Matrix	$E = 70$ GPa
	$\nu = 0.3$
Conductor	$E = 130$ GPa
	$\nu = 0.3$
Insulation	$E_{//} = 33$ GPa
	$E_{\perp} = 18$ GPa

SLAC AHO 2003-032B2f17

F.6 Magnetic Forces

Axial Position (m)	Radial Force (N)	Axial Force (N)
0.038798	4.8415e+05	2233.3
0.10259	4.8443e+05	7396.3
0.16637	4.8501e+05	12666
0.23016	4.8589e+05	18122
0.29395	4.8710e+05	23859
0.35774	4.8863e+05	29989
0.42153	4.9051e+05	36666
0.48532	4.9274e+05	44105
0.54911	4.9532e+05	52636
0.61289	4.9824e+05	62781
0.67668	5.0150e+05	75512
0.74047	5.0509e+05	92409
0.80426	5.0894e+05	1.1819e+05
0.86805	5.1389e+05	1.6088e+05
0.93183	5.1803e+05	2.8105e+05
0.98320	7.3067e+05	4.0092e+05
1.0346	7.3319e+05	1.9313e+05
1.0859	7.3563e+05	94438
1.1373	7.3466e+05	18269
1.1887	7.3171e+05	-46295
1.2401	7.2659e+05	-1.0666e+05
1.2914	7.1924e+05	-1.6581e+05
1.3428	7.0952e+05	-2.2619e+05
1.3942	6.9723e+05	-2.9998e+05
1.4455	6.8209e+05	-3.5971e+05
1.4969	6.6380e+05	-4.3924e+05
1.5483	6.4193e+05	-5.3405e+05
1.5996	6.1645e+05	-6.6068e+05
1.6510	5.8361e+05	-8.4303e+05
1.7024	5.5166e+05	-1.2900e+06

The files are to be found in /home/elnath/john/ansys/babar4

The transition region fine model is in sub-directory cased1 and the end region fine model in sub-directory cased3.

SLAC AHO 2003-032B2f17

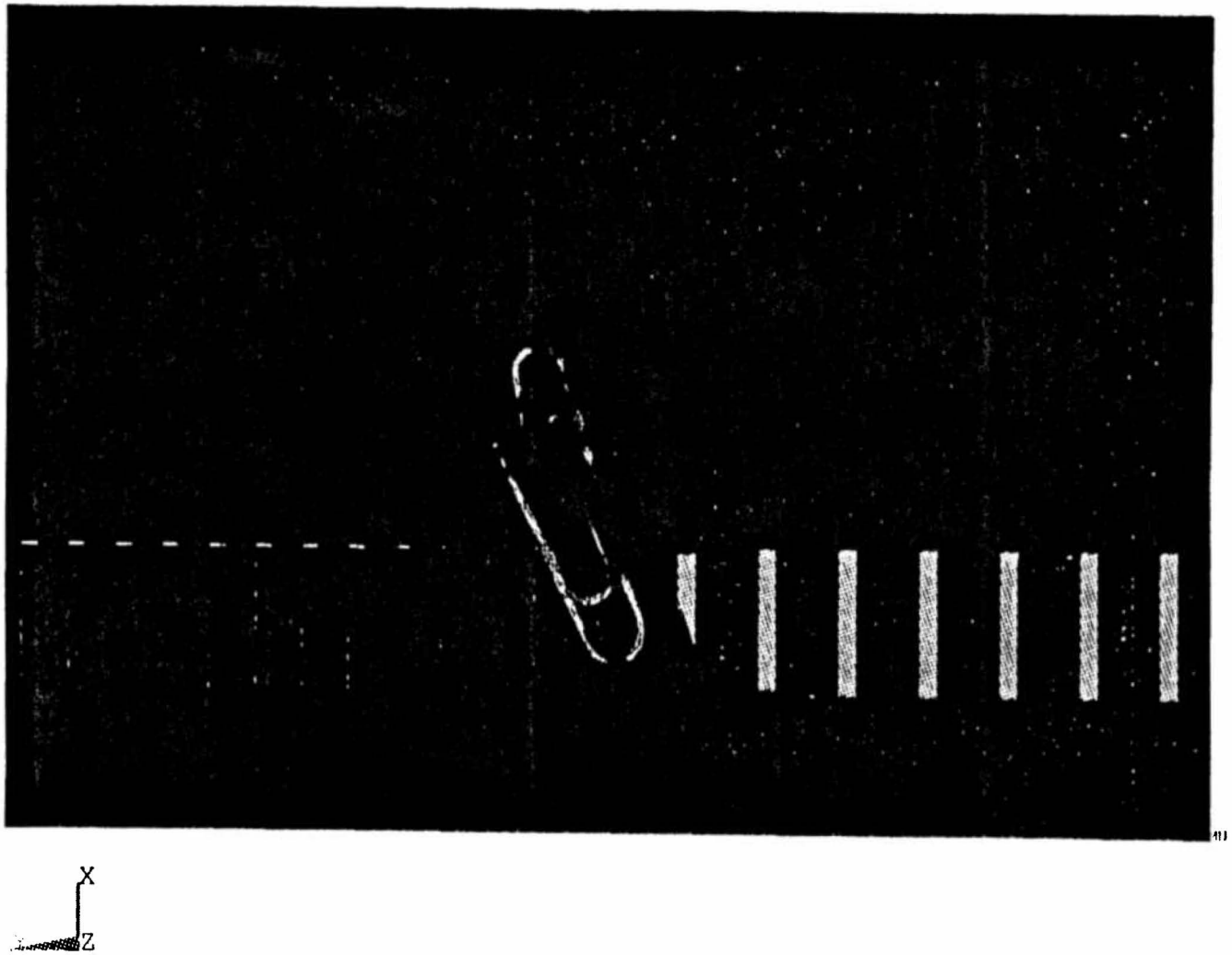

APPENDIX F. Fig. F2
Von Mises Stress
in the fine model,
transition region

SLAC AHO 2003-032B2f17

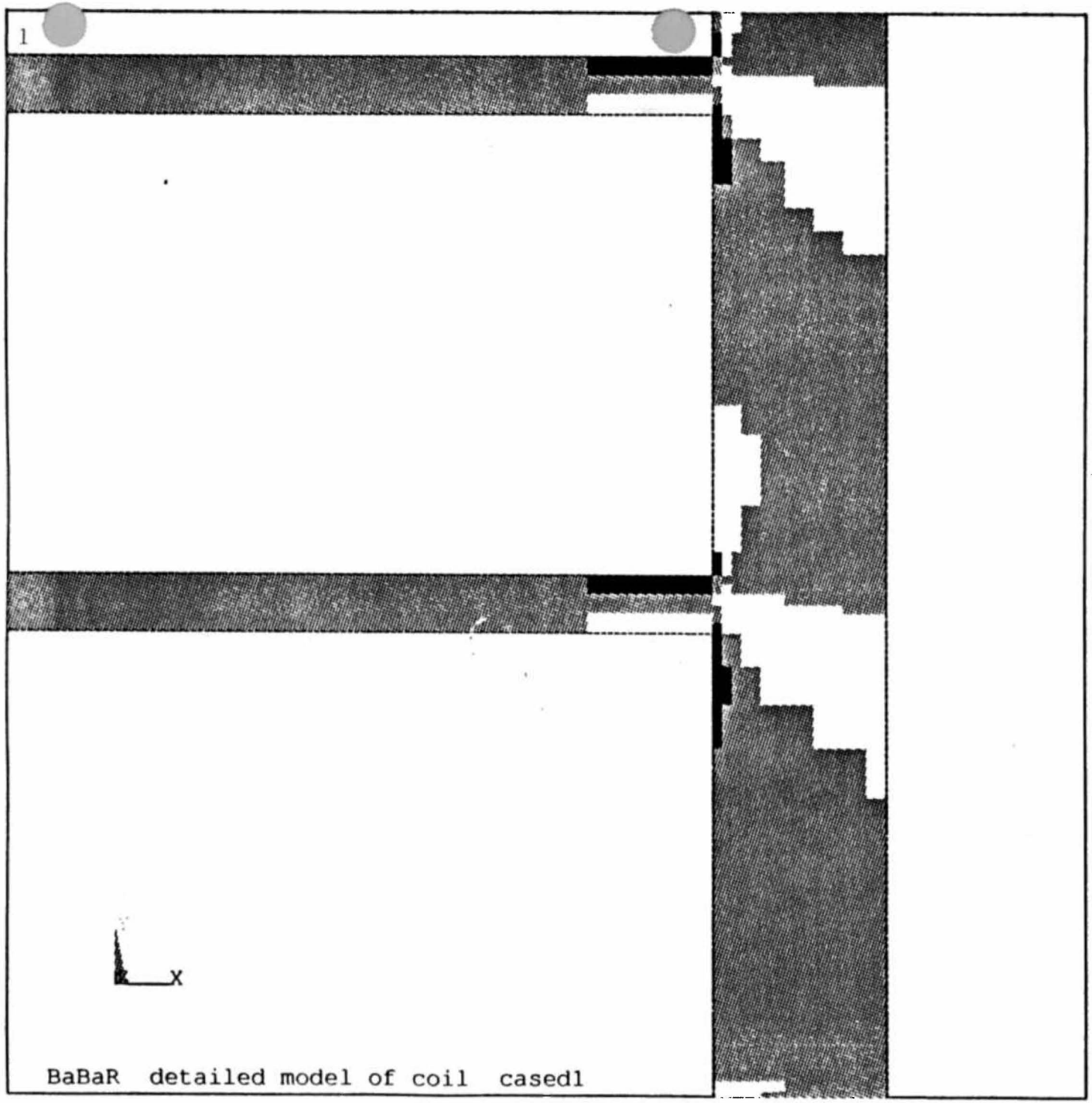

ANSYS 5.1
APR 27 1995
08:49:28
PLOT NO. 1
ELEMENT SOLUTION
STEP=1
SUB =1
TIME=1
SXY (NOAVG)
RSYS=0
DMX =0.650E-03
SMN =-0.103E+07
SMX =0.148E+07

-0.103E+07
-747069
-468430
-189791
88848
367487
646126
924765
0.120E+07
0.148E+07

APPENDIX F. Fig. F4

Shear Stress in the insulation (enclaged and rotated from previous plots), transition region.

1

X

BaBaR detailed model of coil cased3

ANSYS 5.0 A
APR 5 1995
10:53:48
PLOT NO. 1
ELEMENT SOLUTION
STEP=1
SUB =1
TIME=1
SXY (NOAVG)
RSYS=0
DMX =0.389E-03
SMN =-856412
SMX =0.139E+07

-856412
-606899
-357385
-107872
141642
391155
640668
890182
0.114E+07
0.139E+07

APPENDIX F. Fig. F6

Shear Stress in the fine model, at the end of the coil.

SLAC AHO 2003-032B2f17

APPENDIX G

G. ADDENDUM 2: CHANGES TO SUPPORTS, ETC.

Since the main body of this study was written, there have been some changes to the design requirements. This addendum describes the effect of certain changes on the stresses in the vacuum vessel, on the design of the support system, and on the interfaces.

G.1. The changes to the requirements

The earthquake load criteria have changed as a results of the decision to use compliant mounts for the experiment. The design loads are now 0.2g lateral (radial or axial) and 1.4g vertical. (This compares with 1.2g and 2.0g respectively in the previous design).

A knock-on effect of this change is that the axial earthquake loads on the inner detectors no longer need to be supported through the vacuum vessel as described in section 6.4 above.

Another change is to the geometry of the iron yoke; this will now be eight-sided, not six-sided. This affects the positioning of the external supports which can no longer be on the horizontal center line but must occupy spaces 22.5 degrees below it. The supports have been moved to allow for this, and also so that instead of supporting the end-flange of the vacuum vessel they are now located on the outer wall of the vessel. This is shown in the new interface diagram, figures 2a and 2b to this addendum.

The size of the coil has been changed to allow more space inside; all the radii have been increased by 30mm.

G.2. Changes to the overall stresses in the cold mass

The effect of the changes in size will be small. The principal source of stress in the cold mass is the magnetic load, which has not changed. For these reasons, we did not re-run the stress analysis on the overall stress state in the cold mass.

G.3. Changes to the stresses and deflections in the vacuum vessel

(This compares to section 5.2 above)

We have re-run the finite element model of the vacuum vessel with the new dimensions, new support positions, and new loads. There were just four external support positions, placed 22.5 degrees below the horizontal center line on the outer wall of the vessel, in the thickened portion near the end. All four supports were constrained vertically, two (at one end) axially, and two (on one side) horizontally.

Loads from the cold mass were transferred as before, using new values for the mass of the cold mass.

Three load cases were considered. In all cases, the weight of the vessel and the cold mass was included.

SLAC AHO 2003-032B2f17

The loads on the rods (compare with section 6.3, and see figure 1 to this addendum) are now:

Table G.3

		Axial	Radial shared between 4 rods
Nominal	Tensile	10t	20 + .707*7.3 = 25.2
	Compressive	30t	
Earthquake	Tensile	20 + 0.2*7.3 = 21.5t	35.4t
	Compressive	30 + 0.2*7.3 = 31.5t	25t

And the design is now:

Table G.4
(compare with table 6.2 of the design study)

	Units	Axial	Radial
Loads			
Nominal load - tensile	tonne	10	25.2
Nominal load - compressive	tonne	30	
Rods to resist nominal load		6	4
Quake load Tension	tonne	21.5	35.4
Compression	tonne	-31.5	-25.0
Rods to resist quake load		6	4
Material			
Material	Titanium alloy 6%Al, 4%V		
Ultimate stress	MPa	1000	
Yield stress	MPa	900	
Conductivity integral 80K to 4K	W/m	213	
Rod sizes			
Rod diameter - nominal. This is the diameter of the rod over all of its length except the ends, where it is turned down to M20.	mm	25	25
Rod length	mm	350	300
Rod diameter in thread root	mm	16.9 (M20)	16.9 (M20)
Stress, buckling			
Stress under Earthquake load in thread root			
Tension Compression	MPa	160 -234	395 -278
Factor of safety on ultimate stress under earthquake load		4.2 (compressive)	2.5 (tensile)
Factor of safety on buckling (using nominal diameter)		2.9	3.4
Thermal conductivity			
Rods in conductivity calculation		6	8
Total heat load over half the length of the rods	Watts	3.6	5.6

SLAC AHO 2003-032B2f17

Figure 1 to Addendum 2 Forces in cold mass radial support rods

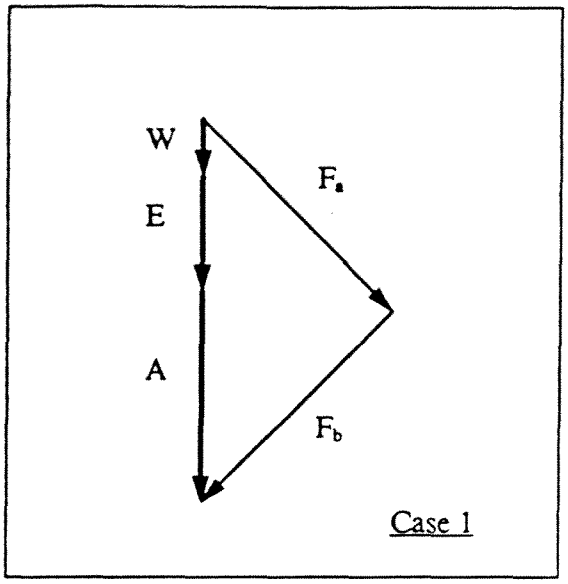

W = weight, 1g gives 7.3t
E = earthquake load, 1.4g gives 10.2t
A = Magnetic alignment error force, 20t
F_a = load in rods, set a (four rods)
F_b = load in rods, set b (four rods)

Case 1 - largest total load

$F_a = F_b = .707 \times (7.3+10.2+20)$
$= 26.5t$

Case 2 - largest load in a set of rods

$F_a = 10.2 + 20 + .707 \times 7.3$
$= 35.4t$

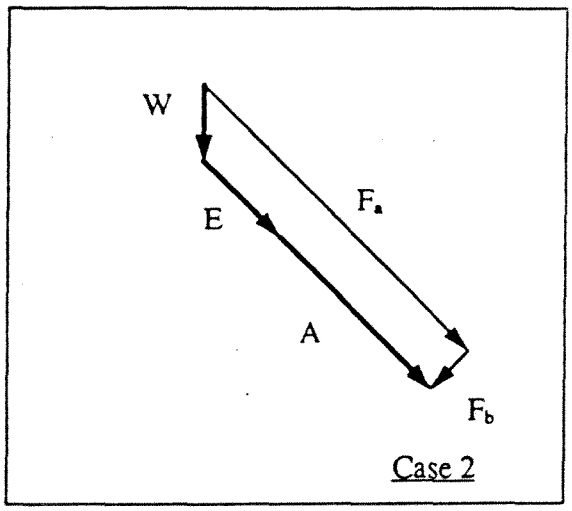

Case 3 - moving forces act sideways

$F_a = .707 \times (7.3 + 10.2 + 20) = 26.5t$
$F_b = .707 \times (7.3 - 10.2 - 20) = -16.2t$
(compressive)

Case 4 - largest compression force
(typical of several possible cases)

$F_b = .707 \times 7.3 - (10.2 + 20) = -25t$
(compressive)

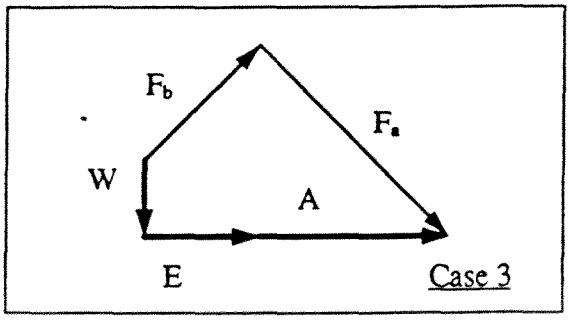

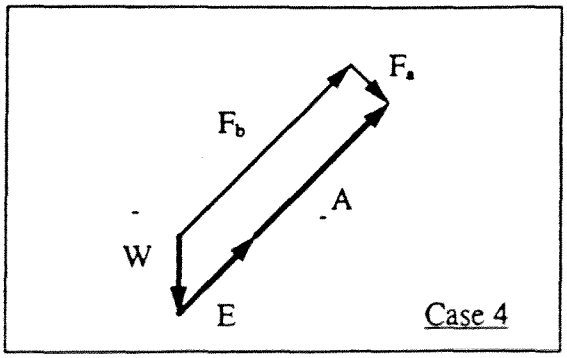

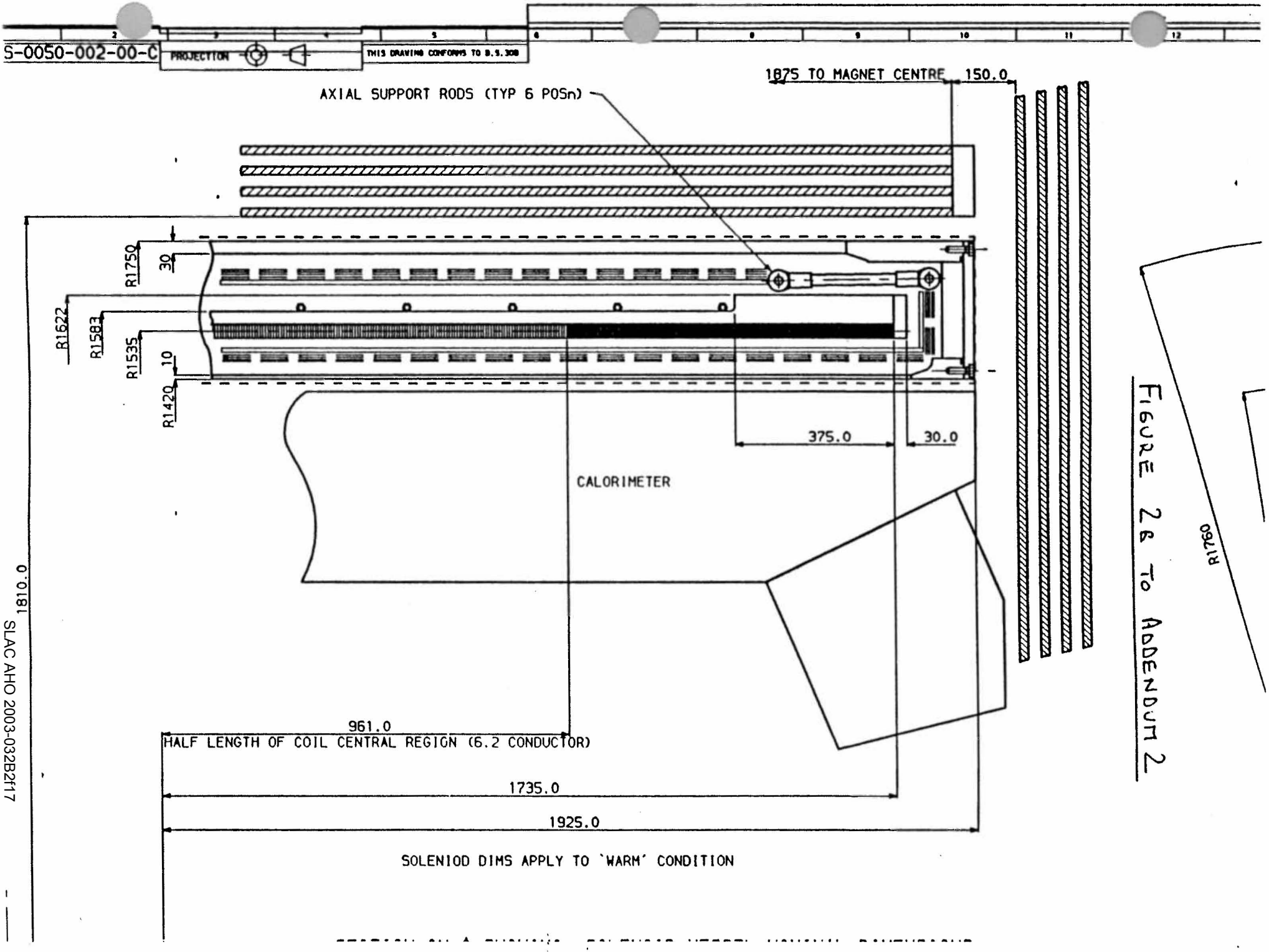

FIGURE 2B TO ADDENDUM 2